國立臺灣大學工學院工程科學及海洋工程研究所

碩士論文

Department of Engineering Science and Ocean Engineering

College of Engineering

National Taiwan University

Master Thesis

仿生型水下載具使用動態壓力訊號分辨壁面之研究

Biomimetic Underwater Vehicle Wall Surface Recognition Using Dynamic Pressure

王膺富

Ying-Fu Wang

指導教授：郭振華博士

Advisor: Jen-Hwa Guo, Ph.D.

中華民國 105 年 2 月

Feb, 2016

國立臺灣大學碩士學位論文
口試委員會審定書

仿生型水下載具使用動態壓力訊號分辨壁面之研究
Biomimetic Underwater Vehicle Wall Surface Recognition Using Dynamic Pressure

本論文係王膺富君（學號 R02525075）在國立臺灣大學工程科學及海洋工程學系完成之碩士學位論文，於民國 105 年 02 月 01 日承下列考試委員審查通過及口試及格，特此證明

口試委員：

____________________（指導教授）

______________ ______________

______________ ______________

______________ ______________

系　主　任 ______________

致謝

碩士兩年多的生涯即將告一段落，準備迎接下個階段的到來，能親手完成一本論文的感動無法言喻，得之於人者太多，出之於己者太少，要感謝的人太多太多，沒有他們的幫助與支持，這本論文也不會如此順利的完成，在這邊我要感謝那些曾經幫助過我的人。

首先我要感謝我的父母及哥哥們，在我碩士的生涯中，讓我可以在沒有經濟壓力的情況下，專心致力於學業，接著我要感謝我的舅舅與舅媽無償地提供我遮風避雨的地方，像照顧自己小孩般的照顧我，是你們分擔了我心頭的壓力，讓我得以順利的完成學業。

感謝指導教授郭振華老師的細心指導和鼓勵，給予我論文的參考方向，也提供機會參與國際研討會，這裡也要感謝鄭逸琳老師、林顯群老師與戴璽恆老師給予論文改進的寶貴建議與指正，使得論文能更加完整。

特別感謝弈倫學長的理論和實作上的建議與指導，幫我處理程式上的問題，讓我每每遇到瓶頸時，總能幫助我找到問題盲點和突破問題。感謝盛煒學長在硬體上的幫助，感謝惟果學長的幫忙與指導，感謝冠宇學長的人生經驗分享及丹林學長的鼓勵。感謝碩班學長：讓我走向不歸路的建汝、認真的泰清與倍豐、讓實驗室像遊樂園的凱閔與漢穎，很正的學姊慧瑩。感謝實驗室的同儕，校草勝凱、辛苦的健柏、自以為世紀很強的志偉、強者英哲，很開心能認識你們，與你們嘴砲玩樂的日子讓我減輕了許多壓力。感謝實驗室的學弟妹：安廷、佳恩、君圃，在我需要幫忙做實驗時撥出時間給予幫助。

最後特別感謝從考研究所開始就一路支持我的欣庭，當我壓力大時總是靜靜的聆聽我的抱怨，幫我分擔所有壓力，義無反顧的支持我的所有決定。感謝所有好友的鼓勵與支持，感謝太陽女神的威力，讓令人煩躁多雨的台北能綻放陽光。最後最後，感謝所有幫助過我的人，有你們，這本論文才得以完成。

中文摘要

本研究利用機器學習與分類理論探討仿生型水下載具游動時周圍的壓力場變化，並藉由實驗來作驗證。本實驗所使用之仿生型載具為長 90 公分、寬 25 公分、高 50 公分之類魚型水下載具，在載具兩側及頭部分別裝載壓力感測器，共七顆壓力感測器，用以感測游動時所產生的周圍壓力變化。

此論文中我們提出一個架構，將壓力感測器所量測到的信號經由濾波器及統計理論的分析過程，抽取出待分類的特徵，再利用支持向量機針對特徵向量來作分類。首先將訊號濾波，將濾波後的訊號作均方根，接著挑選出數種信號特徵作為特徵向量，爾後我們利用一個特徵選擇的方法，從所挑選的數種特徵向量適應性地選取較具代表性的特徵向量，最後再利用支持向量機來對不同類別的特徵向量予以分類。根據本文結論，仿生型載具能在自身游動時，憑藉著裝載的壓力感測器偵測周圍的壓力場變化，予以達到周圍偵測的效果，期許未來能進一步達成群游、避障等目的。

關鍵詞: 仿生型自主水下載具、側線系統、游動運動學、環境偵測

Abstract

Machine learning method is used to study the wall detection possibilities of a swimming Biomimetic Autonomous Underwater Vehicle (BAUV) by measuring the dynamic pressure surrounding the vehicle body. A BAUV of 90cm length, 25cm width and 50cm high with pressure sensors on body sides and on its head was built to sense the pressure around the BAUV.

An architecture for the design of a two-class pressure signals classifier in an underwater environment is proposed. The classifier is based on a support vector machine, features vector are dynamic pressure signals processed by a band-pass filter and then their root-mean-square values are ensemble to represent the feature values. Feature vectors for classification are adaptively selected to form significant feature vectors by a feature selection method. Finally, the classifier is used for classifying the selected features. It is shown that a BAUV could use the dynamic pressure signals to estimate the presence of a solid wall beside it by the classifier.

Keywords: Biomimetic Autonomous Underwater Vehicle, lateral line, swimming kinematics, environmental detection

CONTENTS

LIST OF FIGURE

LIST OF TABLES

LIST OF SYMBOLS

x_i	Input vector
y_i	Class labels
f	The hyperplane
w	Parameters of the classifier
b	Parameters of the classifier
M	Euclidean distance
$\propto_i$	Lagrange multiplier
L	Lagrangian
∂	Partial derivative operator
ξ_i	Slack variables
C	The penalty parameter
γ_i	Lagrange multiplier
$\emptyset$	The nonlinear function
sgn	Sign function
n	The number of support vector
K	The kernel function
γ	The kernel parameter
h	The kernel parameter

d	The kernel parameter
I	Important dimension function
$\boldsymbol{\Omega}_{a,\beta}$	A hyperplane corresponding class a and class β
k	Feature dimension
$\mu_{a,k}$	The mean value of the feature dimension k in class a
$\mu_{\beta,k}$	The mean value of the feature dimension k in class β
$\sigma_{a,k}$	The standard deviation of the feature dimension k in class a
$\sigma_{\beta,k}$	The standard deviation of the feature dimension k in class β

Chapter 1 Introduction

1.1 Motivation

Most fish use the lateral line system as an important sensory organ to make up for lack of other organs, such as the fish in the harsh underwater environment, they must rely on the lateral line system to sense the surroundings for obstacle avoidance and navigation. In this study, we choose the commercial pressure sensors as the lateral line system to measure the change in near field pressure of water flow.

Machine Learning is very popular in recent years, it can find a lot of seemingly meaningless signals which implied useful information through machine learning. Classification is one of the topics discussed in machine learning theory, it analyzes its signal and then classifies them with known categories, in this way, it will be able to establish a model represents the relationship between the input and the output category, then, we classify unknown signals according to the model, finally, the decision results obtained.

There are a variety of classifiers, such as genetic algorithm(GA),artificial neural network(ANN), Bayesian classification method, support vector machine(SVM) and so on. SVM is a machine learning methods for data classification, regression and pattern recognition. Because SVM classification ability is quite good, it has been widely used in

handling with classification problems in recent years.

The pressure sensors inspired by the lateral line system were developed to mimic the sensory capabilities evolved in real fish. Fish are able to sense the surroundings by using the lateral line's feedback, such as detecting of stationary objects, schooling, tracking prey, avoiding obstacles and so on. There are lots of existing studies on artificial lateral lines that measure signals by fixed sensors, In order to implement the sensory systems, we equipped the array of pressure sensors on the surface of the BAUV, and dedicate to distinguish the pressure field around the BAUV by SVM in this thesis. Therefore, our motivation is to find out the different pressure signals by the pressure sensors between the BAUV swims along the wall and in the open field, and distinguish the pressure signals in two cases (along the wall and in the open field) by machine learning theory.

1.2 Literature review

In the sight of unclear underwater environment, the lateral line system is an important sensory organ for fish to sense surroundings [1], The lateral line consists of arrays of hair cell sensors, it allows an aquatic animal to identify objects of near field and perform hydrodynamic imaging of the environment, therefore, fish are able to detect predators/prey [2], school [3] and detection of stationary objects [4] by the lateral line system.

The biological lateral line system has inspired the effort to engineer artificial lateral lines for applications in underwater vehicles, It provides a useful supplement to existing sensing instruments, such as cameras and sonars. In order to mimic this sensing system, some pressure sensors were employed to measure the hydrodynamics information to estimate distance detection and location. Coombs [5] develop the flow sensor and used the gradient of pressure to detect amplitude and distance of a dipole. Fernandez [6] identified both passive and active objects from pressure signals measured by pressure sensor array.

In Neuro-physiological studies, the distance and amplitude of a dipole source could be estimated by pressure difference. An analysis of mottled sculpin responding to a vibrating source also was discussed in his research. And the result is consistent with the assumption in which fish would detect distance and direction of a vibrating source. To

engineer such a biologically inspired sensing system, numbers of artificial lateral line systems were developed to detect for fish-like underwater sensing [7].

Pressure difference of flow field of swimming fish were provided to study the behavior of aquatic locomotion, there are various types of model for different purposes have been demonstrated in discussing different topics, such as fish school, saving energy, and BAUV designing. Windsor et al attempted to compare the hydrodynamic imaging in different situation by Blind Mexican cave fish depend on the flow field [8] [9].

The support vector machine (SVM) is developed based on the idea of structural risk minimization (SRM) induction principle [10] that aims at minimizing a bound on the generalization error, rather than minimizing the mean square error.

In many applications, SVM has been shown to provide higher performance than traditional learning machines and has been introduced as powerful tools for solving various classification and regression problem [11] [12], for the classification case, SVM has been used for isolated handwritten digit recognition [13], speaker identification, face detection in images, knowledge-based classifiers [14], and text categorization [15].

As in traditional pattern-recognition systems, the model consists of three main modules [16]; a feature extractor that generates feature vectors from the signals; the feature selection method that choose the important feature vectors for classification, and a

feature classifier that outputs the class label based on the selected features.

1.3 Thesis organization

This thesis is organized as follows. In chapter 2, we introduce the concepts of SVM classifier, kernel function, and select parameters by the cross-validation method.

In chapter 3, we explain the scheme of pressure signal analysis used in this study, then we describe the feature extraction and the feature selection methods. In chapter 4, the system architecture of the BAUV are described, we first briefly introduce hardware of the BAUV and the product of commercial pressure sensors. The experimental setup are described, then, we presents two-class (near the wall and in the open field) classified experiment results of the tested system and discussed. Finally, we conclude this study in chapter 5.

Chapter 2 Feature Classification by Support Vector Machine

Support Vector Machine (SVM) is one of the most powerful technique for data classification, it has proven to provide higher performance than traditional learning machines and has been introduced as powerful tools for solving intractable classification and regression problem, so we choose SVM as the classification model make us classify signals in the underwater environment.

2.1 Support Vector Machine

2.1.1 Linear Classification

Consider the two different kinds of data in a two-dimensional plane, it is shown in Fig 2.1, the training data from two classes $[(x_1, y_1), (x_2, y_2), \dots, (x_\ell, y_\ell)]$ with input vector x_i and output data y_i, the class labels $y_i \in \{+1, -1\}$. Because these data are linearly separable, we can use a line to separate the two types of data, this line is equivalent to a hyperplane and it can be represented by classification function

$$f(x) = w^T x + b \tag{2.1}$$

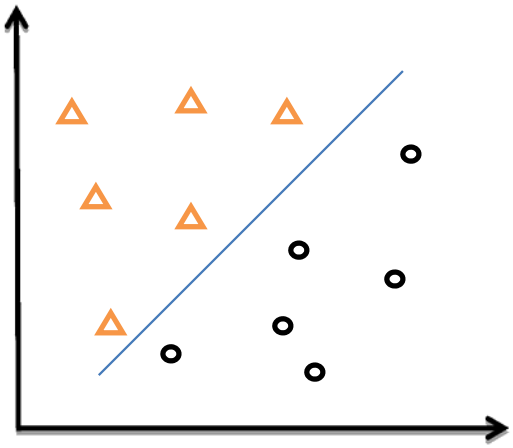

Fig. 2.1 Two different kinds of data in a two-dimensional

Where w and b are the parameters of the classifier, and there exists parameters w and b such that

$$\begin{cases} w^T x + b \geq +1, & y_i = +1 \\ w^T x + b \leq -1, & y_i = -1 \end{cases} \tag{2.2}$$

and equivalently

$$y_i(w^T x_i + b) \geq 1, \qquad i = 1, \ldots, \ell \tag{2.3}$$

Fig. 2.2 depicts the classification problem.

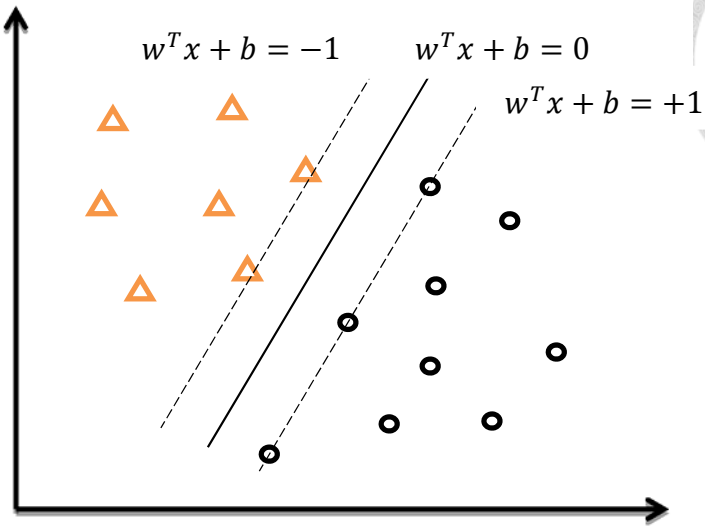

Fig. 2.2 The classification problem

When the data point farther away from the hyperplane, and the confidence of the classifier is better, therefore, we need to find the gap have maximal margin. Fig. 2.3 shows a simple case of the maximal margin and the small margin in a two-dimensional input space.

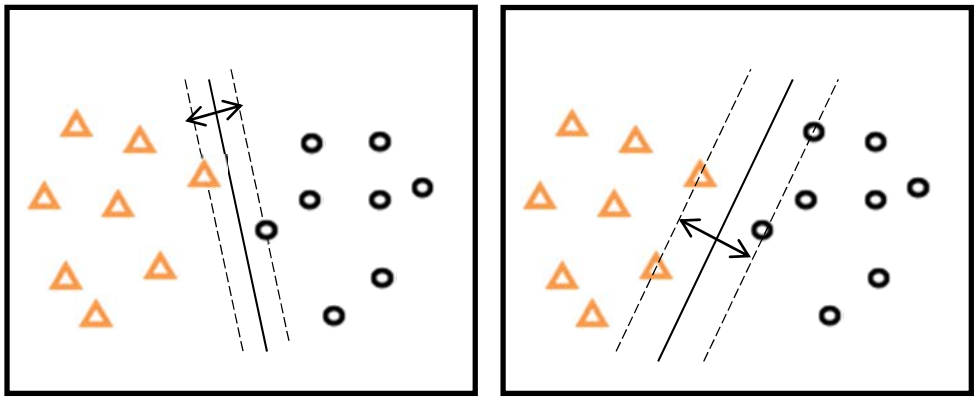

Small Margin Maximal Margin

Fig. 2.3 The case of the optimal separating hyperplane

There are two parallel planes $H_1: w^T x + b = +1$ and $H_2: w^T x + b = -1$ both side of the separating hyperplane, and the same distance from the hyperplane, they can be represented as Euclidean distance.

$$\mathrm{M} = \frac{|w^T x + b|}{\|w\|} + \frac{|w^T x + b|}{\|w\|} = \frac{2}{\|w\|} \tag{2.4}$$

Where $\|w\| = \sqrt{w^T w}$ is the Euclidean norm of parameter vector *w*. From (2.4), the problem of SVM is

$$\begin{aligned} &\max && \frac{2}{\|w\|} \\ &subject\ to && y_i(w^T x_i + b) \geq 1\ ,\ i = 1, \dots, l \end{aligned} \tag{2.5}$$

and is equivalent to

$$\begin{aligned} &\min && \frac{1}{2}\|w\|^2 \\ &subject\ to && y_i(w^T x_i + b) \geq 1\ , i = 1, \dots, l \end{aligned} \tag{2.6}$$

Now the objective function is quadratic, each constraint will coupled with a Lagrange multiplier $\propto_i \geq 0$ in the Lagrange function let the problem converted to dual variable optimization problem

$$L(w, b, \alpha) = \frac{1}{2}\|w\|^2 - \sum_{i=1}^{l} \alpha_i [y_i(w^T x_i + b) - 1] \quad (2.7)$$

The Lagrangian *L* must be minimized with respect to the primal variables w and *b* and maximized with respect to the dual variables α_i, the solution to parameters *w* and *b* is equivalent to determining the saddle point of the Lagrangian. At the saddle point, the derivatives of *L* with respect to primal variables will vanish.

$$\frac{\partial L}{\partial w} = 0 \quad \rightarrow \quad w = \sum_{i=1}^{l} \alpha_i y_i x_i \quad (2.8)$$

$$\frac{\partial L}{\partial b} = 0 \quad \rightarrow \quad \sum_{i=1}^{l} \alpha_i y_i = 0 \quad (2.9)$$

Let (2.8) and (2.9) substituting into Lagrangian (2.7), it eliminates the primal variables *w* and *b*, resulting in the following quadratic programming problem as the dual problem in the Lagrange multipliers, so the dual problem is solved in $\alpha = [\alpha_1, \alpha_2, \ldots \alpha_l]$ instead of *w*.

$$\max_{\alpha} \quad \sum_{i=1}^{l} \alpha_i - \frac{1}{2} \sum_{i,j=1}^{l} \alpha_i \alpha_j y_i y_j x_i^T x_j$$

$$\text{subject to} \quad \sum_{i=1}^{l} \alpha_i y_i = 0 \tag{2.10}$$

$$\alpha_i \geq 0, \quad i = 1, \ldots, l$$

The Karush-Kuhn-Tucker theorem plays an important role in the theory of SVM, owing to the problem of SVM is the convex problem, the Karush-Kuhn-Tucker (KKT) conditions means that is a non-linear programming problems can have the optimal solution of necessary and sufficient conditions for w, b, α. Thus solving the SVM problem is equivalent to finding a solution to the KKT conditions. According to this, the solution of problem (2.10) has the equality

$$\alpha_i [y_i (w^T x_i + b) - 1] = 0, \qquad i = 1, \ldots, l \tag{2.11}$$

The dual problem (2.10) is solved in $\alpha = [\alpha_1, \alpha_2, \ldots \alpha_l]$ instead of w, then we can determine the parameters w and b by (2.8) and (2.11).

About the hyperplane, data classification is a point x substitutes into (2.1) calculates the results, and according to its sign to the category. From (2.1), the classifier for binary classification problem can thus be written as

$$f(x) = \sum_{i=1}^{n} \alpha_i y_i \langle x_i \cdot x \rangle + b \tag{2.12}$$

We only need to calculate the inner product for the new point *x* and the training data points, in fact, only non-zero Lagrange multipliers α_i take part in establishing the final classifiers. These points that have non-zero corresponding Lagrange multipliers are called *Support Vectors* (SV). Support Vector are the point of the closest hyperplane in two groups of data, so the hyperplane is to decide which point is Support Vector. Therefore, where n is the number of Support Vector. Fig. 2.4 demonstrates the support vectors and non-support vectors in a linearly separable classification case.

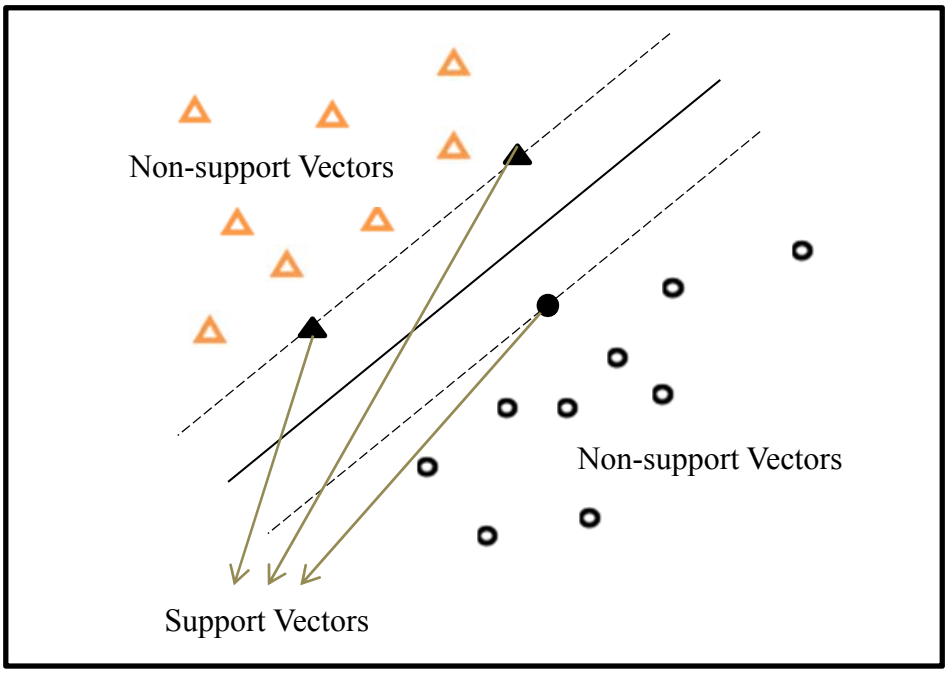

Fig. 2.4 The support vector and the separating hyperplane

2.1.2 Non-Separable Cases

Previously, we all assume that the classification problem is linearly separable data, but most data sets are not able to be classified by linear hyperplanes in real world. The data sets may not be nonlinear but simply because the data sets are noisy and cannot be linearly classified, when a data point is misclassified, an error will occur and exert an influence on the decision hyperplane, and these data that left the normal position are called Outlier, it is shown in Fig. 2.5.

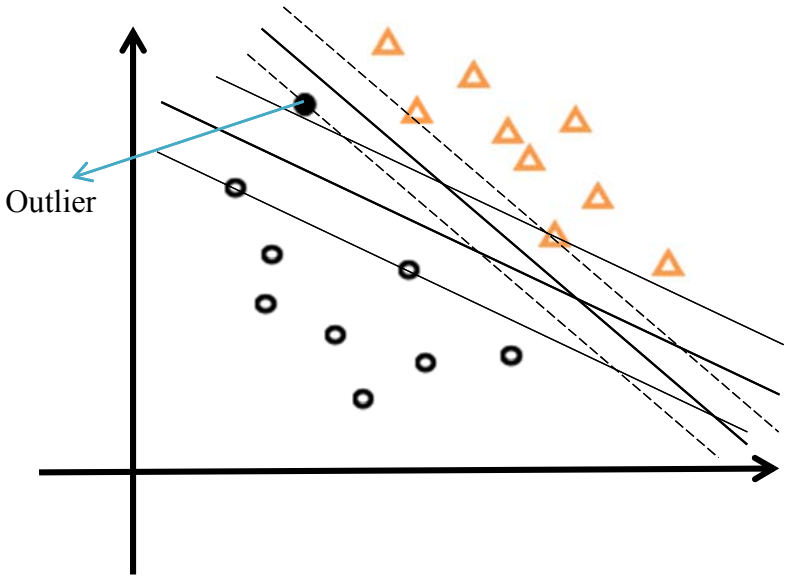

Fig. 2.5 The separating hyperplane have data left the normal position

The soft margin is allowed to tolerate misclassifications in such non-separable case, the algorithm was introducing non-negative slack variables $\xi_i \geq 0,\ i = 1, \cdots, l$ in the optimization problem [30]. The objective function to be minimized involves a second term to account for the overlapping data and the constraints need to modified, therefore, the equation (2.6) will be written as

$$\begin{aligned} \min_{w,b} \quad & \frac{1}{2}\|w\|^2 + C\sum_{i=1}^{l}\xi_i \\ \text{subject to} \quad & y_i(w^T x_i + b) \geq 1 - \xi_i \\ & \xi_i \geq 0, \quad i = 1, \ldots, l \end{aligned} \tag{2.13}$$

Where *C* is a penalty parameter that accounts for the weights between margin maximization and error minimization. A larger *C* corresponds to assigning a greater penalty to errors. Such that the goal tends to put more emphasis on minimizing the second term (training error) in the objective function (2.13). Simultaneously, this results in larger weights, i.e. the margin is narrower. For a smaller *C*, more error can be tolerated (more data can be misclassified), resulting in a wider margin. Note that for linearly separable case, the penalty parameter *C* is equal to infinity.

The constraint is added to the objective function in a similar way as that in a preceding subsection. By introducing Lagrange multipliers $\alpha \geq 0$ and $\gamma \geq 0$, the new primal Lagrangian is

$$L(w, b, \xi, \alpha, \gamma) = \frac{1}{2}\|w\|^2 + C\sum_{i=1}^{l}\xi_i - \sum_{i=1}^{l}\alpha_i\left[y_i(w^T x_i + b) - 1 + \xi_i\right] - \sum_{i=1}^{l}\gamma_i\xi_i \tag{2.14}$$

Again, the saddle point of the Lagrange function needs to be determined, the Lagrangian is minimized with respect to *w*, *b* and ξ_i, and maximized with respect to α_i and γ_i. The problem can be solved in the dual space in the same manner as above.

$$\frac{\partial L}{\partial w} = 0 \quad \rightarrow \quad w = \sum_{i=1}^{l}\alpha_i y_i x_i \tag{2.15}$$

$$\frac{\partial L}{\partial b} = 0 \quad \rightarrow \quad \sum_{i=1}^{l}\alpha_i y_i = 0 \tag{2.16}$$

$$\frac{\partial L}{\partial \xi_i} = 0 \quad \rightarrow \quad C - \alpha_i - \gamma_i = 0 \tag{2.17}$$

And the KKT condition is

$$\begin{aligned} &\alpha_i[y_i(w^T x_i + b) - 1 + \xi_i] = 0 \\ &\gamma_i \xi_i = 0, \;\; i = 1, \cdots, l \end{aligned} \tag{2.18}$$

The same, substituting (2.15), (2.16) and (2.17) into (2.14), we can get a same result in the following dual quadratic programming (QP) problem, and the only difference between separable case and non-separable case in QP lies in a bound *C* of the Lagrange multipliers α_i.

$$\begin{aligned} \max_{\alpha} \quad & \sum_{i=1}^{l} \alpha_i - \frac{1}{2} \sum_{i,j=1}^{l} \alpha_i \alpha_j y_i y_j x_i^T x_j \\ \text{subject to} \quad & \sum_{i=1}^{l} \alpha_i y_i = 0 \\ & 0 \le \alpha_i \le C, \quad i = 1, \ldots, l \end{aligned} \tag{2.19}$$

The data point that have nonzero Lagrange multipliers are termed support vectors and involve in constructing the decision hyperplane, among them, the points for which $0 \le \alpha_i \le C$ can be identified that $\xi_i = 0$. These support vectors are referred to as *margin support vectors*. The points for which $\alpha_i = C$ are misclassified and their corresponding $\xi_i > 0$. These support vectors are called *bounded support vectors*. And

the decision hyperplane of a soft margin classifier is in the same form as question (2.12).

2.1.3 Nonlinear Support Vector Classification

In real world problems, many data sets may exhibit nonlinear characteristics and thus are not able to classified by linear hyperplanes. For the nonlinear case, SVM approach is to map the data into a high dimensional space to solve the original space linearly inseparable problem, Fig. 2.6 shows data cannot be classified in two-dimensional space and thus mapped to the three-dimensional space is classified.

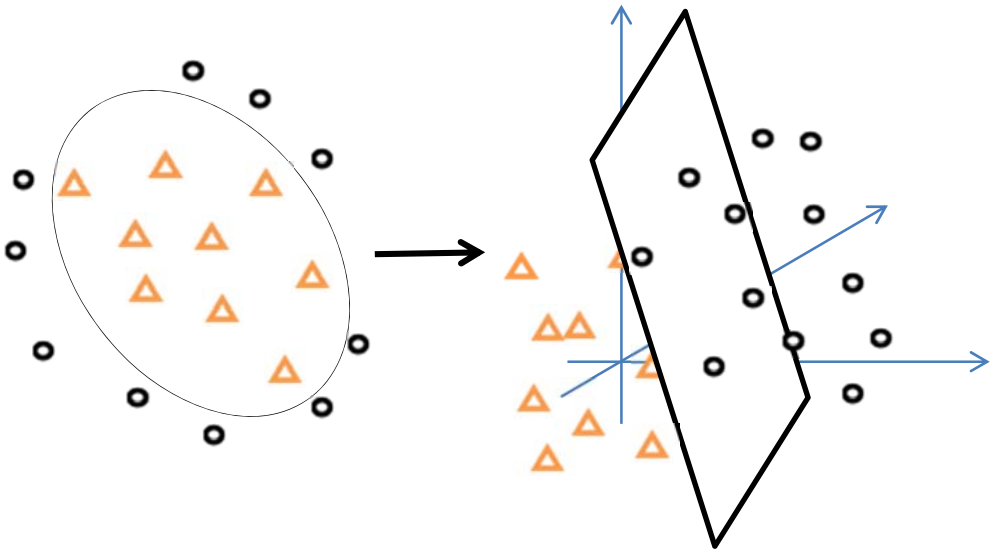

Fig. 2.6 Data of nonlinear classification is mapping into a high dimensional space

Let an input vector *x* be mapped into a feature space by a nonlinear function $\emptyset(x)$, and we can use the linear classifier in the feature space. Thus, the nonlinear classifier is

$$f(\boldsymbol{x}) = \mathbf{sgn}[\boldsymbol{w^T}\emptyset(\boldsymbol{x}) + \boldsymbol{b}] \tag{2.20}$$

And the separating hyperplane satisfies

$$y_i(w^T\emptyset(x_i) + b) \geq 1, \qquad i = 1, \dots, l \tag{2.21}$$

The objective function and the constraints become

$$\begin{aligned} \min_{w,b,\xi} \quad & \frac{1}{2}\|w\|^2 + C\sum_{i=1}^{l}\xi_i \\ \text{subject to} \quad & y_i(w^T\emptyset(x_i) + b) \geq 1 - \xi_i \\ & \xi_i \geq 0, \quad i = 1, \dots, l \end{aligned} \tag{2.22}$$

The Lagrangian is

$$L(w,b,\xi,\alpha,\gamma) = \frac{1}{2}\|w\|^2 + C\sum_{i=1}^{l}\xi_i - \sum_{i=1}^{l}\alpha_i\{\, y_i[\, w^T\emptyset(x_i + b)\,] - 1 + \xi_i\,\} - \sum_{i=1}^{l}\gamma_i\xi_i \tag{2.23}$$

The solution is solved by the saddle point of the Lagrange function.

$$\frac{\partial L}{\partial w} = 0 \quad \rightarrow \quad w = \sum_{i=1}^{l}\alpha_i y_i \emptyset(x_i) \tag{2.24}$$

$$\frac{\partial L}{\partial b} = 0 \quad \rightarrow \quad \sum_{i=1}^{l}\alpha_i y_i = 0 \tag{2.25}$$

$$\frac{\partial L}{\partial \xi_i} = 0 \quad \rightarrow \quad C - \alpha_i - \gamma_i = 0 \tag{2.26}$$

And the KKT conditions are

$$\begin{aligned} &\alpha_i\{\, y_i[\, w^T\emptyset(x_i) + b\,] - 1 + \xi_i\,\} = 0 \\ &\gamma_i\xi_i = 0, \;\; i = 1,\cdots,l \end{aligned} \tag{2.27}$$

Substituting (2.24), (2.25) and (2.26) into (2.23), the QP problem becomes

$$\begin{aligned} \max_{\alpha} \quad & \sum_{i=1}^{l} \alpha_i - \frac{1}{2} \sum_{i,j=1}^{l} \alpha_i \alpha_j y_i y_j \emptyset(x_i)^T \cdot \emptyset(x_j) \\ \text{subject to} \quad & \sum_{i=1}^{l} \alpha_i y_i = 0 \\ & 0 \leq \alpha_i \leq C, \quad i = 1, \dots, l \end{aligned} \tag{2.28}$$

Also, the data points that have nonzero Lagrange multipliers are support vector, the decision hyperplane of a nonlinear classifier is constructed using support vector as

$$f(x) = \text{sgn}\left[\sum_{i=1}^{n} \alpha_i y_i \emptyset(x_i)^T \cdot \emptyset(x) + b \right] \tag{2.29}$$

Where n is the number of support vector.

2.2 Kernel Function

When using the nonlinear algorithms in the preceding subsection, the computation of inner product $< \emptyset(x_i)^T \cdot \emptyset(x_j) >$ in the feature space will be very complex and computationally prohibitive, thus, the computation can be performed in the inner products in the feature space using a kernel function $K(x_i, x_j) = \emptyset(x_i)^T \cdot \emptyset(x_j)$ to yield the inner products in the feature space. And the QP problem of nonlinear classifier with kernels can be formulated as

$$\begin{aligned} \max_{\alpha} \quad & \sum_{i=1}^{l} \alpha_i - \frac{1}{2} \sum_{i,j=1}^{l} \alpha_i \alpha_j y_i y_j \, K(x_i, x_j) \\ \text{subject to} \quad & \sum_{i=1}^{l} \alpha_i y_i = 0 \\ & 0 \le \alpha_i \le C, \quad i = 1, \dots, l \end{aligned} \tag{2.30}$$

There are four basic kernels:

1. Linear kernel

$$K(x_i, x_j) = x_i^T \cdot x_j \tag{2.31}$$

2. Polynomial kernel

$$K(x_i, x_j) = \left[\gamma(x_i^T \cdot x_j) + h\right]^d \tag{2.32}$$

3. Radial Basis Function (RBF) kernel

$$K(x_i, x_j) = \exp\left(-\gamma \left\| x_i - x_j \right\|^2\right) \quad (2.33)$$

4. Sigmoid kernel

$$K(x_i, x_j) = \tanh\left[\gamma\left(x_i^T \cdot x_j\right) + h\right] \quad (2.34)$$

Where γ, h and d are kernel parameters.

Since the nonlinear SVM model is employed, a kernel function has to be selected from the qualified functions. From [17], it suggested the Gaussian RBF kernel, because it unlike the linear kernel, the RBF can nonlinearly map the data into the feature space so that it can handle the data with nonlinear attributes. Moreover, the linear kernel is a special case of RBF kernel [18], and the sigmoid kernel behaves like RBF kernel for certain parameters [19]. But, the sigmoid kernel is not inner product of two vectors under some parameters [12]. The polynomial kernel has more parameters than the RBF kernel, the RBF kernel has only one parameter, and therefore it has less numerical difficulties. In addition, the values of the polynomial kernel may go to infinity or zero when the degree is large, while the value of the RBF kernel is between zero and one. For these reasons, the RBF kernel seems to surpass other commonly used kernels, so we finally choose the RBF kernel in this study.

2.3 Parameters of Support Vector Machine

The penalty parameter *C* controls the flatness or smoothness of the approximation function. A larger *C* corresponds to assigning a greater penalty to error, indicates that the goal tends to put more emphasis on minimizing the second term (training error) in the objective function in (2.22). This will result in larger weights, which makes the learning machine more complex. A smaller *C* may cause the errors too be excessively tolerated, yielding a learning machine with poor approximation. If the data are noisy, then smaller *C* values, which penalize the error less, may be preferred.

The radial basis function (2.33) has only a parameter γ, which is related to the spread of the function around its center. A larger γ results in a smaller spread, and a smaller γ causes a wider shape of the radial basis function. Fig. 2.7 shows some examples of the radial basis function for different γ values.

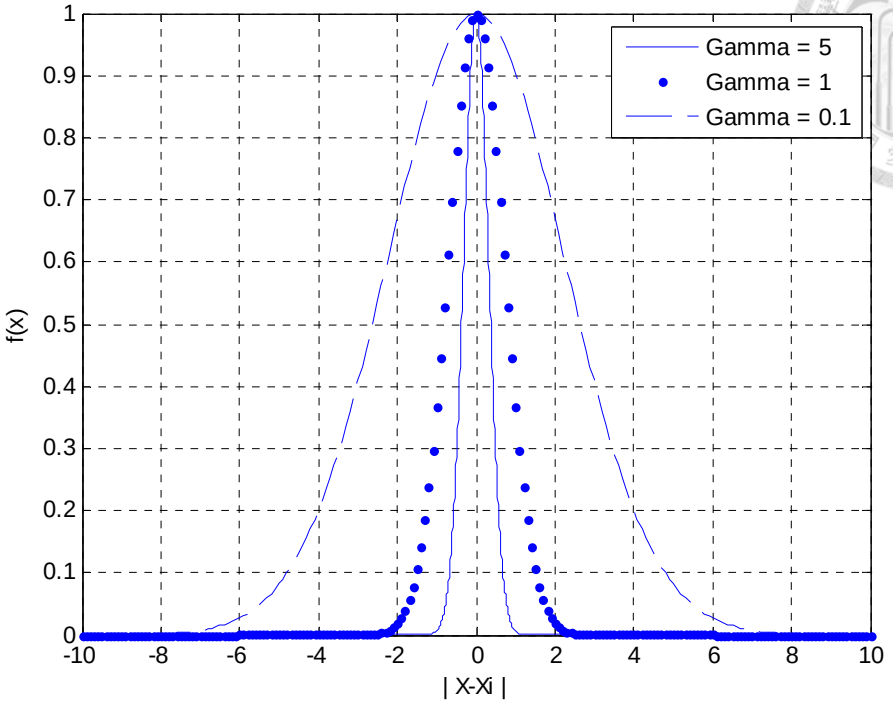

Fig. 2.7 Radial basis function

2.3.1 Parameter Optimization

The SVM model used in this study has two independent parameters (C,γ) to be determined. These parameters are often obtained by a manual trial and error method in literature. And the grid search method is a straightforward and exhaustive method, it is used to calibrate these parameters more effectively and overcome the probable drawback of the manual trial and error method. Hsu *et al* [17] suggested the application of a two-step grid search method. First, a coarser grid search (for example, $C = 2^{-5}, 2^{-3}, \ldots, 2^{11}$; $\gamma = 2^{-5}, 2^{-3}, \ldots, 2^{3}$) are used to determine the best region of grids. Then, a finer grid search (for example, $C = 2^{1}, 2^{1.25}, \ldots, 2^{5}$; $\gamma =$

$2^{-1.5}, 2^{-1.25}, \ldots, 2^{1.5}$) is conducted to find the optimal parameters. The optimization scheme used in this study is based on the above mentioned two-step grid search method.

2.3.2 Cross-validation

As the previous section 2.3.1, the purpose is to identify the best (C,γ) that let the classifier increased accuracy. A common way is to separate database to two parts of which one is considered unknown in testing the classifier. Then the prediction accuracy on this set can more precisely reflect the performance on classifying unknown data. And this procedure is cross-validation.

In *k*-fold cross-validation, we first divide the dataset into *k* subsets of equal size. Sequentially one subset is tested using the classifier trained on the remaining *k*-1 subsets. Thus, each instance of the whole database is predicted once so the cross-validation accuracy is the percentage of data which are correctly classified.

The cross-validation can prevent the overfitting problem. We use Fig. 2.8 which is a binary classification problem to illustrate this issue. Filled circles and triangles are the training data while hollow circles and triangles are the testing data. The testing accuracy the classifier in Fig. 2.8 (a) and (b) is not good since it overfits the training data. If we think training and testing data in Fig. 2.8(a) and (b) as the training and validation sets in cross-validation, the accuracy is not good. On the other hand, classifier in Fig. 2.8(c)

and (d) without overfitting training data gives better cross-validation as well as testing accuracy.

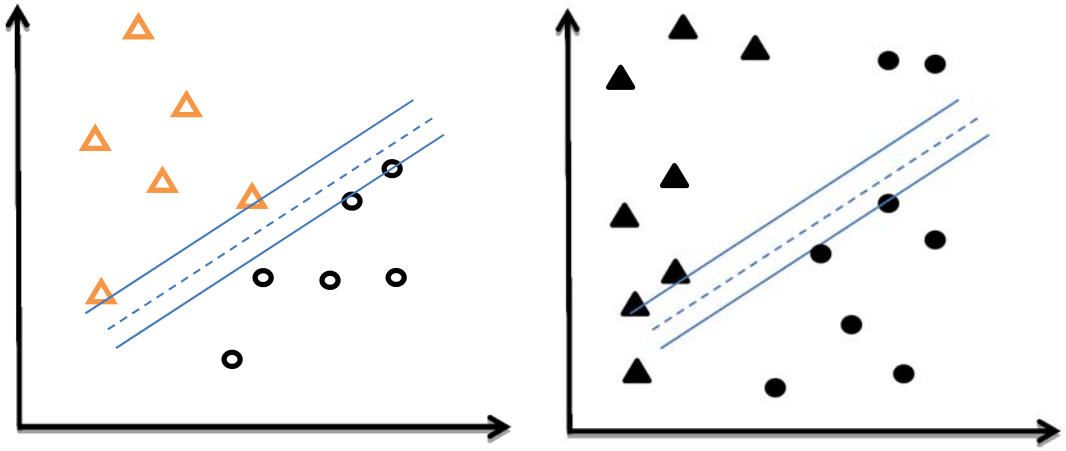

(a) Training data and an overfitting classifier

(b) Appling an overfitting classifier on testing data

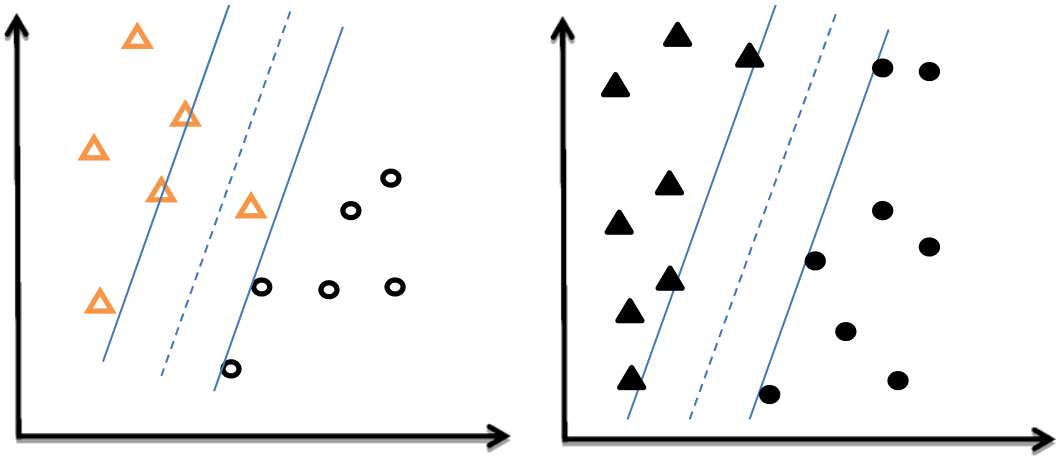

(c) Training data and a better classifier

(d) Appling a better classifier on testing data

Fig. 2.8 An overfitting classifier and a better classifier

(● and ▲: training data; ○ and △: testing data)

Chapter 3 Pressure Signal Processing

3.1 Data Preprocessing

In the experiments, it's difficult to distinguish signals in the complex underwater environments, therefore, signal processing must be done before SVM classification so that the signal can represent useful information. Figure 3.1 illustrates the pressure data measured by the commercial sensors attached on the robot fish.

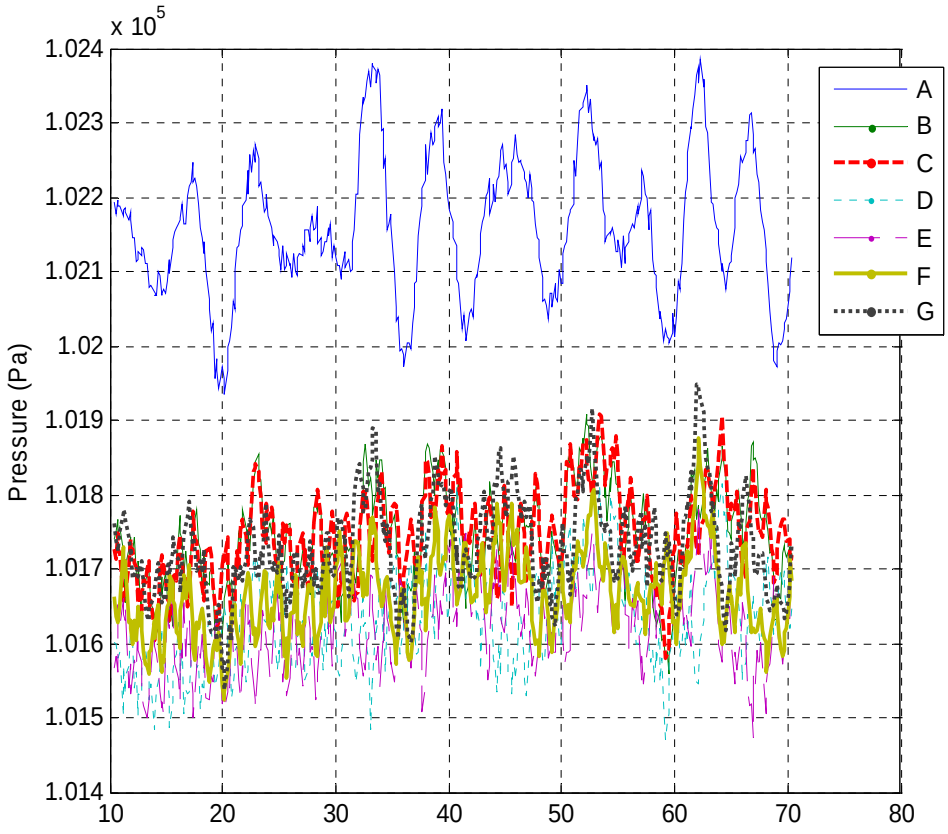

Fig. 3.1 Pressure measured by the commercial sensors attached on the robot fish

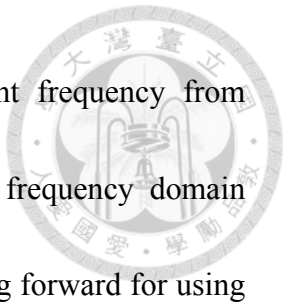

We used a band-pass filter to extract the pressure with different frequency from commercial sensors. Figs. 3.2 3.15 present the filtered data and frequency domain analysis by Fourier Transformation. Since the robot fish tail fin swing forward for using the frequency of 0.76Hz, In Fig. 3.3, Fig. 3.5, Fig. 3.7, Fig. 3.9, Fig. 3.11, Fig. 3.13 and Fig. 3.15, the domain frequency is about 0.76Hz, which is the tail flapping frequency. Besides, the amplitude of the interval between 0~0.3Hz is caused by the change of depth during the fish swimming.

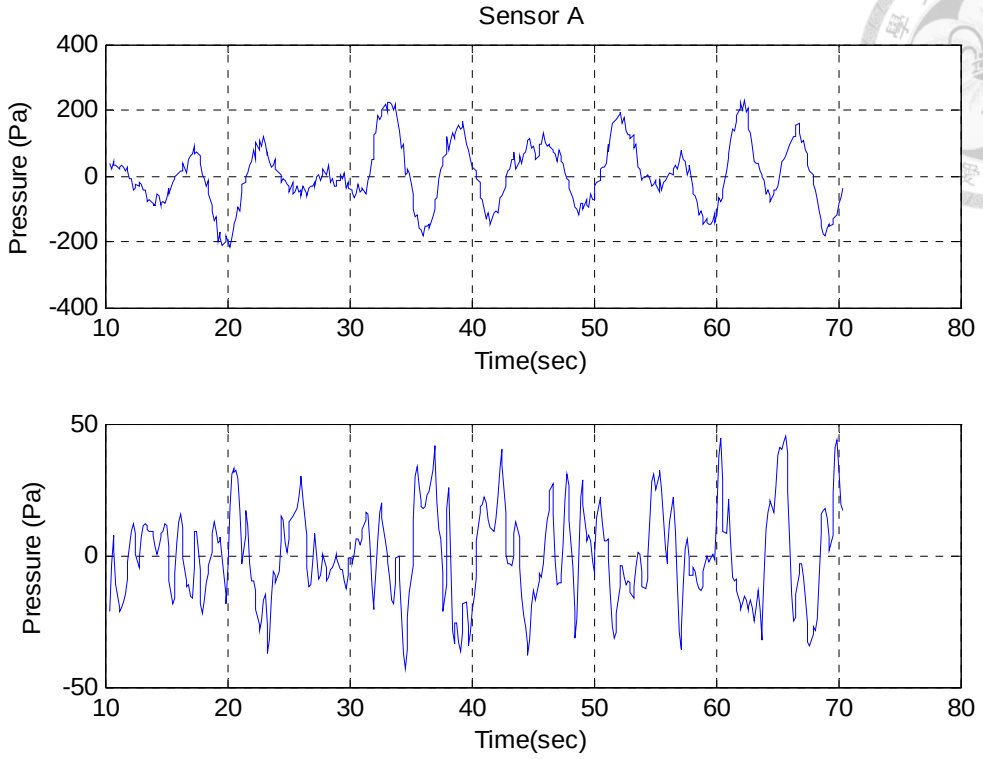

Fig. 3.2 Experimental pressure signal measured from sensor A (upper panel) and the result filtered after a band-pass filter with 0.5~1.2Hz (lower panel)

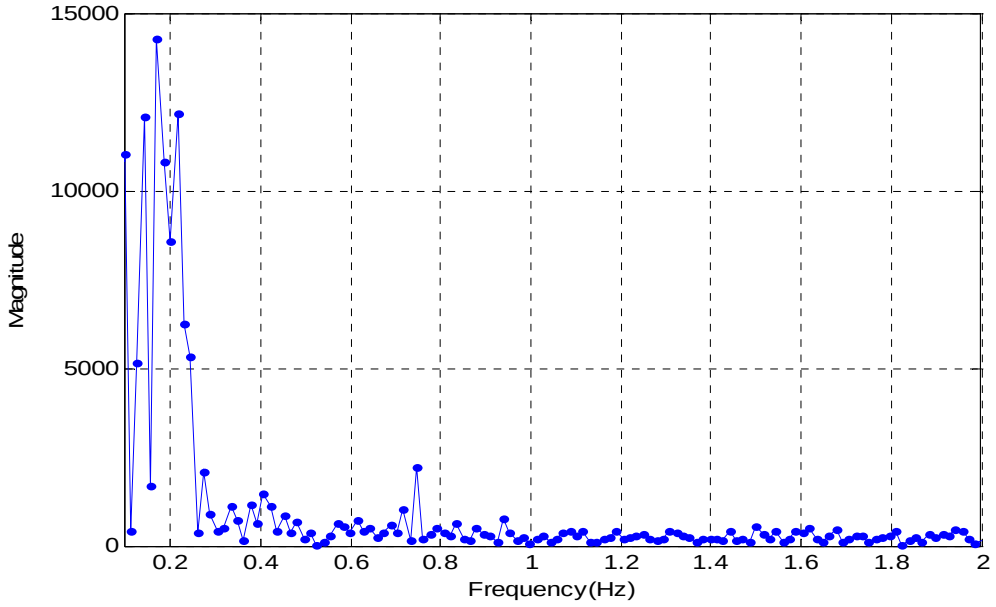

Fig. 3.3 The frequency domain analysis of the experimental pressure signal of sensor A by means of Fourier transformation

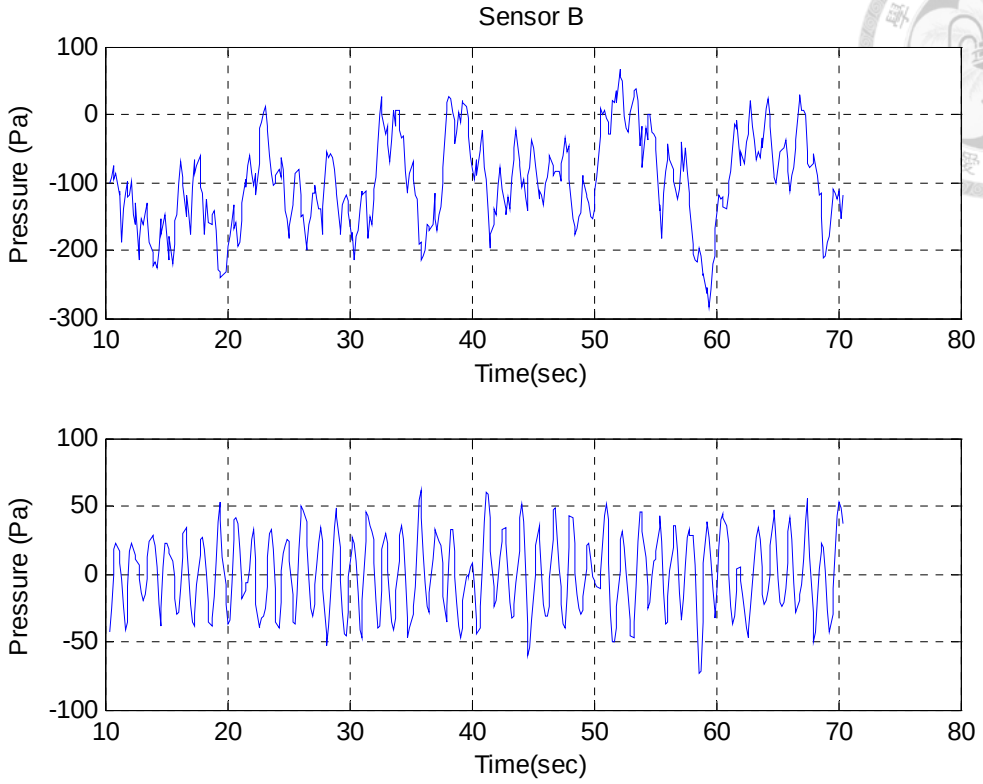

Fig. 3.4 Experimental pressure signal measured from sensor B (upper panel) and the result filtered after a band-pass filter with 0.5~1.2Hz (lower panel)

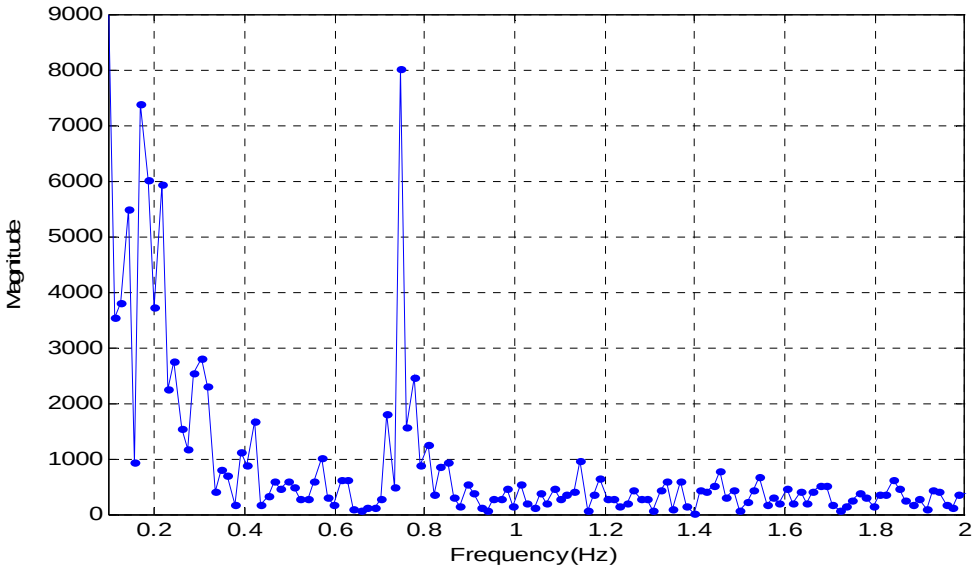

Fig. 3.5 The frequency domain analysis of the experimental pressure signal of sensor B by means of Fourier transformation

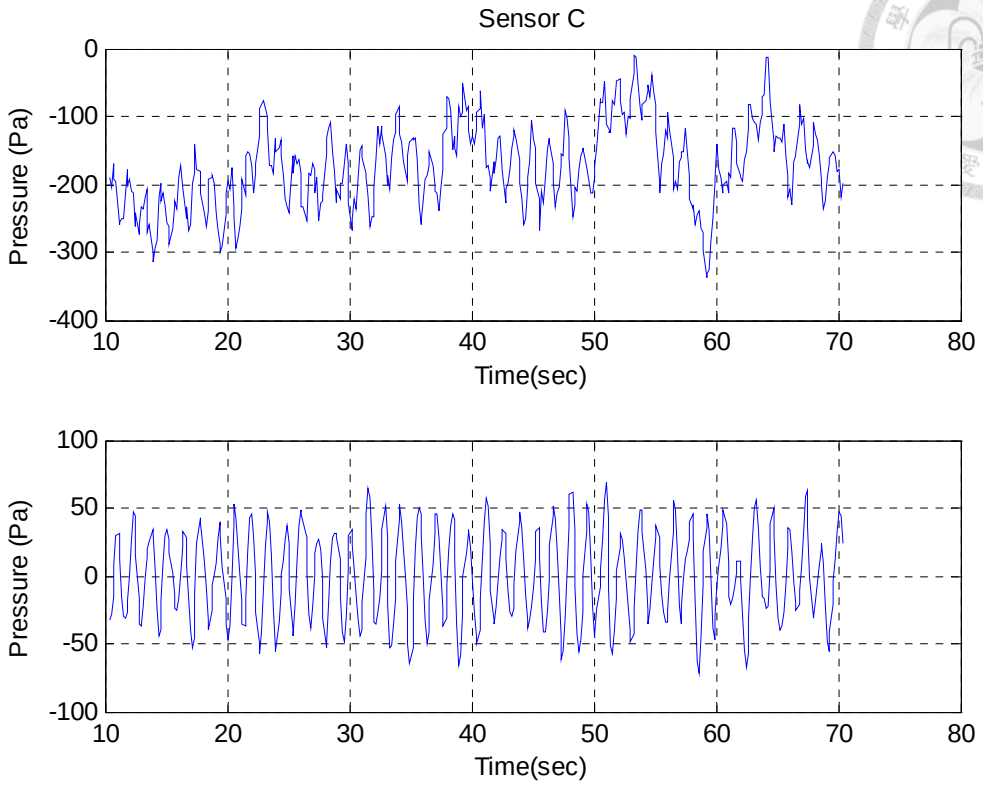

Fig. 3.6 Experimental pressure signal measured from sensor C (upper panel) and the result filtered after a band-pass filter with 0.5~1.2Hz (lower panel)

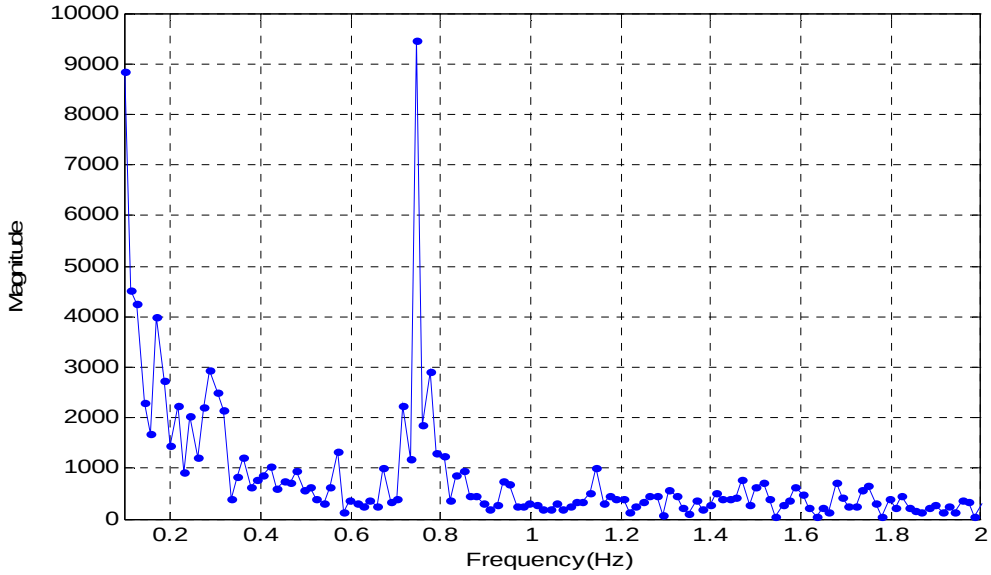

Fig. 3.7 The frequency domain analysis of the experimental pressure signal of sensor C by means of Fourier transformation

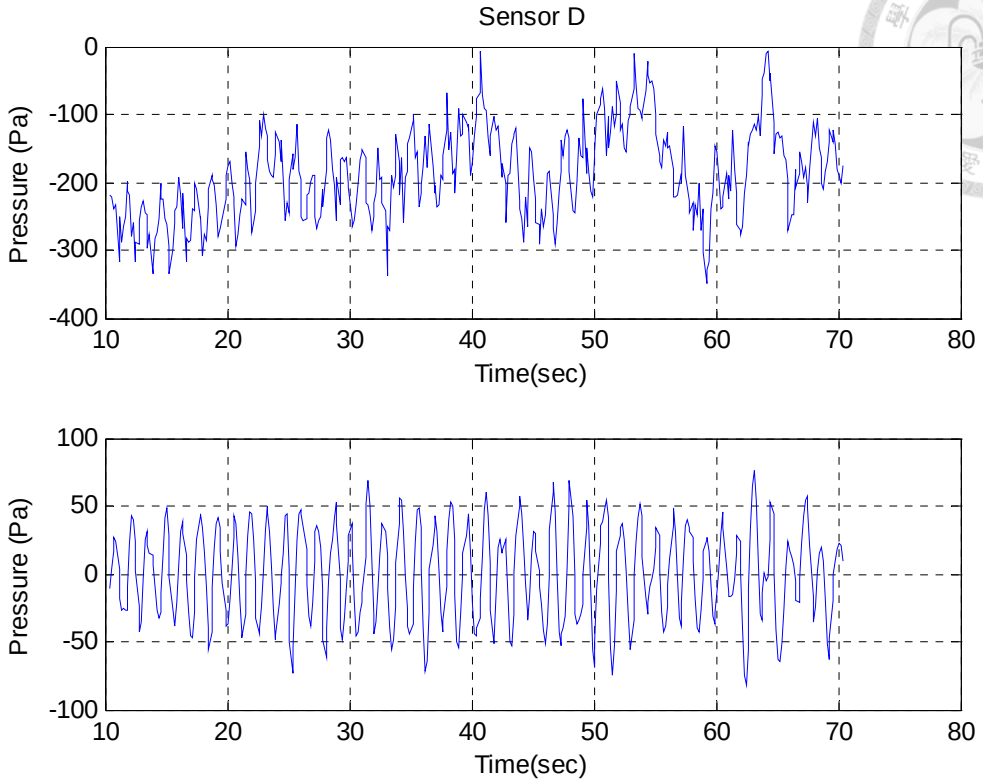

Fig. 3.8 Experimental pressure signal measured from sensor D (upper panel) and the result filtered after a band-pass filter with 0.5~1.2Hz (lower panel)

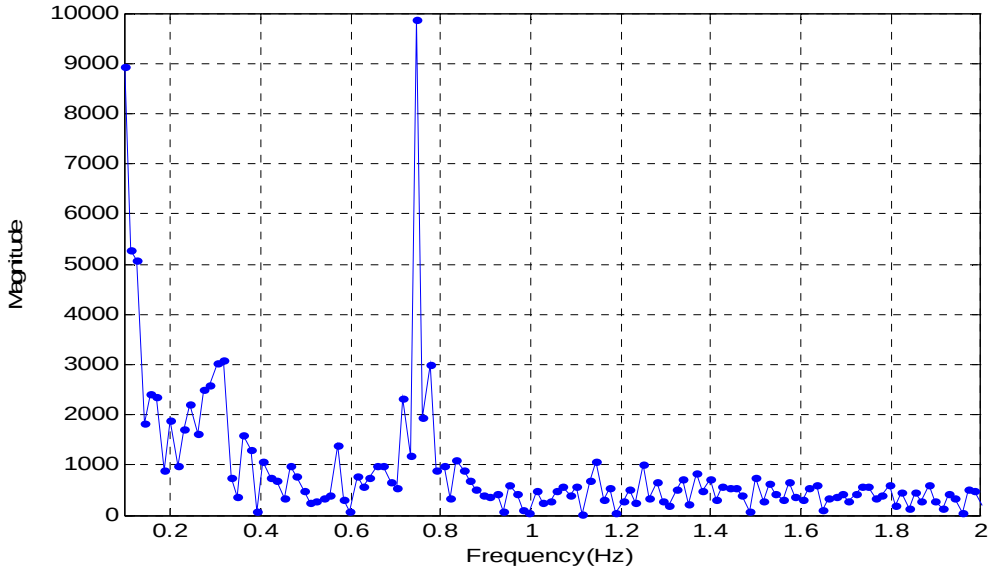

Fig. 3.9 The frequency domain analysis of the experimental pressure signal of sensor D by means of Fourier transformation

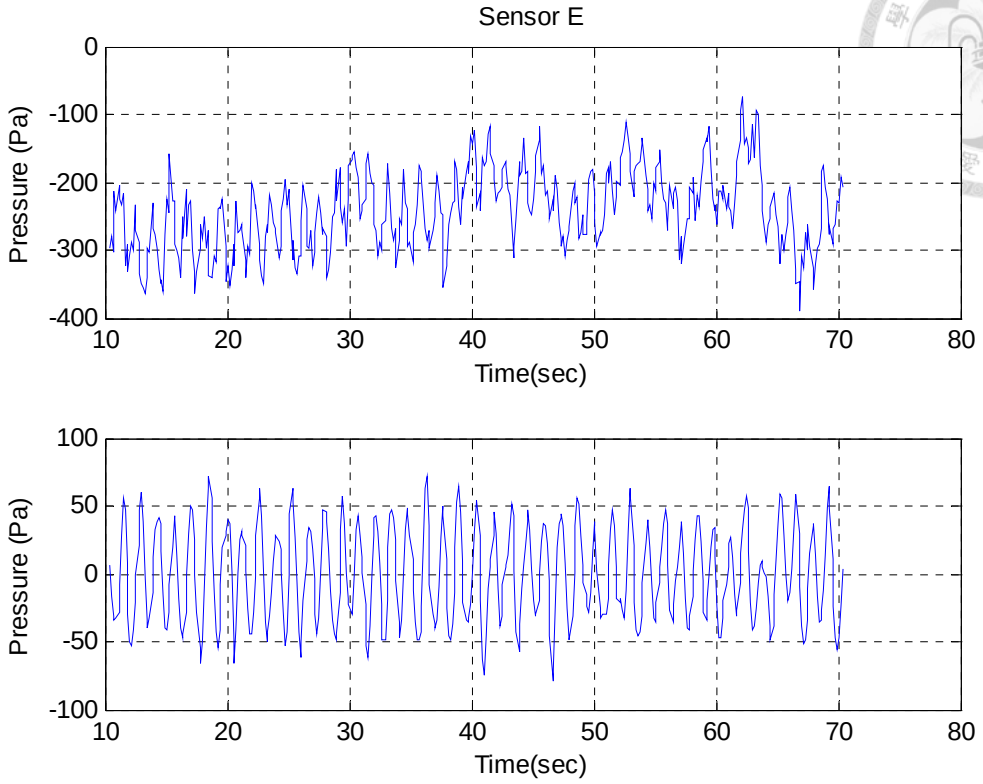

Fig. 3.10 Experimental pressure signal measured from sensor E (upper panel) and the result filtered after a band-pass filter with 0.5~1.2Hz (lower panel)

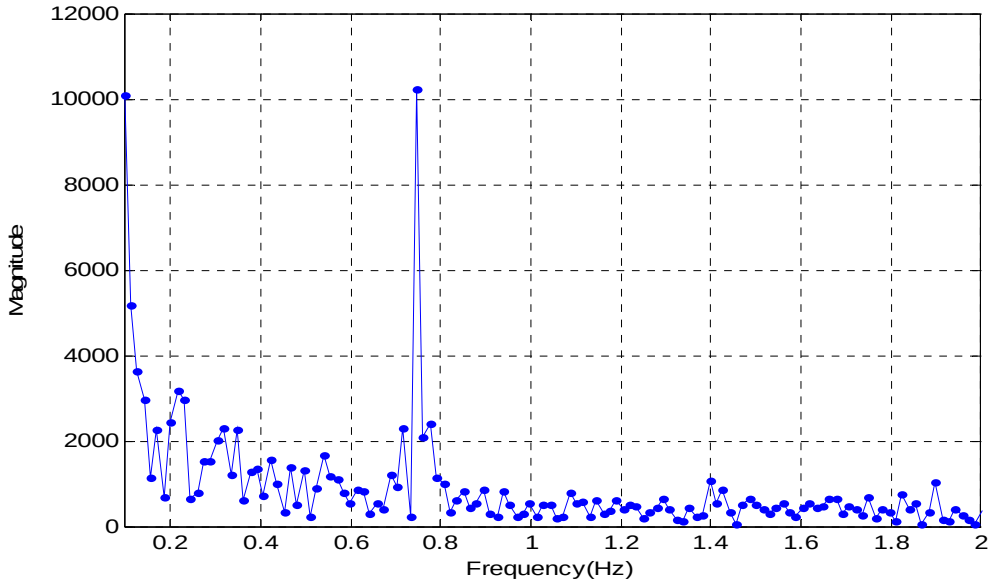

Fig. 3.11 The frequency domain analysis of the experimental pressure signal of sensor E by means of Fourier transformation

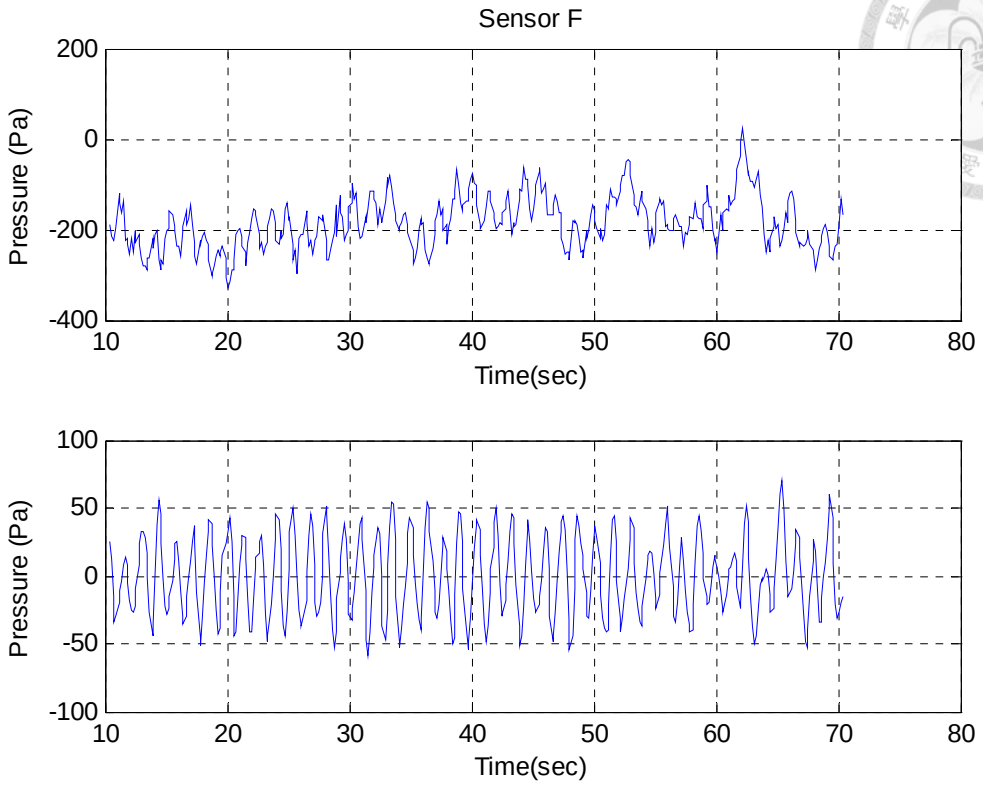

Fig. 3.12 Experimental pressure signal measured from sensor F (upper panel) and the result filtered after a band-pass filter with 0.5~1.2Hz (lower panel)

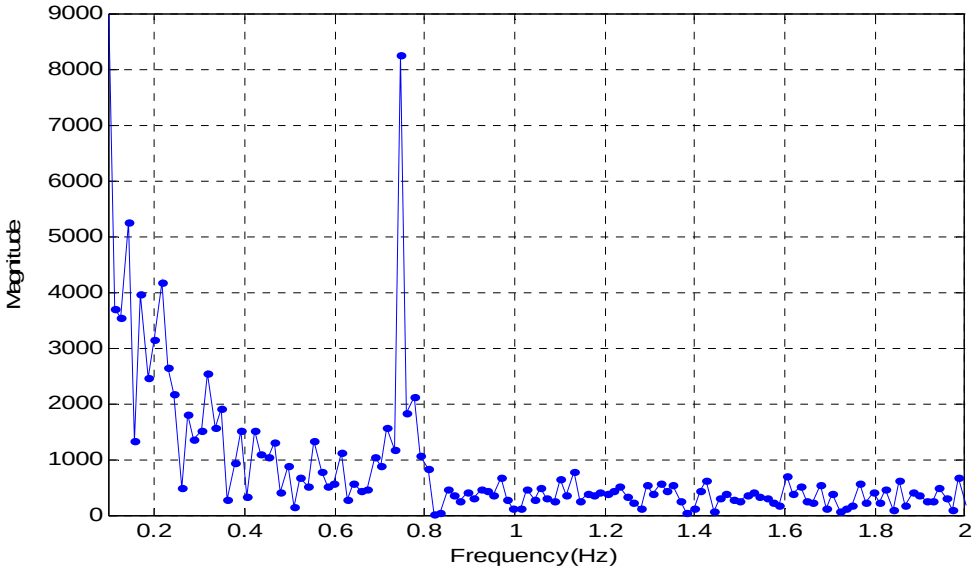

Fig. 3.13 The frequency domain analysis of the experimental pressure signal of sensor F by means of Fourier transformation

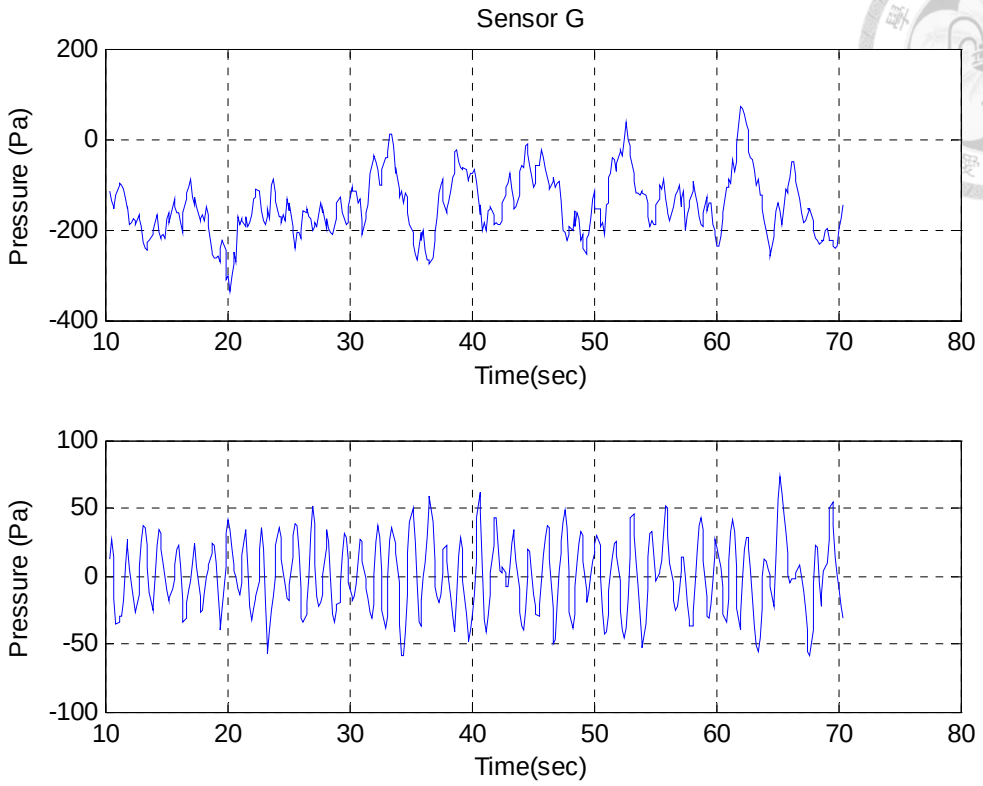

Fig. 3.14 Experimental pressure signal measured from sensor G (upper panel) and the result filtered after a band-pass filter with 0.5~1.2Hz (lower panel)

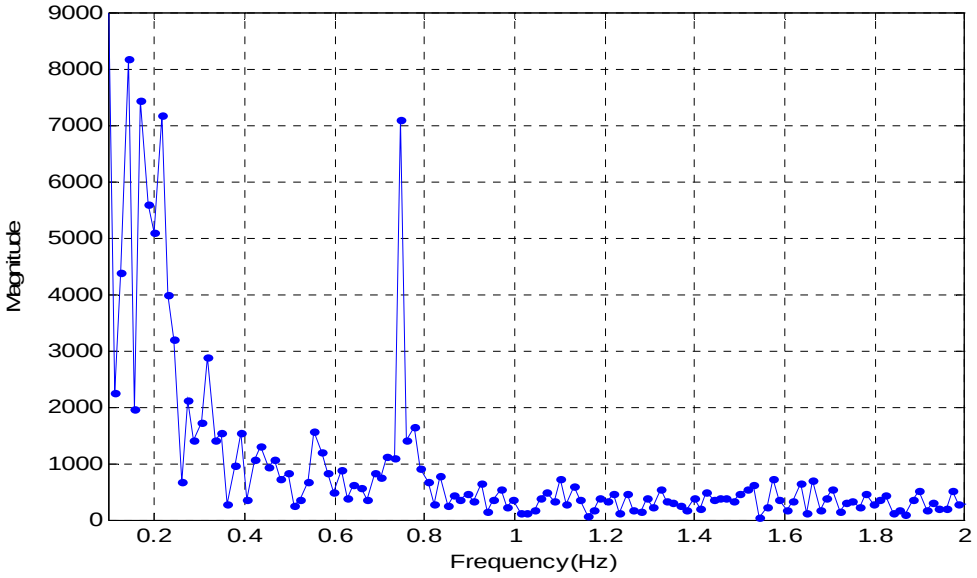

Fig. 3.15 The frequency domain analysis of the experimental pressure signal of sensor G by means of Fourier transformation

As we know, swimming along the wall has different magnitude of hydrodynamic pressure with swimming in the open field, as a result [8] [9], we use root mean square (RMS) value to obtain the magnitude of hydrodynamic pressure. In order to compare the measured pressure along the wall and away the wall, we try to observe the difference RMS values when the BAUV swims in two cases. The RMS values of the filtered pressure signals measured by the sensors are shown in Fig. 3.16, Fig. 3.17, Fig. 3.18 and Fig. 3.19.

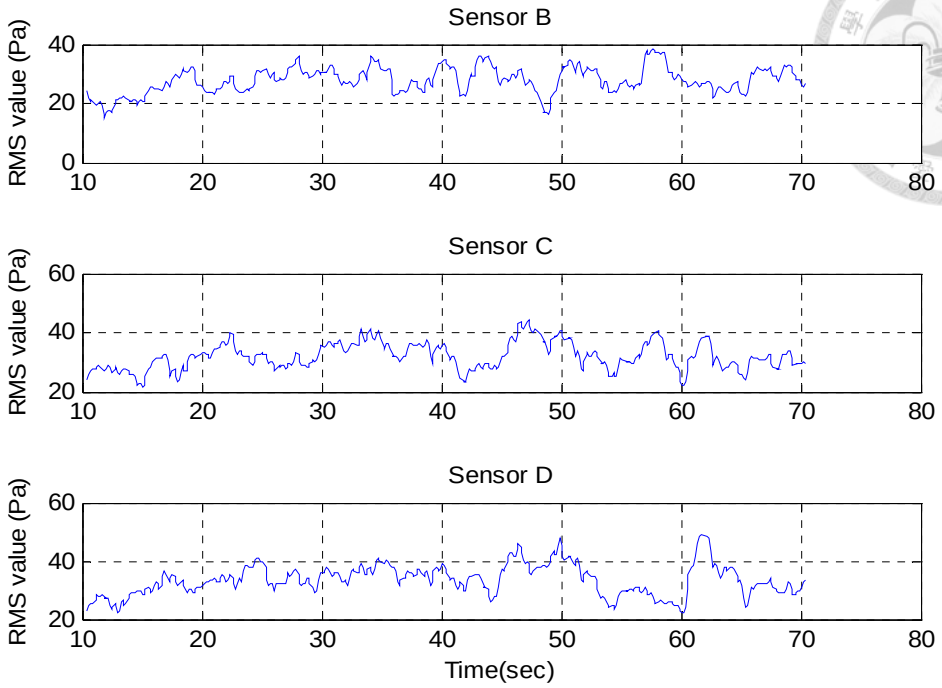

Fig. 3.16 RMS values of the filtered pressure signals measured by the left side sensors while the BAUV swims along the left side wall

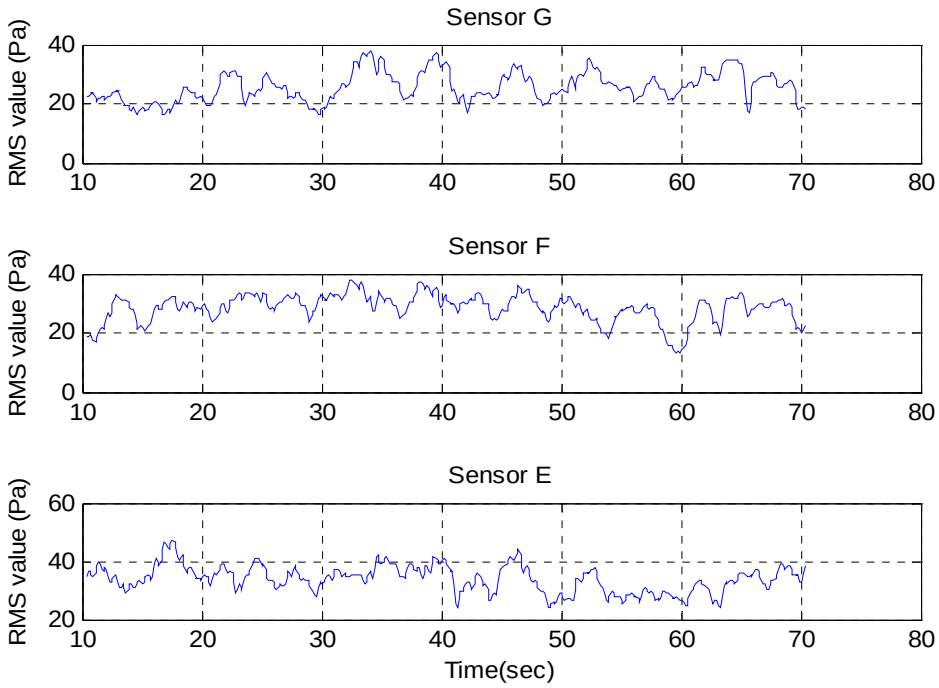

Fig. 3.17 RMS values of the filtered pressure signals measured by the right side sensors while the BAUV swims along the left side wall

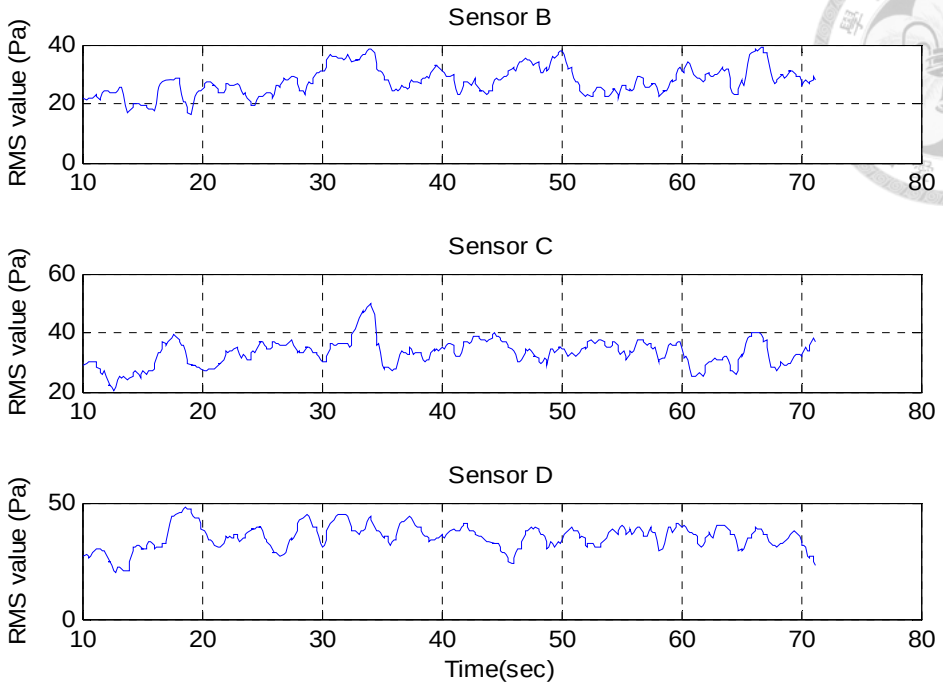

Fig. 3.18 RMS values of the filtered pressure signals measured by the left side sensors while the BAUV swims in open field

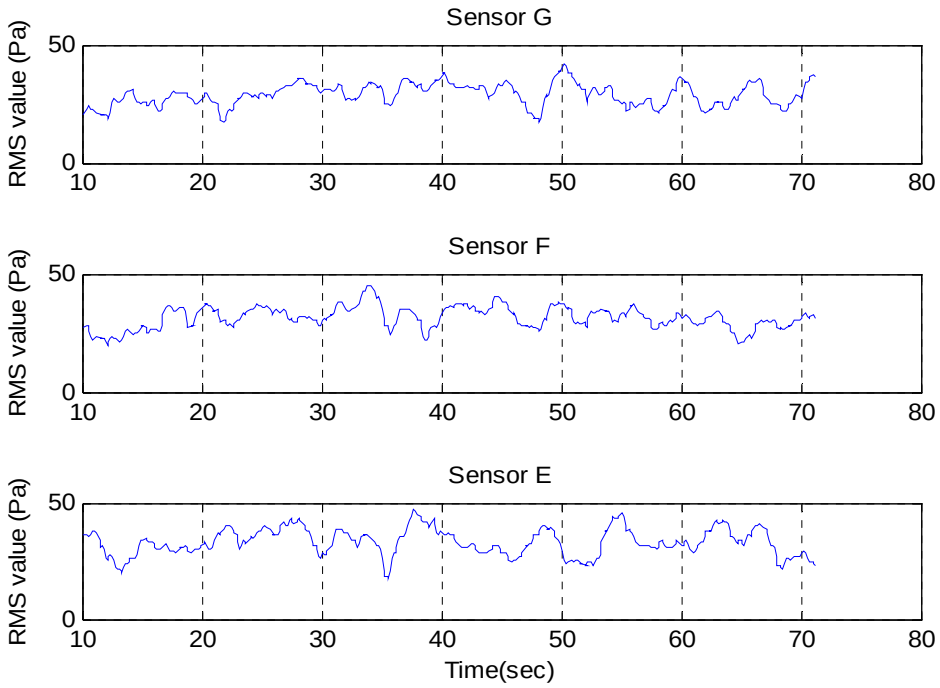

Fig. 3.19 RMS values of the filtered pressure signals measured by the right side sensors while the BAUV swims in open field

Compare the RMS values of hydrodynamic pressure in Fig. 3.16 and Fig. 3.18, it seems the variation increases while the robot fish swims along the wall, one of the possible reasons is due to the wall effect. However, recognition capacity cannot effectively improve if we only compared the differences with the single sensor, so we calculate the ratio and difference of the RMS value of pressure at both side sensors, and they are shown in Fig. 3.20, Fig. 3.21, Fig. 3.22, Fig. 3.23, Fig. 3.24 and Fig. 3.25.

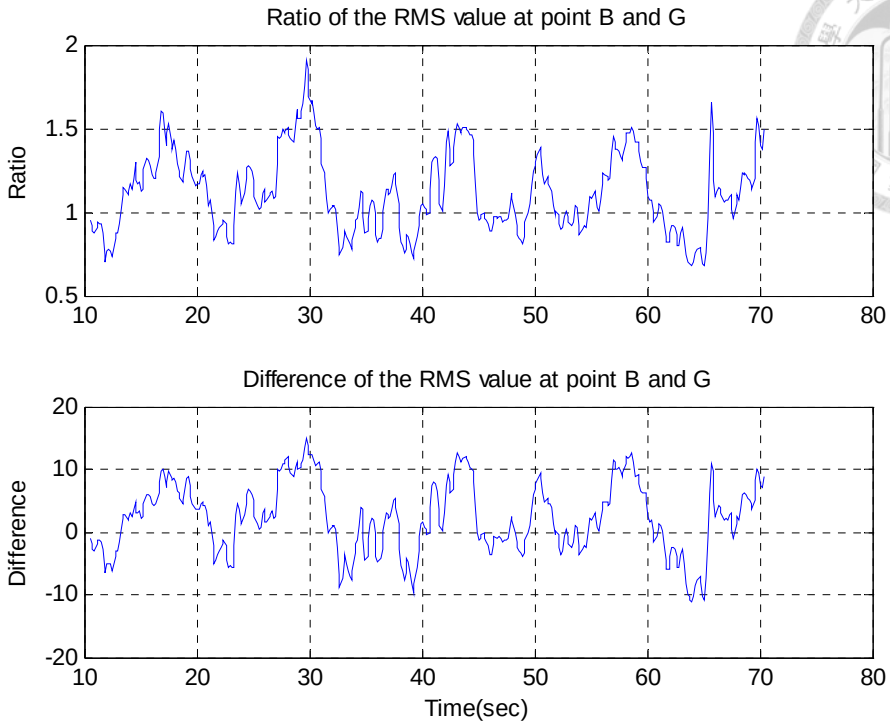

Fig. 3.20 Ratio and difference of the RMS value of pressure at point B and G while the BAUV swims along the wall

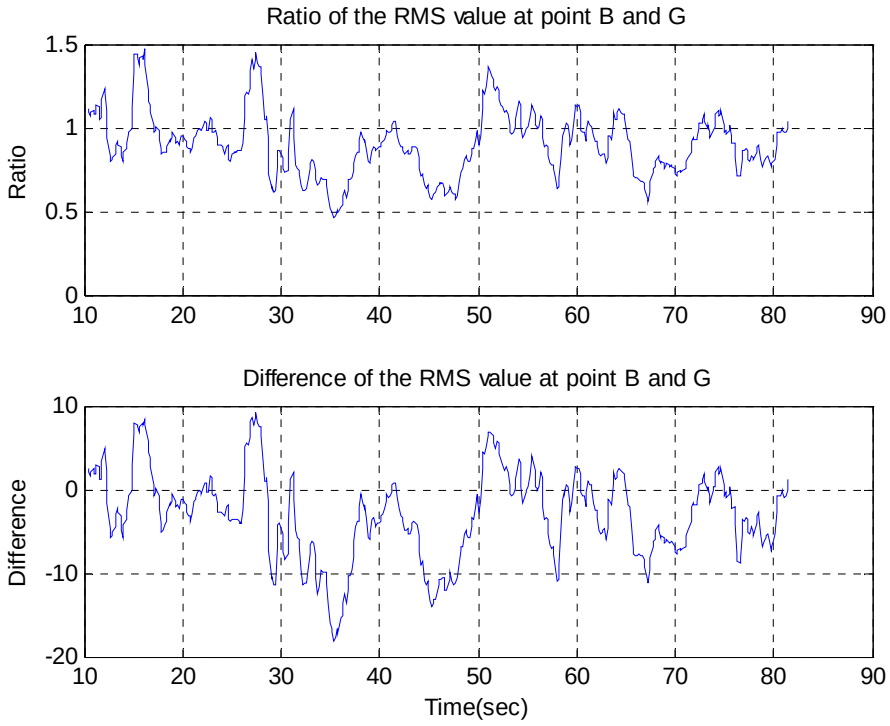

Fig. 3.21 Ratio and difference of the RMS value of pressure at point B and G while the BAUV swims in open field

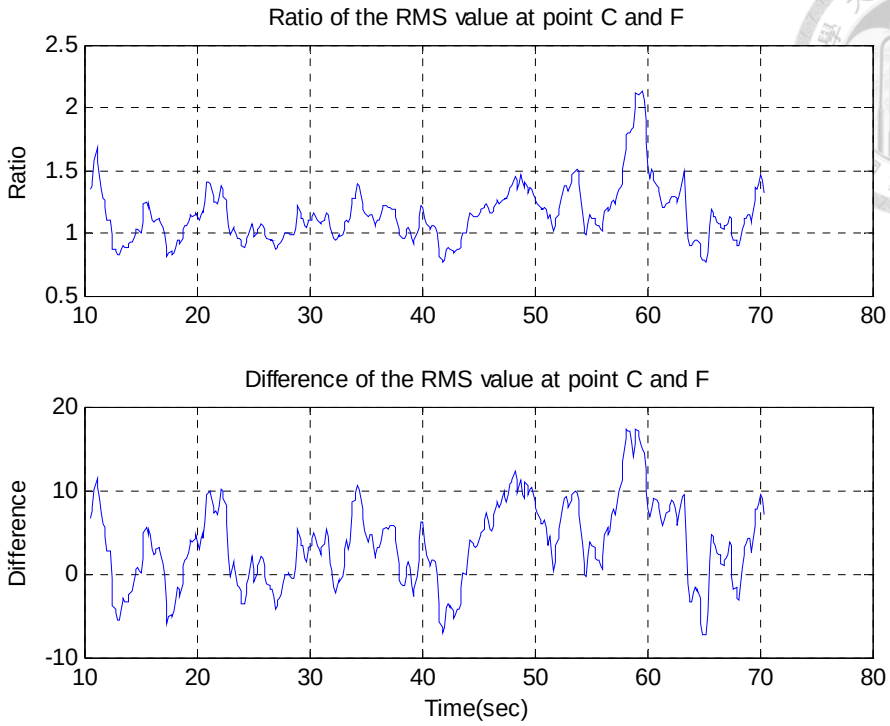

Fig. 3.22 Ratio and difference of the RMS value of pressure at point C and F while the BAUV swims along the wall

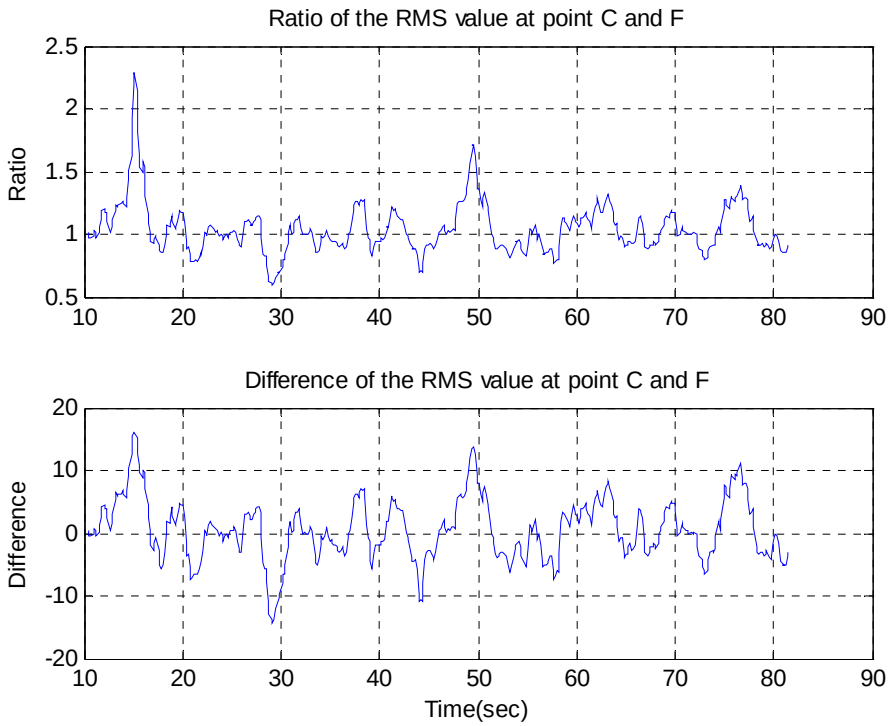

Fig. 3.23 Ratio and difference of the RMS value of pressure at point C and F while the BAUV swims in open field

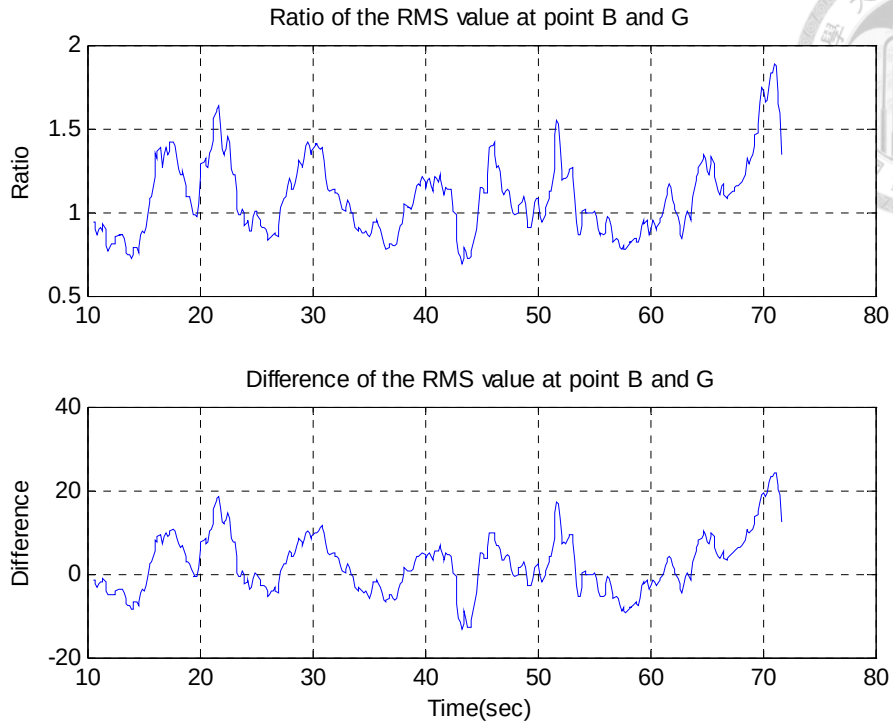

Fig. 3.24 Ratio and difference of the RMS value of pressure at point D and E while the BAUV swims the wall

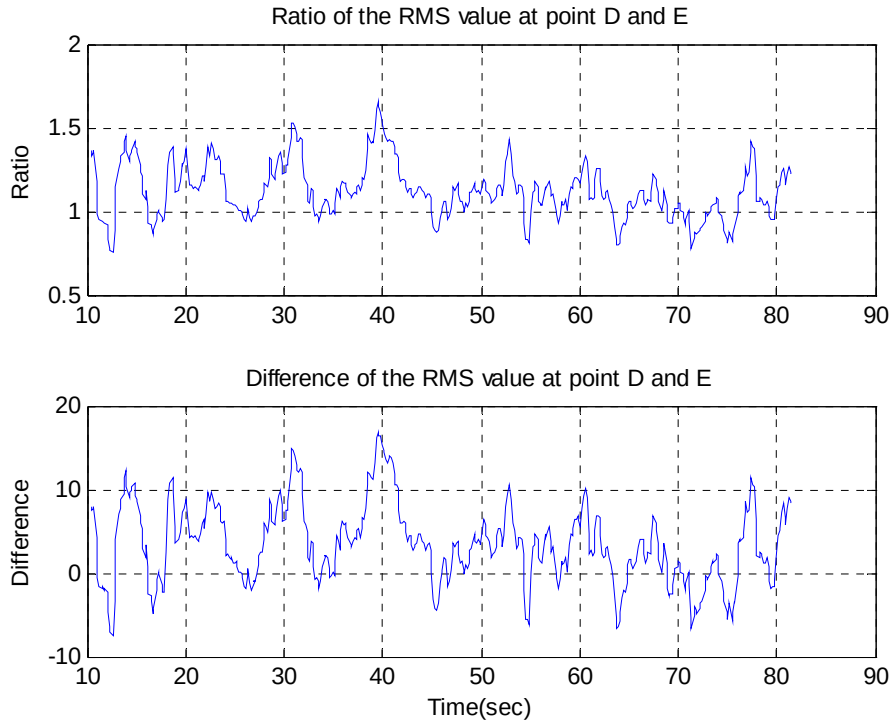

Fig. 3.25 Ratio and difference of the RMS value of pressure at point D and E while the BAUV swims in open field

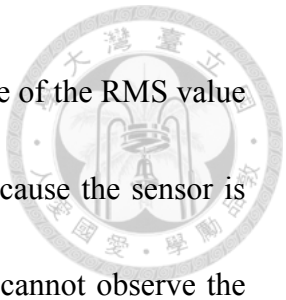

In Figs. 3.20 to 3.25, we can find out that the ratio and difference of the RMS value far away the tail has larger difference between two cases, this is because the sensor is greater impact when the pressure sensor near the tail, that make us cannot observe the effect of the wall.

Above this reason, the sensor A which location is on the head of the BAUV is the farthest away the tail, so it is not affected by the impact of caudal fin swing and also not affected by the two cases (near the wall and in the open field), thus, we made the RMS value of pressure of sensor A as a standard value, and calculated the ratio and difference of the RMS value of pressure between sensor A and each sensors to compare the difference of the two cases, and they are shown in Fig. 3.26, Fig. 3.27, Fig. 3.28, Fig. 3.29, Fig.3.30, Fig. 3.31, Fig. 3.32 and Fig. 3.33.

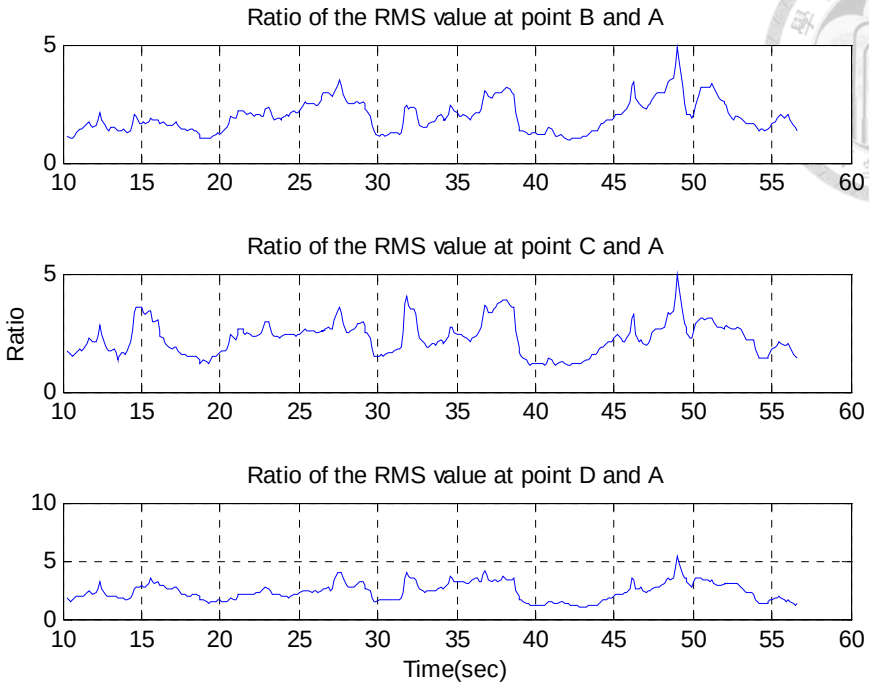

Fig. 3.26 Ratio of the RMS value of pressure between the left side sensors and sensor A while the BAUV swims along the wall

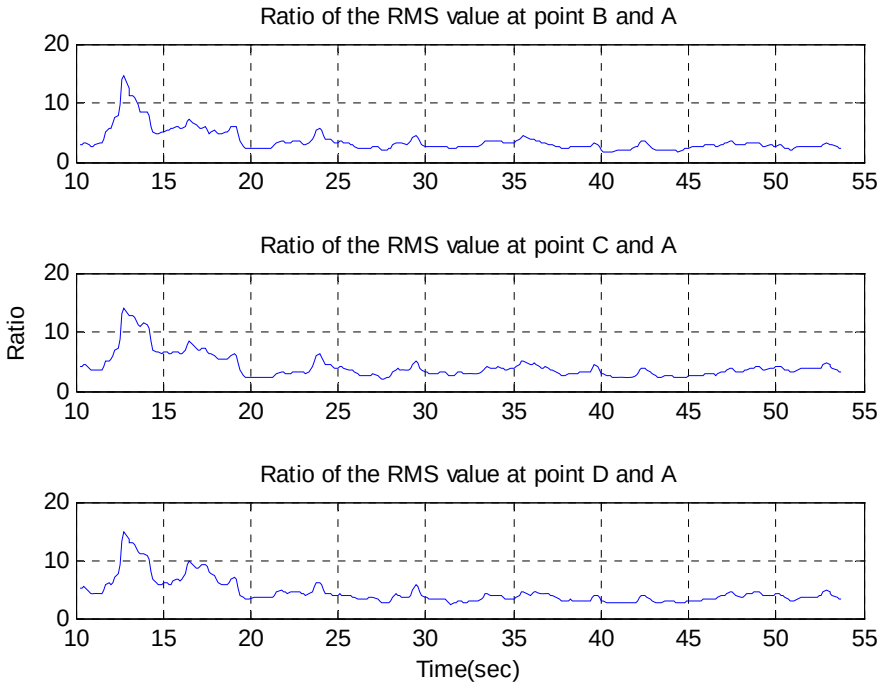

Fig. 3.27 Ratio of the RMS value of pressure between the left side sensors and sensor A while the BAUV swims in open field

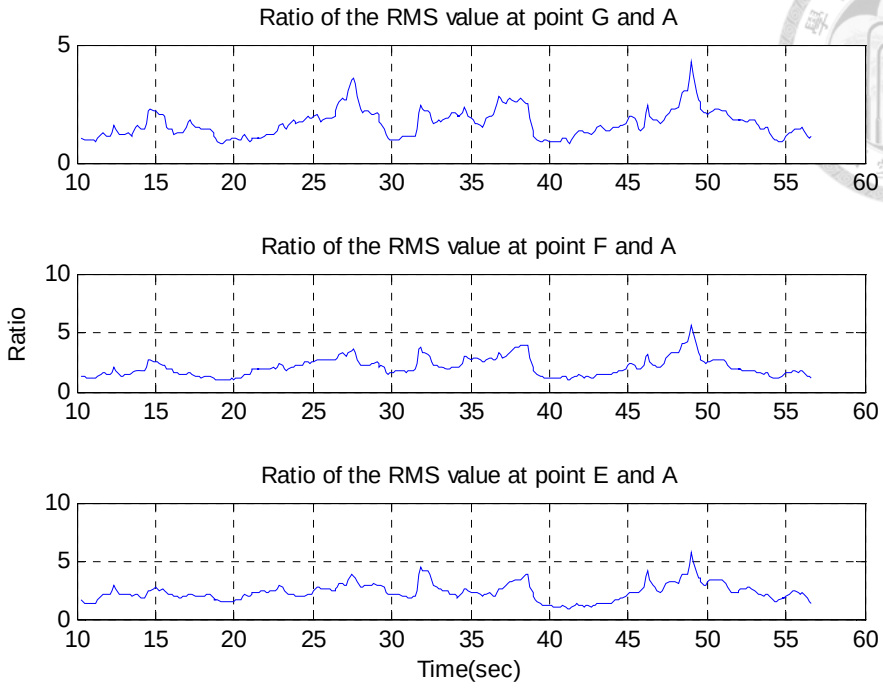

Fig. 3.28 Ratio of the RMS value of pressure between the right side sensors and sensor A while the BAUV swims along the wall

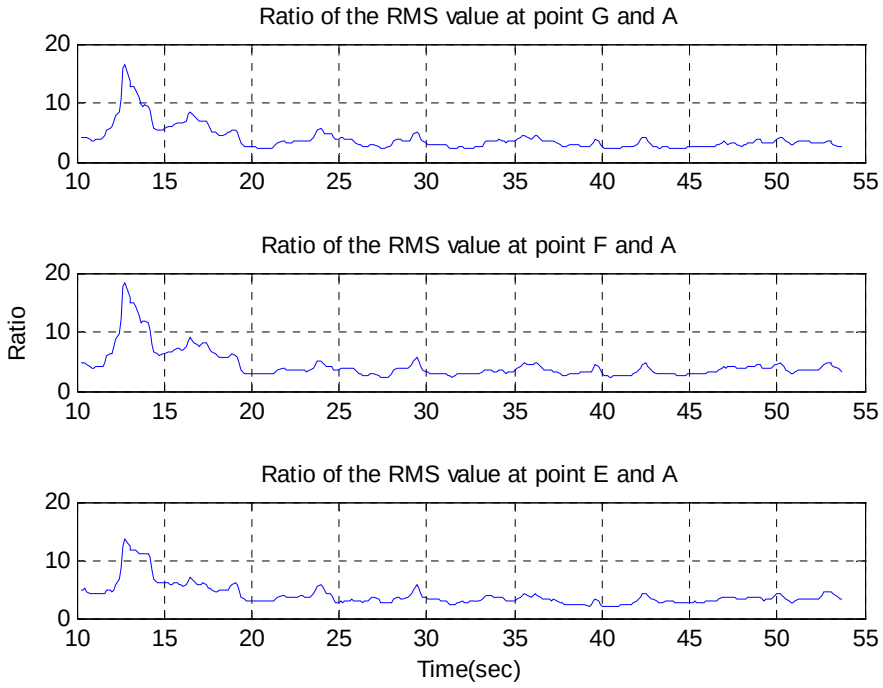

Fig. 3.29 Ratio of the RMS value of pressure between the right side sensors and sensor A while the BAUV swims in open field

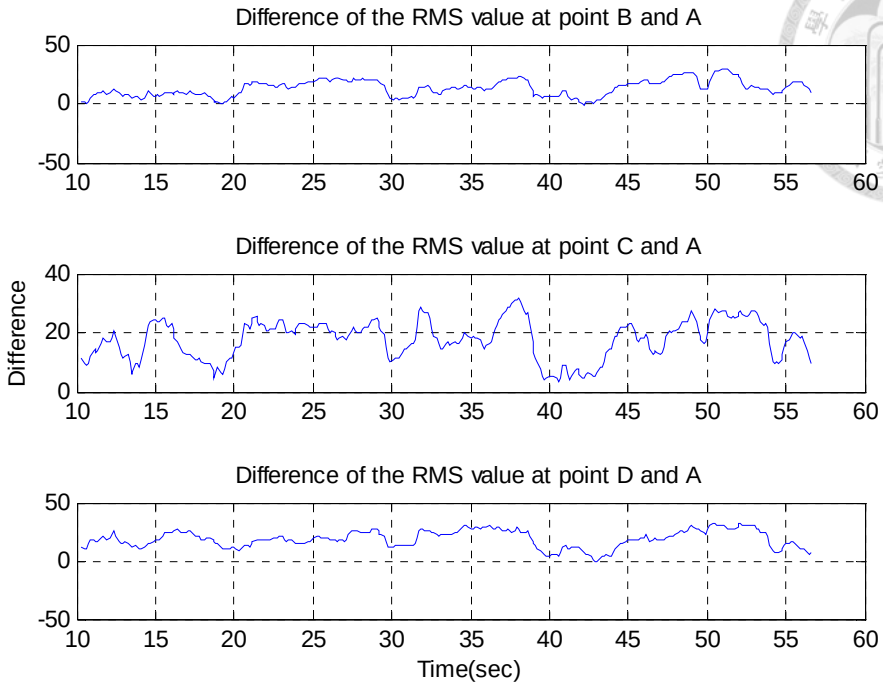

Fig. 3.30 Difference of the RMS value of pressure between the left side sensors and sensor A while the BAUV swims along the wall

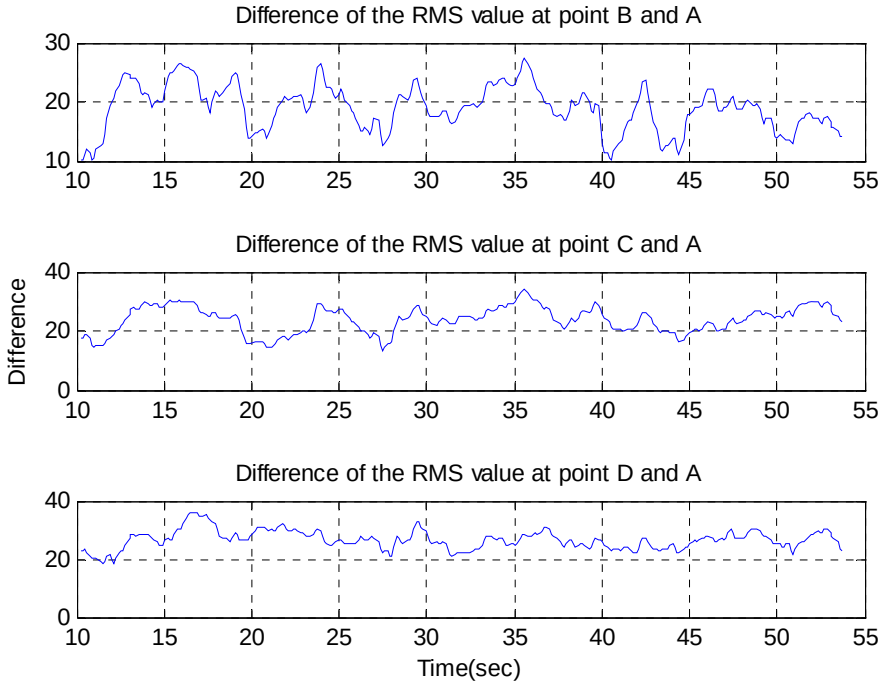

Fig. 3.31 Difference of the RMS value of pressure between the left side sensors and sensor A while the BAUV swims in open field

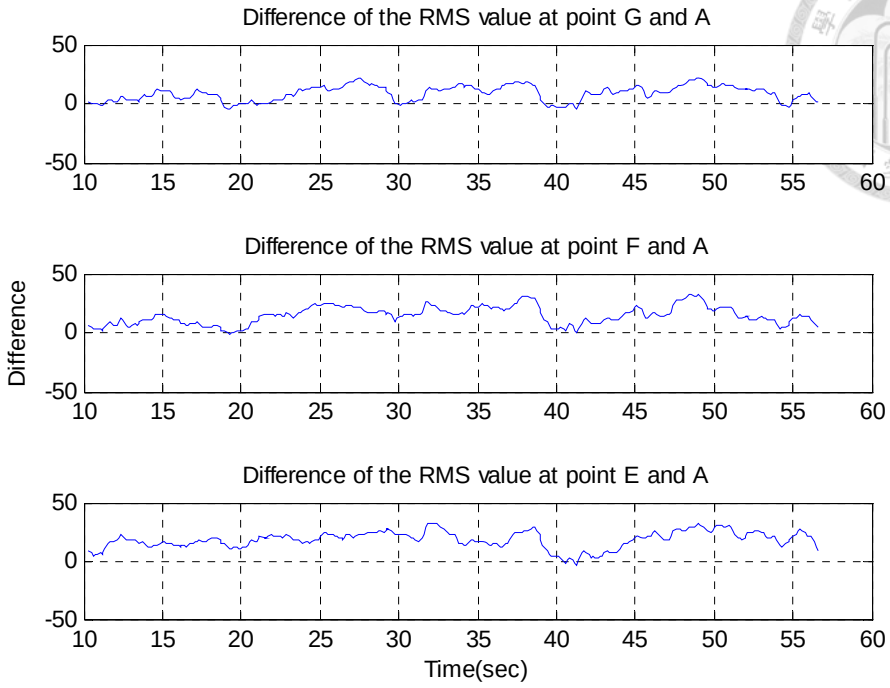

Fig. 3.32 Difference of the RMS value of pressure between the right side sensors and sensor A while the BAUV swims along the wall

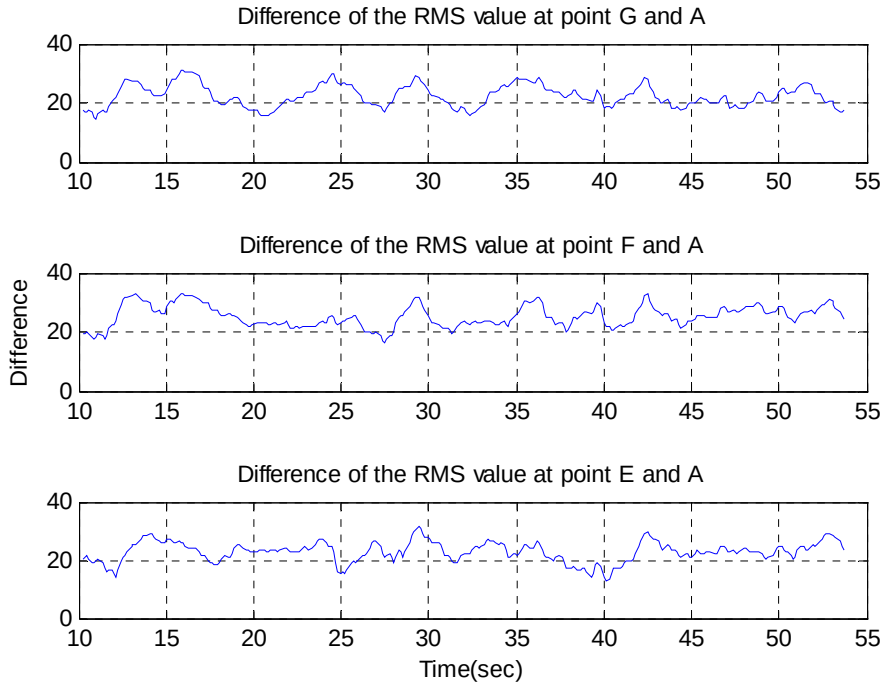

Fig. 3.33 Difference of the RMS value of pressure between the right side sensors and sensor A while the BAUV swims in open field

3.2 Feature Extraction

The purpose of feature extraction is to effectively describe the pressure signals in different cases, a representative feature not only can reproduce signals significance but also increase the efficiency and accuracy of the classification system. Feature extraction can provide the abilities of event detection and classification for the classification system, therefore, it is an important step in recognition system design.

In this study, we try to find out useful information to represent our cases, therefore, according to Figs. 3.16 to 3.19, the RMS values of the filtered pressure measured may be able to provide an effective information, so we chose all sensors as our seven features. And in Figs. 3.20 to 3.33, the ratio and difference of the RMS value of pressure between the sensors are also able to make us to increase the accuracy of classification.

It is shown that the extracted diverse features are different from each other, therefore, we decided that they can serve as useful parameters in classifying the underwater pressure signals.

3.3 Feature Selection

The extracted feature vectors described in section 3.2, before fed the feature vectors into support vector machine classifier, we used a feature selection method. The purpose of feature selection is to select the best features of some of the characteristics can make recognizable to achieve the best. These features which have better recognition ability not only simplify the classifier machine of the calculation but also help us understand the issue of causation in this category.

The feature selection help us to find out the important dimension from extracted features in two-class classification, however, the dimensions of feature vectors used in two-class classification are not like the common signal recognition algorithms. We defined a simple equation to evaluate the importance $I(a, \beta, k)$ of a specific feature dimension k, $1 \leq k \leq x$ for a hyperplane $\boldsymbol{\Omega}_{a,\beta}$ corresponding class a and class β.

$$I(a, \beta, k) = \frac{(\mu_{a,k} - \mu_{\beta,k})^2}{\sigma_{a,k}^2 - \sigma_{\beta,k}^2} \tag{3.1}$$

Where the $\mu_{a,k}$ denotes the mean value of the feature dimension k for all training samples in class a, and the $\sigma_{a,k}$ denotes the standard deviation of the feature dimension k for all training samples in class a.

Equation (3.35) aims at evaluating differentiation capability between the two

classes as well as the stability in the same class for a given feature dimension k, each dimension of extracted features is needed to be calculated first for hyperplane of SVM classifier. It is more important feature when $I(a,b,k)$ values are larger. Finally, we chose the first 10 dimensions as the input feature vectors of SVM classifier. Fig. 3.34 illustrates the process of feature selection.

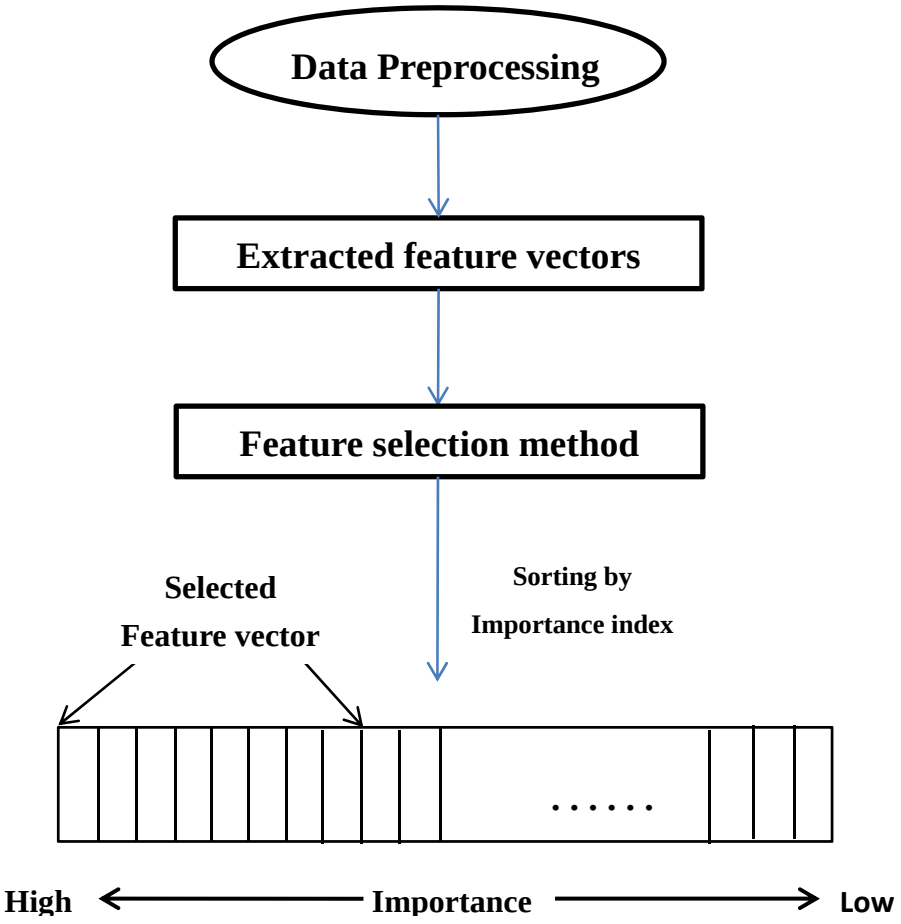

Fig. 3.34 Process of feature selection

Chapter 4 Experiments

In our all experiments, we control the amplitude and the frequency of the caudal fin, tail beating frequency was selected about 0.7 to 0.8 Hz. The BAUV was programmed to swim forward straightly by controlling the flapping tail to maintain the BAUV stably swam.

The lateral line system will record the surrounding pressures while the BAUV is swimming. We set up two main cases, the first case is letting the BAUV swims in the open field, and the second case is swimming along the wall, in both cases, we use the measured values as the training data.

4.1 Hardware of the BAUV

4.1.1 Biomimetic Autonomous Underwater Vehicle

The BAUV was used as a tested for our experiment, its body 90cm length, 25cm width and 50cm high. Taking into account both the appearance and performance of the robot fish required, the BAUV divided the 45cm length rigid head and 45cm length flexible tail in two segments, about the tail section, the motor was used to drive two steel wires to swing the whole tail, and an elastic mechanism on the tail makes the BAUV swim more like a real fish. The mechanism of the tail is shown in Fig. 4.1(a).

And the tail of BAUV was covered with a rubber flexible material on its outside and it is shown in Fig. 4.1(b).

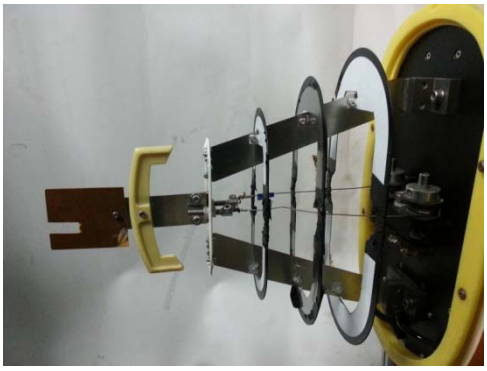

(a) The mechanism of the tail

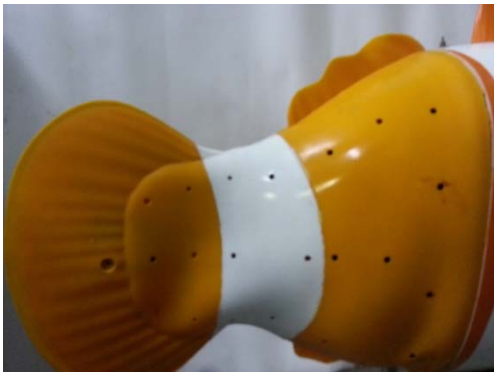

(b) Rubber material on its outside

Fig. 4.1 The tail of the BAUV

In addition, the rigid head part was composed by waterproof container, a buoyancy engine, a compass and one pair of cameras. Both of the robot's computer and motor controller were set up in the waterproof container. The internal view of the BAUV is shown in Fig. 4.2 (a). Furthermore, the BAUV body was covered with a plastic material, and it is shown in Fig. 4.2 (b).

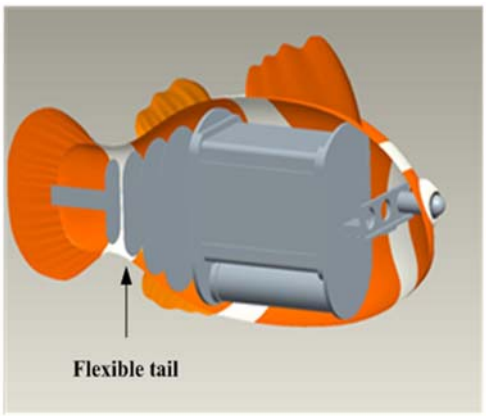

(a) Internal view of the BAUV

(b) Plastic material on its outside

Fig. 4.2 The body of the BAUV

4.1.2 Pressure Sensors

The lateral line system has the ability to sense minor variation of the ambient field, it is indispensable sensory organs for fish. In this study, we chose commercial pressure sensors MS5803-01BA to mimic the fish lateral line. It is optimized for underwater measurement systems with pressure resolution, it module includes a high linear pressure sensor and an ultra-low power 24 bit ΔΣ ADC with internal factory calibrated coefficients. It provides a precise digital 24 Bit pressure and temperature value and different operation modes that allow the user to optimize for conversion speed and current consumption. The MS5803-01BA operating range is 1000 to 1300000 pa and -40 to +85 °C, its size are 0.5 cm diameter. This new sensor module generation is based

on leading MEMS technology and latest benefits from MEAS proven experience and know-how in high volume manufacturing of altimeter modules, which have been widely used for over a decade. The sensing principle employed leads to very low hysteresis and high stability of both pressure and temperature signal.

Since commercial pressure sensors MS5803-01BA with high resolution, its resolution of 1.2 Pa, the pressure sensors were used in the BAUV experiments as shown in Fig. 4.3. Fig. 4.4 displays the position of the sensors installed on the BAUV. There are three sensors on left side starting from the sensor closest to the head were sensor B, sensor C and sensor D, three sensors on right side starting from the sensor closest to the tail were sensor E, sensor F, sensor G and a sensor A on the head.

Fig. 4.3 MS5803-01BA commercial pressure sensors

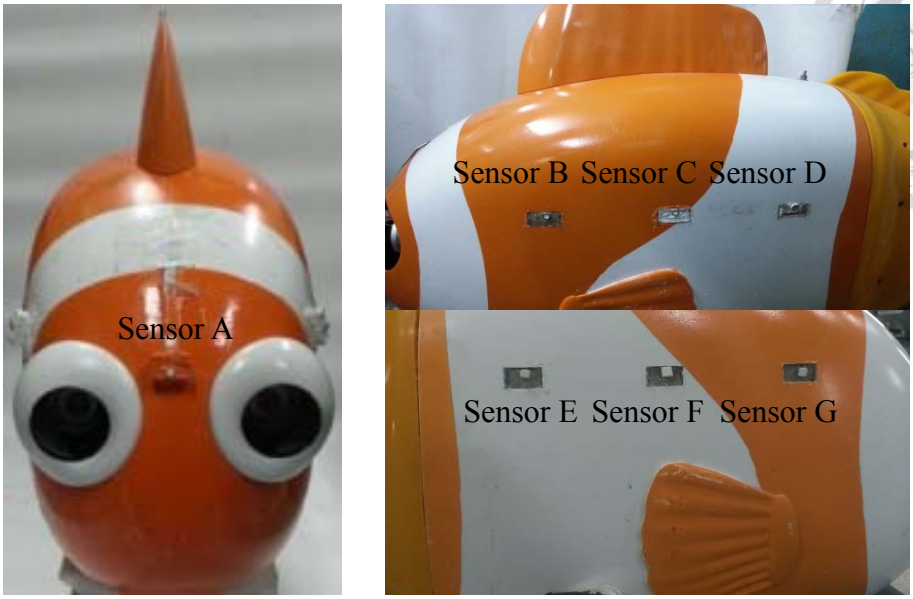

Fig. 4.4 Position of sensors attached on the BAUV

4.2 Experimental Setup

In order to compare the difference of pressure measured by sensors between the BAUV swimming along the wall and in the open field, the BAUV is programed to swim along the wall, the distance between the pressure sensors on the surface of the BAUV and the wall is about 10~30 cm, since the robot fish is very small compared to the solid wall in water tank, the pressure sensor in order to sense the wall must be as close as possible. The BAUV swims in the open field, the distance between the pressure sensors on the surface of the BAUV and the wall is about 50 cm above. Besides, the pressure sensors will be below the water level about 40cm.

The experiment is designed to test the classification capability of the SVM, the

experiments were performed in the water tank belongs to the department of Engineering Science and Ocean Engineering, National Taiwan University, and it is shown in Fig. 4.5 and Fig. 4.6.

Fig. 4.5 Water tank

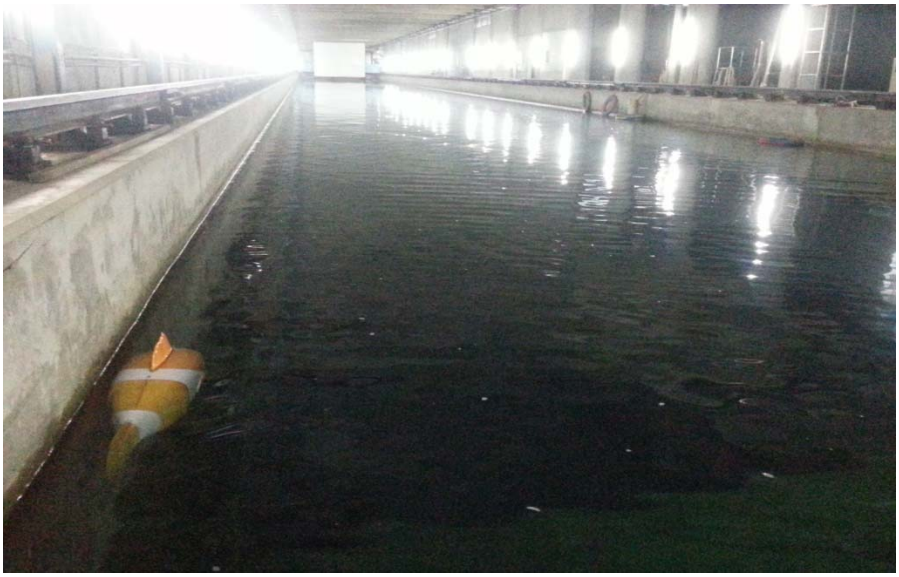

Fig. 4.6 The BAUV swims along the wall

4.3 Experimental Results

In order to test the quality of our training results, we did two experiments (near the wall and in an open field) to comparison the training results. Besides, a representative feature is very important to our classification system, so in this study, we propose the useful feature vectors to represent our case, and the extracted feature vectors described in section 3.2 and 3.3, we have totally 25 dimensions, we also used the importance $I(a, \beta, k)$ to sort feature vectors from extracted feature vectors, the importance value are established in Table 1, and the features of the experimental result are shown in Fig. 4.7 to Fig. 4.22.

Table 1 Index of extracted feature vectors

	Features	Importance
1	RMS values of pressure by A sensor	0.391
2	RMS values of pressure by B sensor	0.031
3	RMS values of pressure by C sensor	0.0042
4	RMS values of pressure by D sensor	0.0312
5	RMS values of pressure by E sensor	0.0464
6	RMS values of pressure by F sensor	0.3997

7	RMS values of pressure by G sensor	0.35
8	Ratio of the RMS value of pressure at point B and G	0.19
9	Ratio of the RMS value of pressure at point C and F	0.3636
10	Ratio of the RMS value of pressure at point D and E	0.0001
11	Difference of the RMS value of pressure at point B and G	0.182
12	Difference of the RMS value of pressure at point C and F	0.5
13	Difference of the RMS value of pressure at point D and E	0.0006
14	Ratio of the RMS value of pressure at point B and A	0.73
15	Ratio of the RMS value of pressure at point C and A	0.661
16	Ratio of the RMS value of pressure at point D and A	0.53
17	Ratio of the RMS value of pressure at point E and A	0.357
18	Ratio of the RMS value of pressure at point F and A	0.89
19	Ratio of the RMS value of pressure at point G and A	1.017
20	Difference of the RMS value of pressure at point B and A	0.771
21	Difference of the RMS value of pressure at point C and A	0.567
22	Difference of the RMS value of pressure at point D and A	0.265
23	Difference of the RMS value of pressure at point E and A	0.266
24	Difference of the RMS value of pressure at point F and A	1.26
25	Difference of the RMS value of pressure at point G and A	1.63

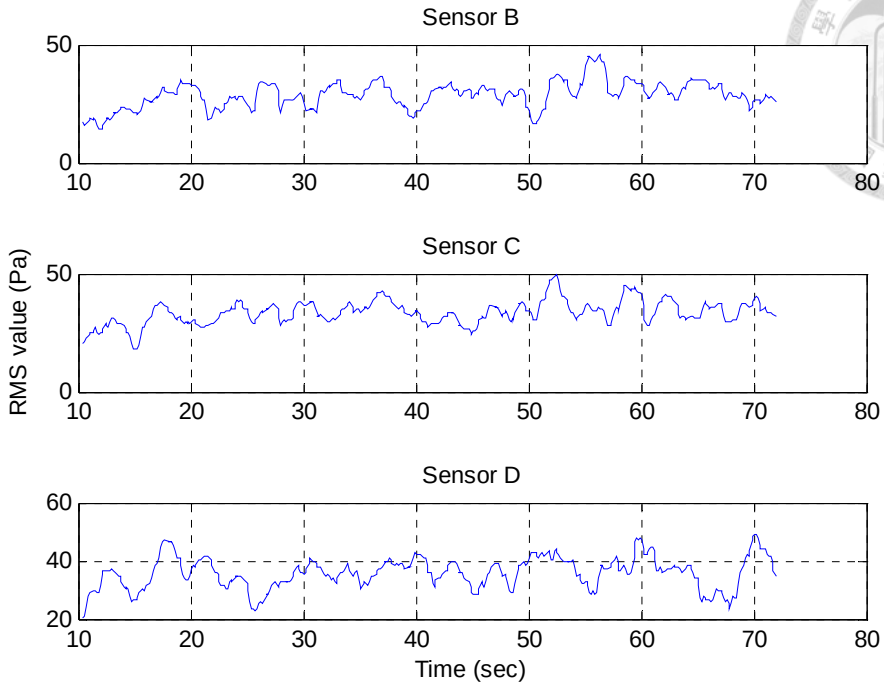

Fig. 4.7 RMS values of the filtered pressure signals measured by the left side sensors while the BAUV swims along the left side wall

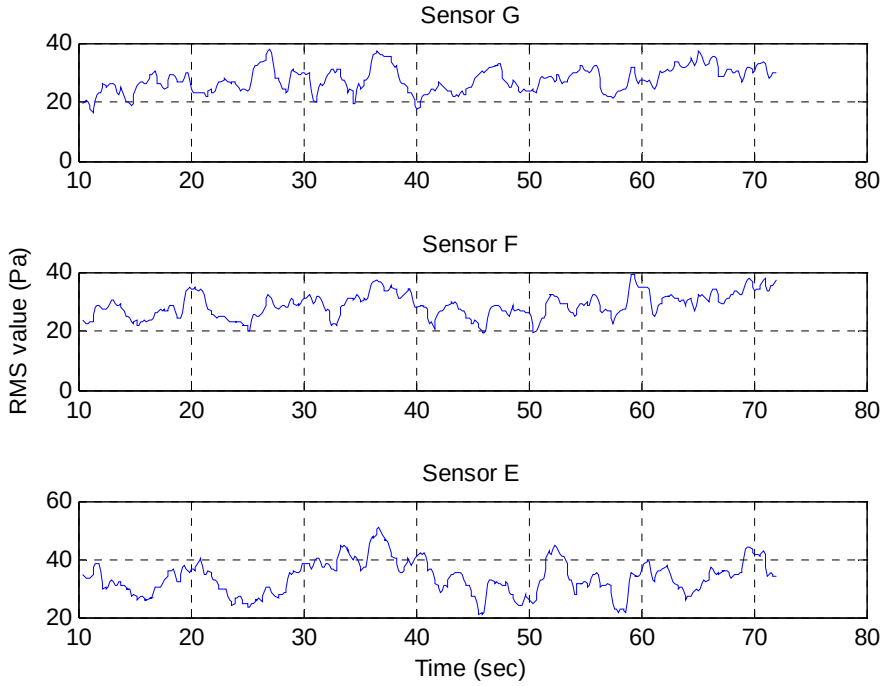

Fig. 4.8 RMS values of the filtered pressure signals measured by the right side sensors while the BAUV swims along the left side wall

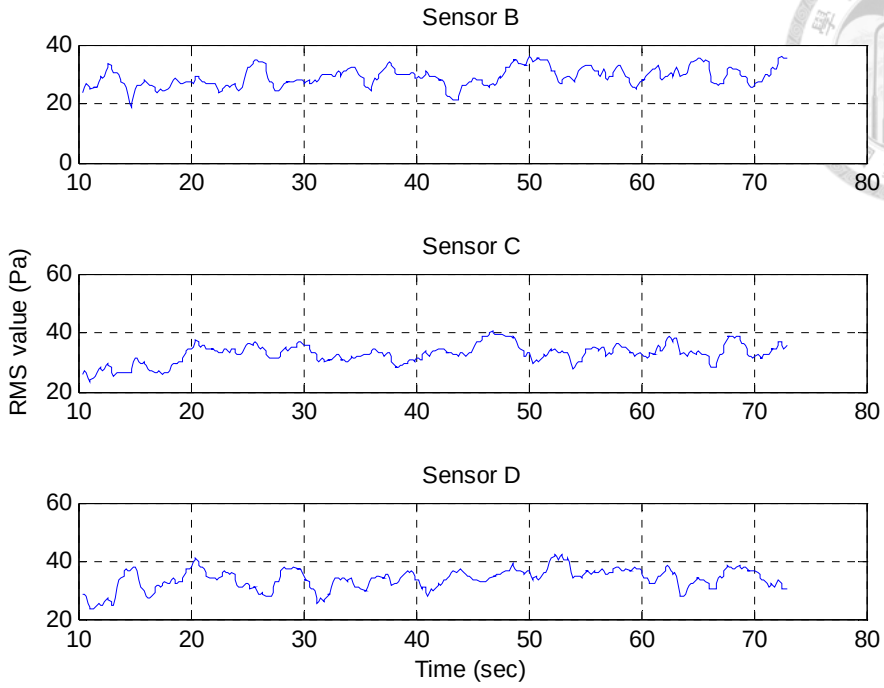

Fig. 4.9 RMS values of the filtered pressure signals measured by the left side sensors while the BAUV swims in an open water

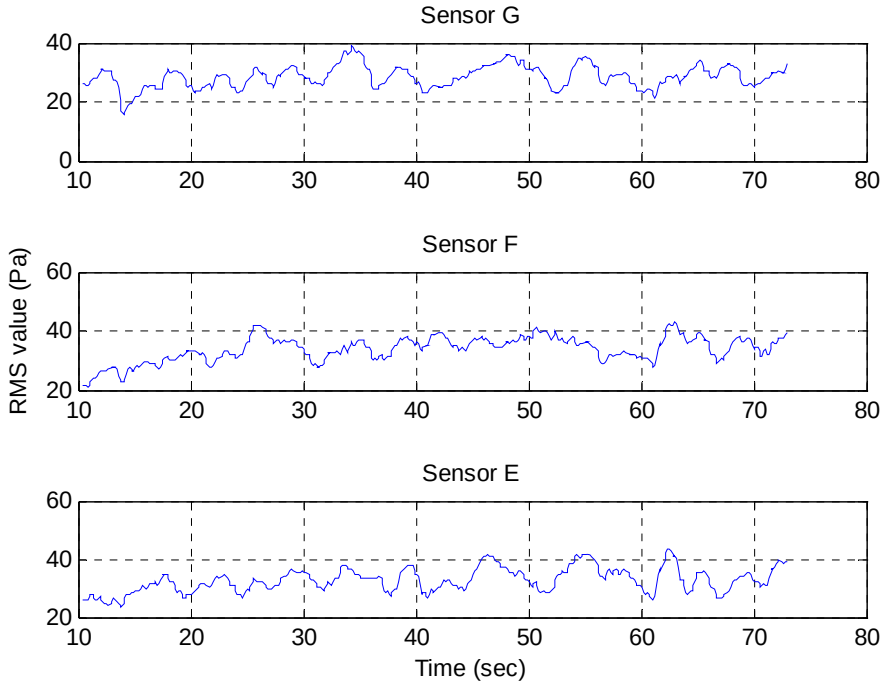

Fig. 4.10 RMS values of the filtered pressure signals measured by the right side sensors while the BAUV swims in an open water

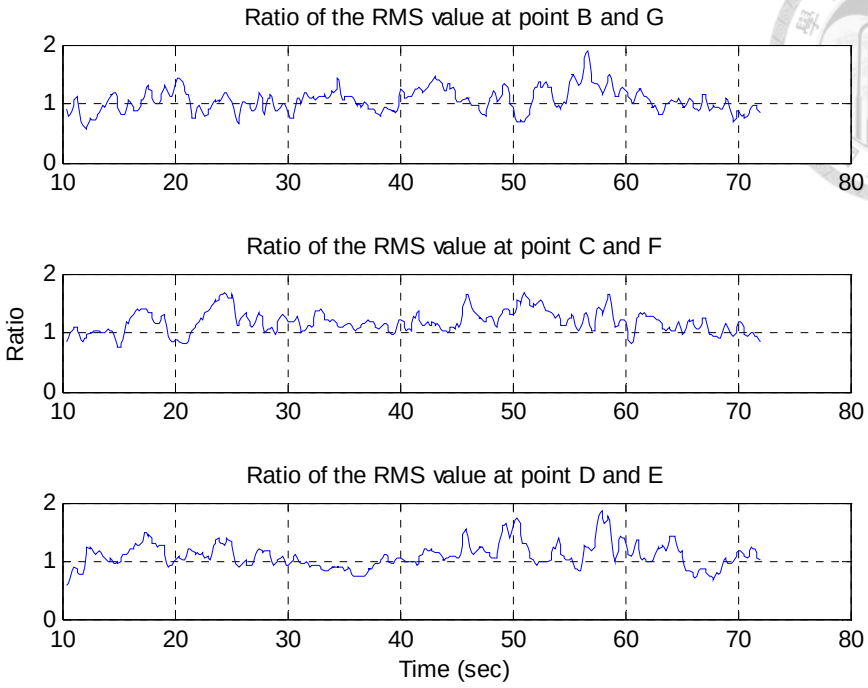

Fig. 4.11 Ratio of the RMS value of pressure at both side sensors while the BAUV swims along the wall

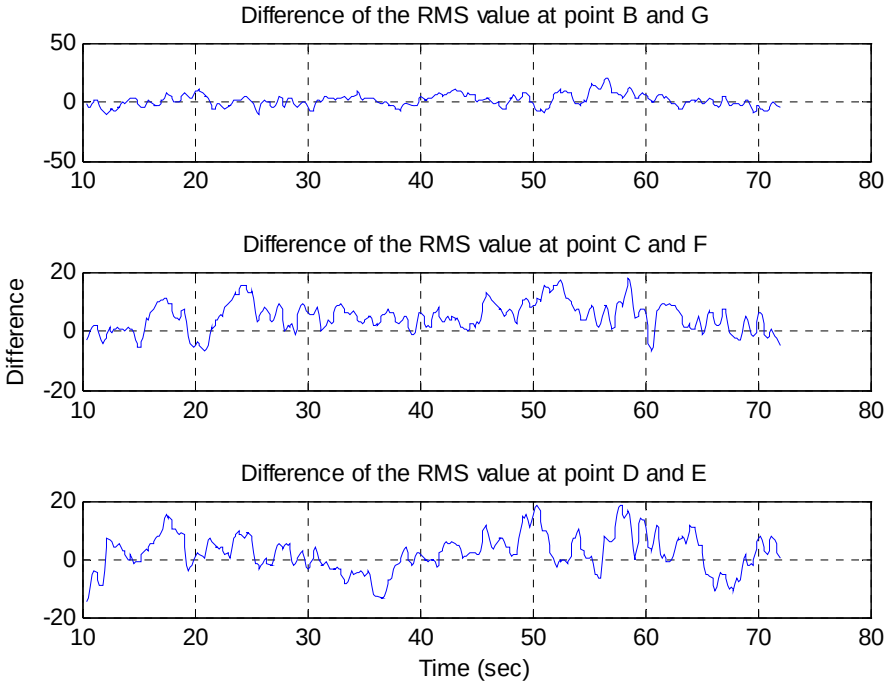

Fig. 4.12 Difference of the RMS value of pressure at both side sensors while the BAUV swims along the wall

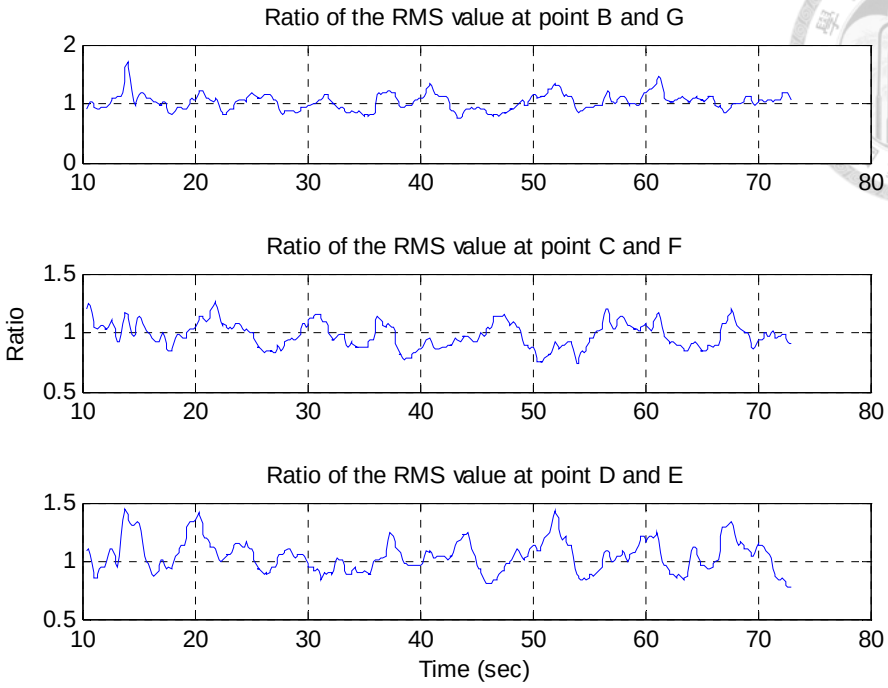

Fig. 4.13 Ratio of the RMS value of pressure at both side sensors while the BAUV swims in an open water

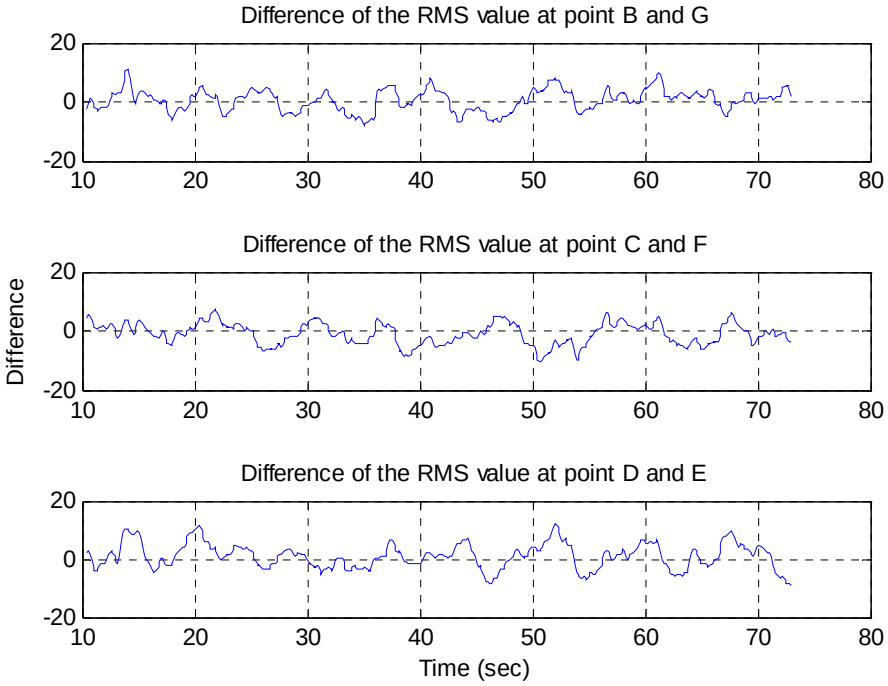

Fig. 4.14 Difference of the RMS value of pressure at both side sensors while the BAUV swims in an open water

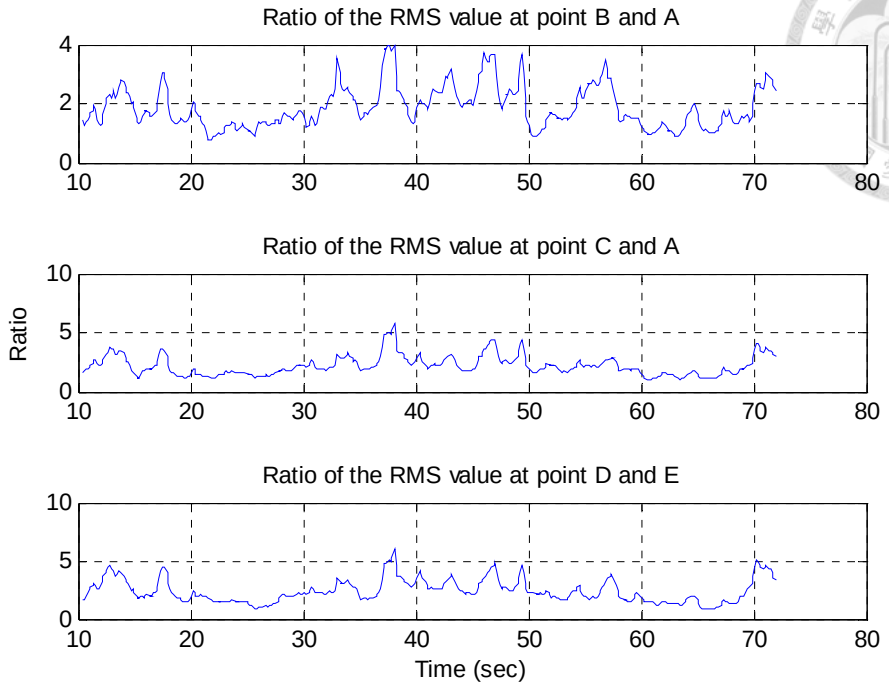

Fig. 4.15 Ratio of the RMS value of pressure between the left side sensors and sensor A while the BAUV swims along the wall

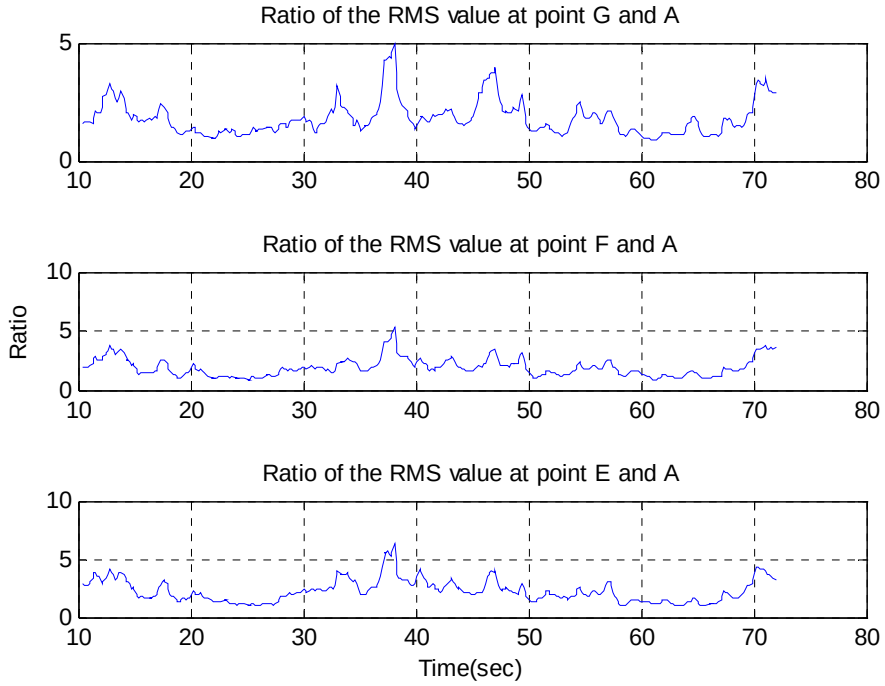

Fig. 4.16 Ratio of the RMS value of pressure between the right side sensors and sensor A while the BAUV swims along the wall

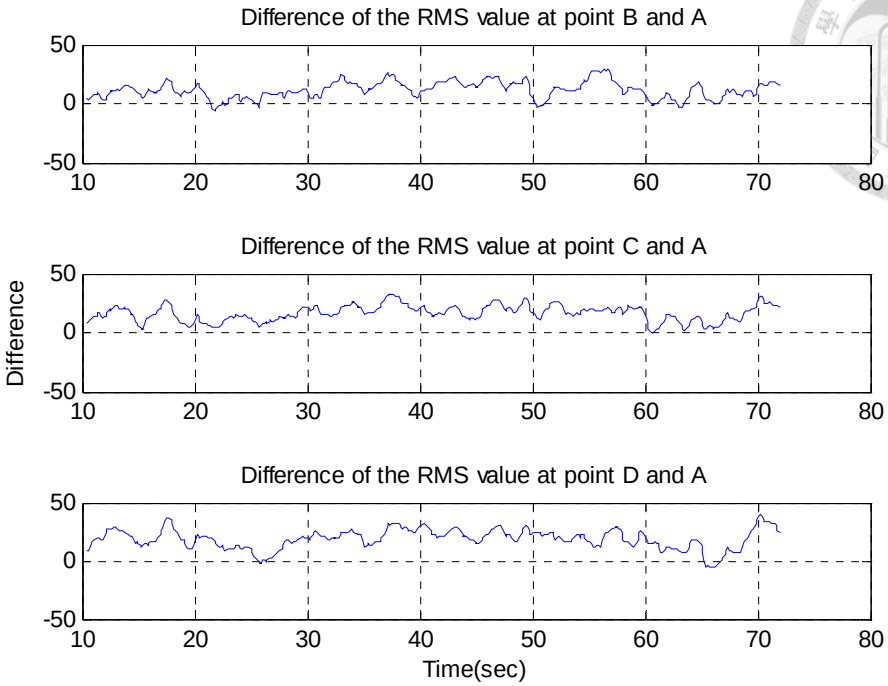

Fig. 4.17 Difference of the RMS value of pressure between the left side sensors and sensor A while the BAUV swims along the wall

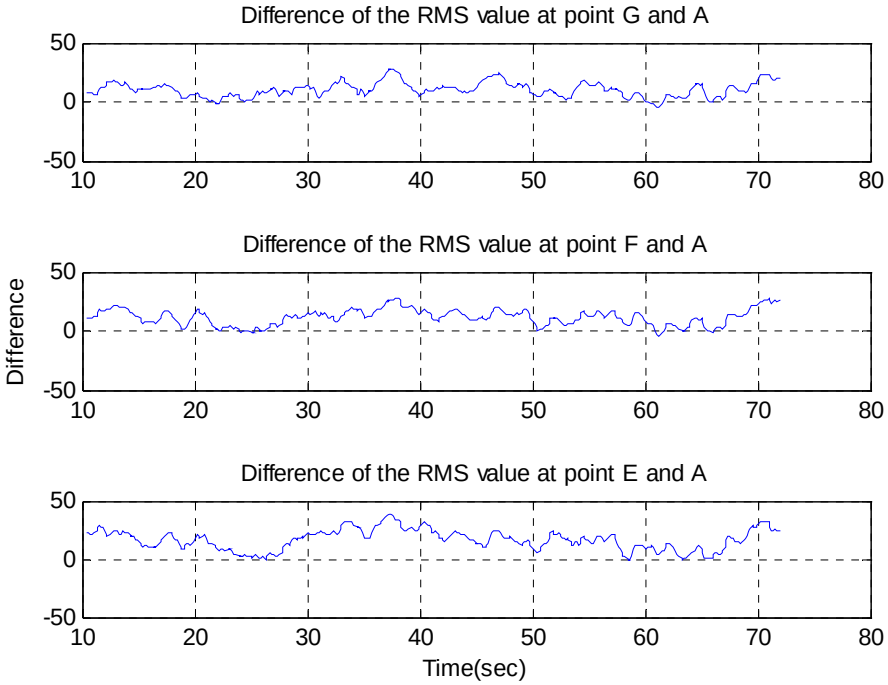

Fig. 4.18 Difference of the RMS value of pressure between the right side sensors and sensor A while the BAUV swims along the wall

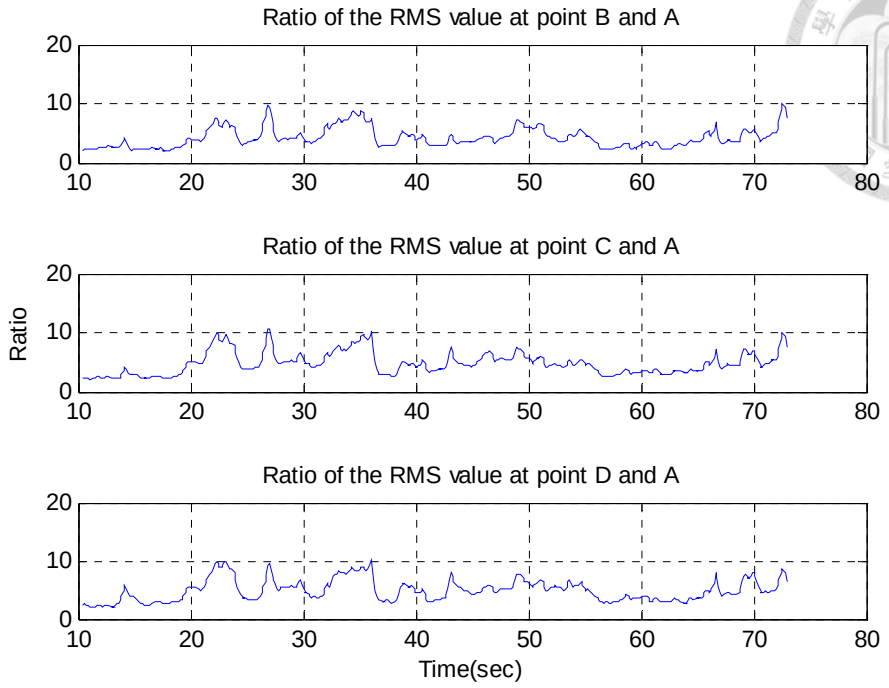

Fig. 4.19 Ratio of the RMS value of pressure between the left side sensors and sensor A while the BAUV swims in an open water

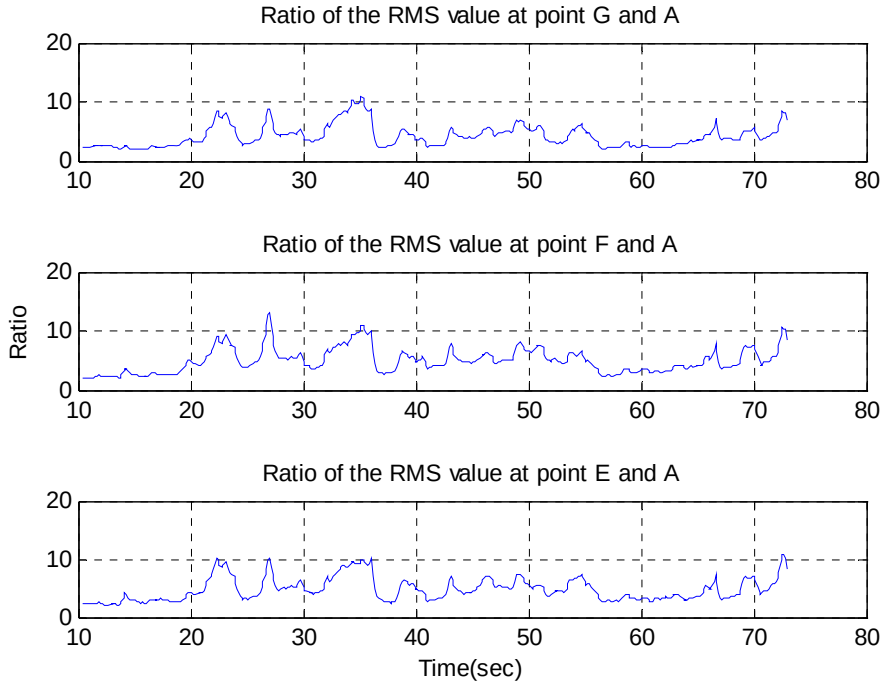

Fig. 4.20 Ratio of the RMS value of pressure between the left side sensors and sensor A while the BAUV swims in an open water

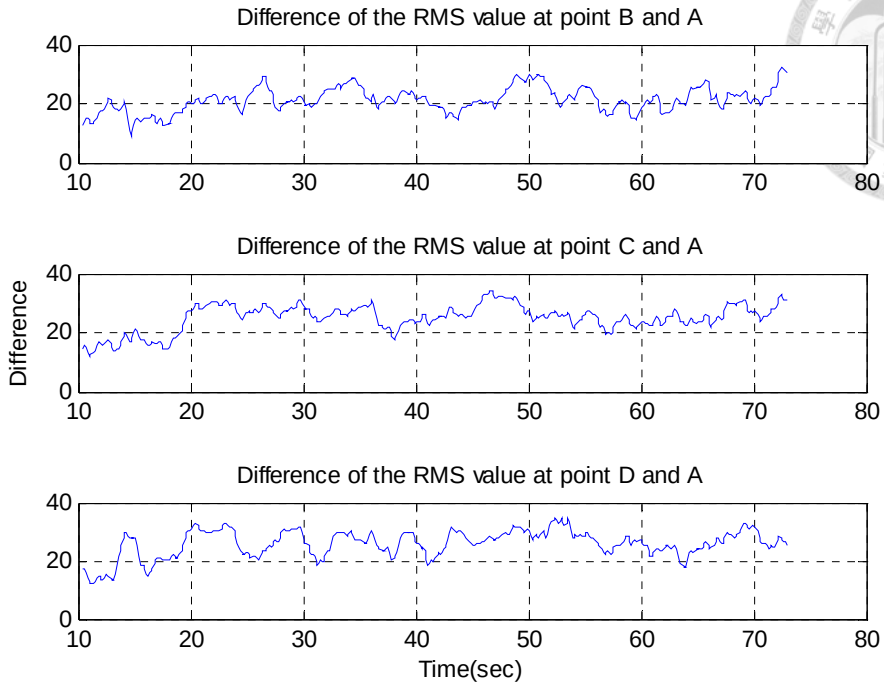

Fig. 4.21 Difference of the RMS value of pressure between the left side sensors and sensor A while the BAUV swims in an open water

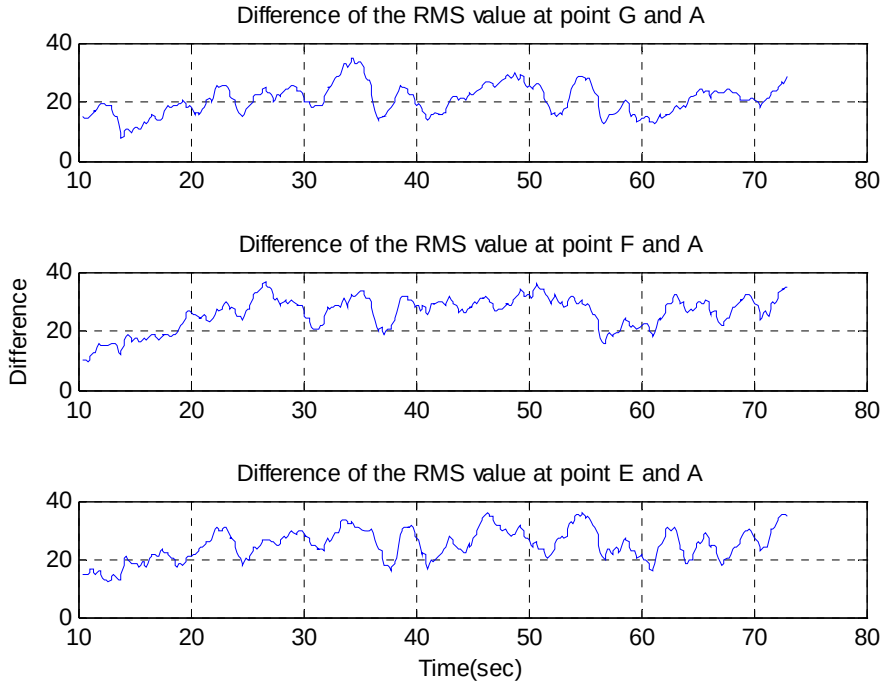

Fig. 4.22 Difference of the RMS value of pressure between the right side sensors and sensor A while the BAUV swims in an open water

4.4 Experimental Results of Classification

Before feeding the feature vectors into SVM classifier, we used the feature selection method to reduce the dimension of extracted feature vectors, this step can help us to choose the important features from extracted feature vectors. There are 28 experiments and total 12600 samples for each class (near the wall and in an open water) were used for training the SVM classifiers, 2 experiments and total 1330 samples for each class were used for testing the SVM classifiers.

We performed three different feature vectors to compare the results of SVM classifier. Firstly, we took all the feature vectors to SVM classifier, the classification accuracy was 85%. Secondly, we choose 10 features based on experience as our feature vectors, and the 10 features are chosen in Table 2, the classification accuracy was 76.1%.

Table 2 Manually selected feature

Two-class	10 features									
Wall vs Open field	2	3	8	9	11	12	15	16	21	22

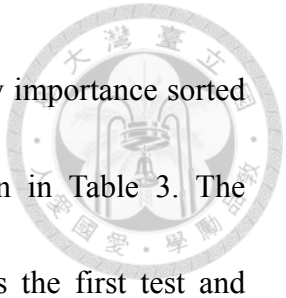

Finally, the feature selection method selected top 10 features by importance sorted as feature vectors from extracted feature vectors, they are shown in Table 3. The classification accuracy was 84%, it had roughly same accuracy as the first test and greater than the second test, we can say that the feature selection method not only reduced the dimension and decreased the time of SVM classifier but also can indeed pick out the more representative characteristics. In Table 3, the elected features mostly related with the sensor on the forehead, it is found that the ratio and difference of the RMS values of each sensors on the lateral sides and on forehead sensor are greatly reduced the effect of water depth and the pitching of the vehicle, it eliminate the interference of underwater environment such that the classification can accurately distinguish with along the wall and in open water.

Table 3 Selected feature by importance

Two-class	10 features sorted by importance									
Wall vs Open field	12	14	15	16	18	19	20	21	24	25

4.5 Environmental Detection

In this section, in order to validate our capability of perception, the BAUV was set to swim in a straight line by controlling the flapping tail from the open field, and we set up two man-made walls in the BAUV trip. Two man-made walls area are 80cm length and 65cm width, they are apart 80cm. Fig. 4.23 depicts the setup of the model for water tank experiments.

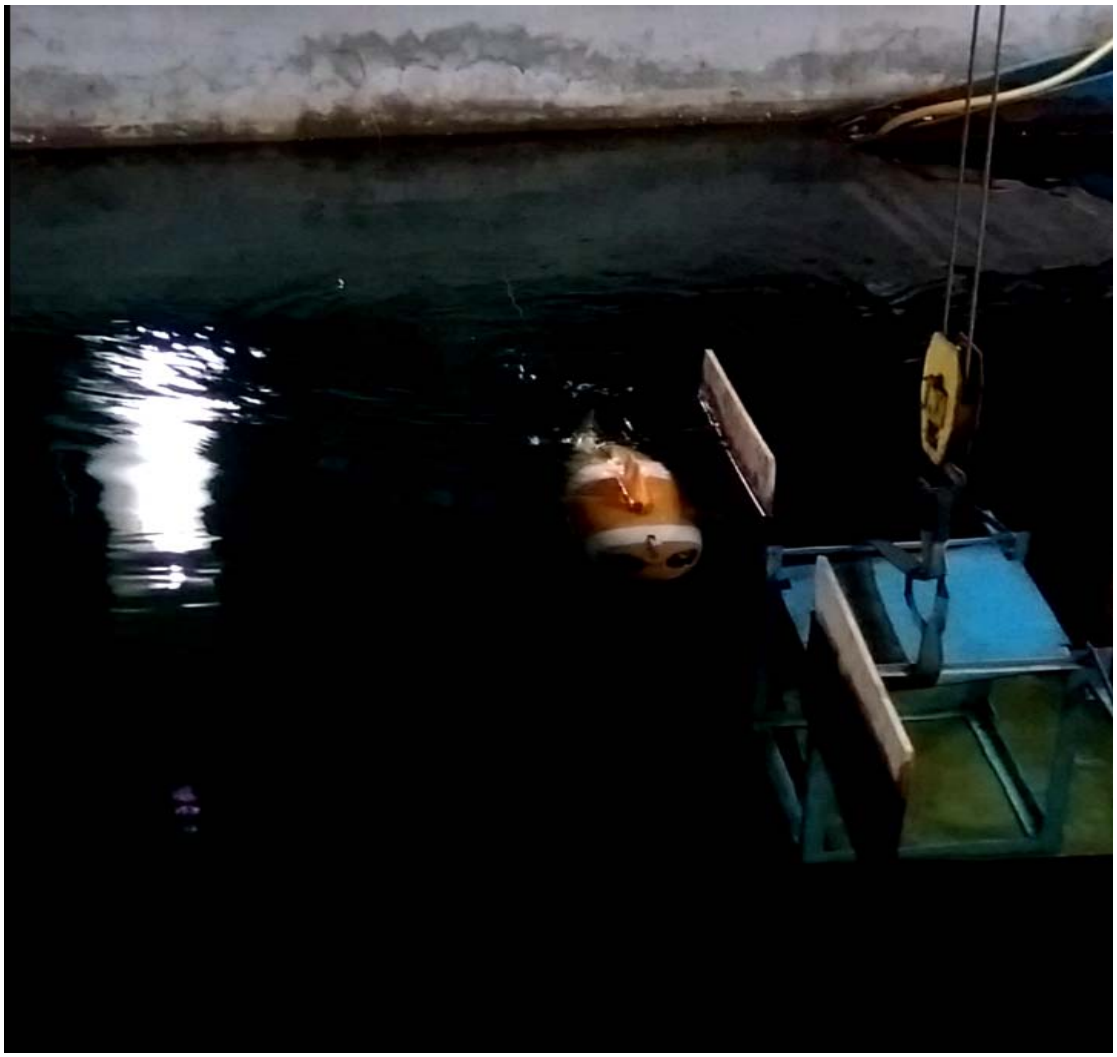

Fig. 4.23 Tank layout of the experiment

The BAUV forward velocity controlled by the tails amplitude and the frequency, the recorded times spent and traveled a forward distance are presented in Fig. 4.24, total travel time is about 34 second.

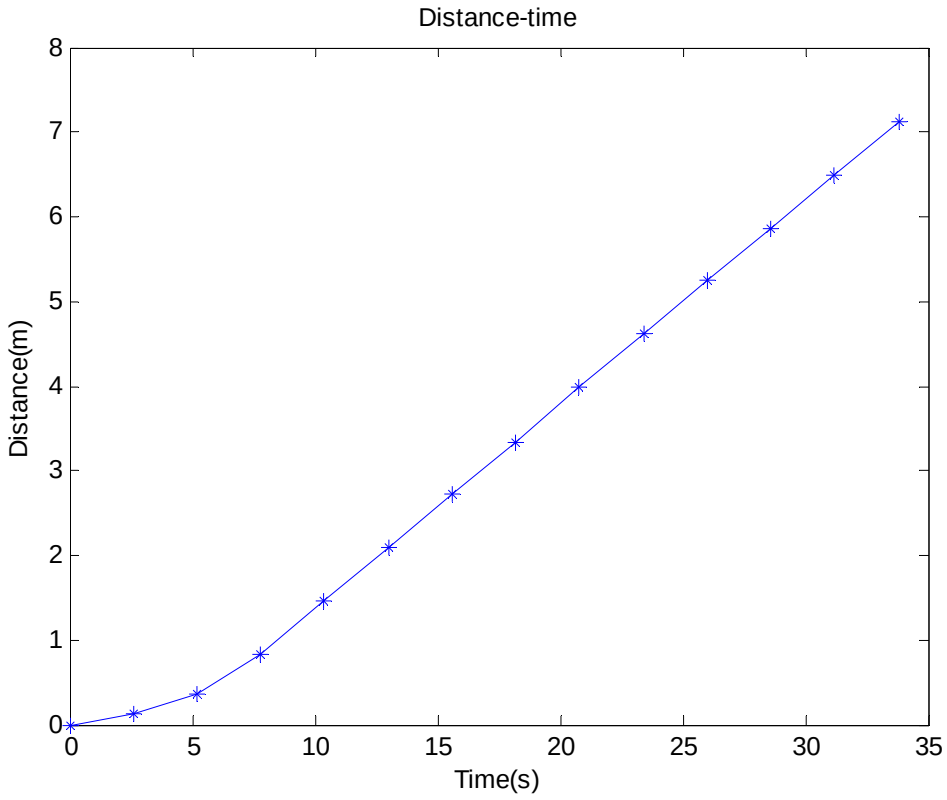

Fig. 4.24 Distance-time plot of the BAUV motion

The selected features of experimental results are shown in Fig. 4.25 to Fig. 4.27, we can clearly see in 12 seconds and 18 seconds each with a peak from selected features of experimental results, the reason by causing this peak is the BAUV swam close the wall.

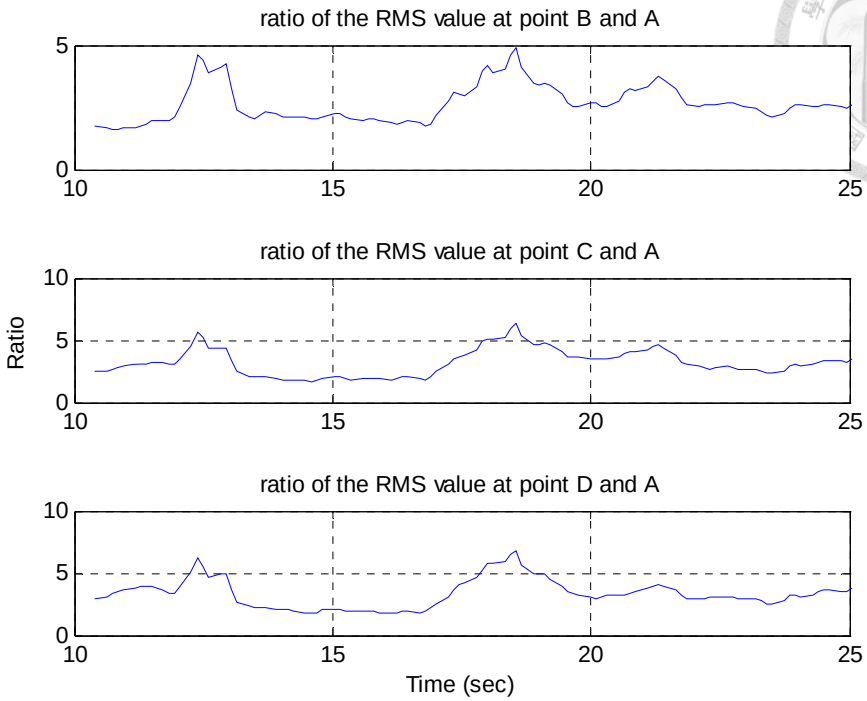

Fig. 4.25 The selected features of experimental results (3 features out of 10)

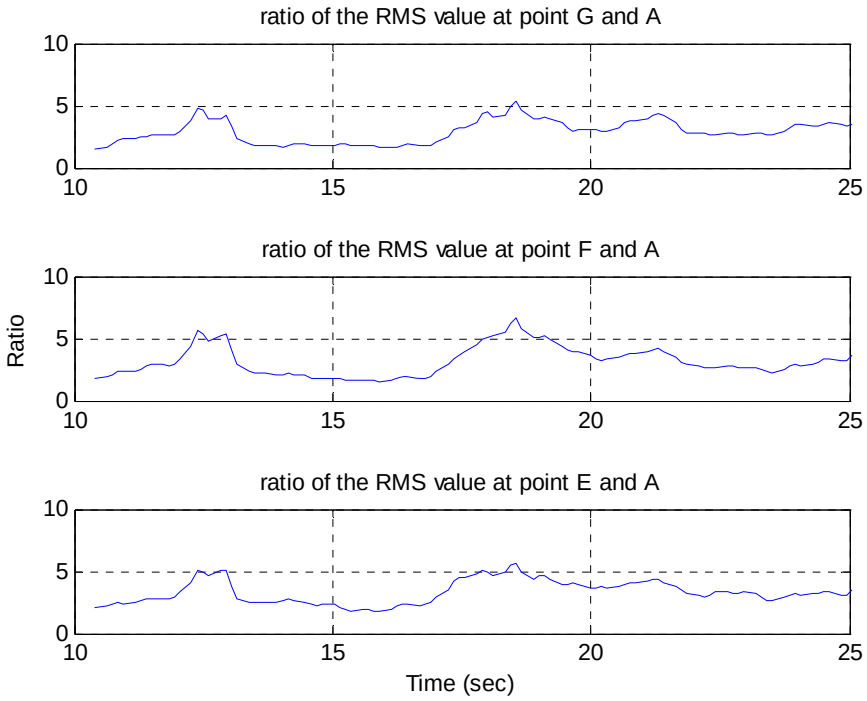

Fig. 4.26 The selected features of experimental results (another 3 features out of 10)

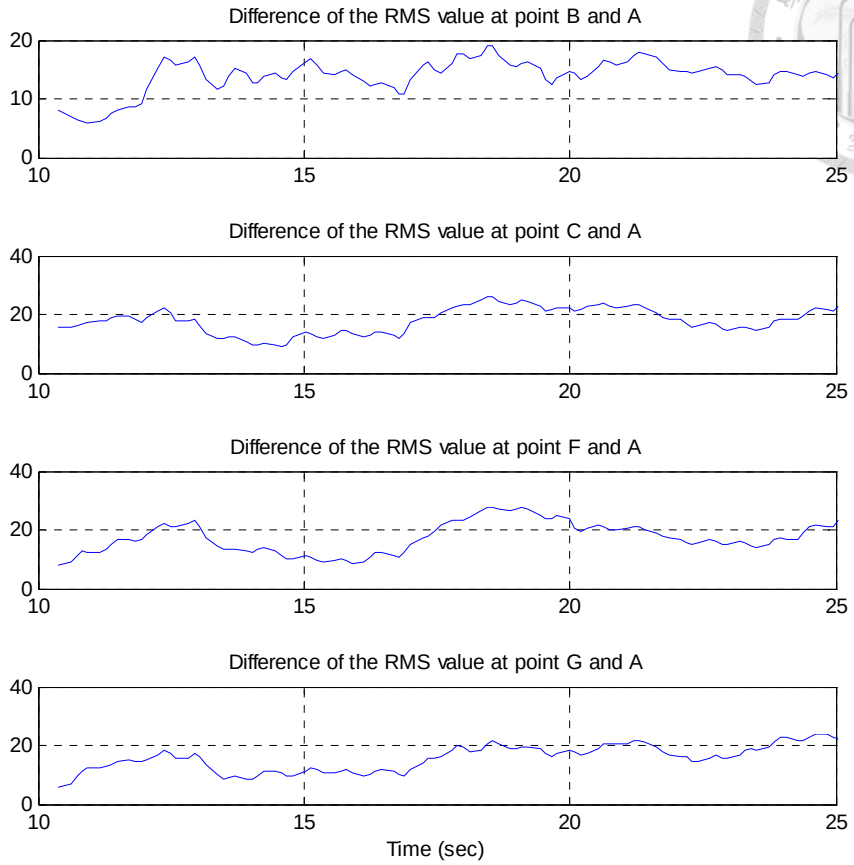

Fig. 4.27 The selected features of experimental results (4 features out of 10)

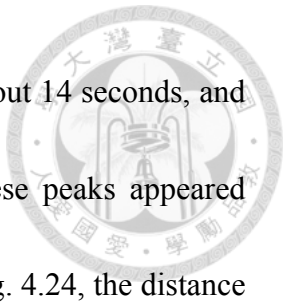

However, the BAUV passed through the first wall of time is about 14 seconds, and passed through the second wall of time is about 20 seconds. These peaks appeared earlier 2 seconds than the actual location of the wall, according to Fig. 4.24, the distance from the BAUV and the wall are apart about 20 ~ 50cm. In other words, as long as the BAUV swims close to the wall less than 50cm range, the lateral line systems will be able to sense the wall.

Fig. 4.28 to Fig. 4.30 illustrates the results of wall detection and shows the tail's motor position of the BAUV. When the BAUV swims close to the wall, it will produce rebound force because of the relationship between the wall, therefore, we control the flapping tail to let the BAUV maintain to swim near the wall so that the robot would not depart too far from the wall.

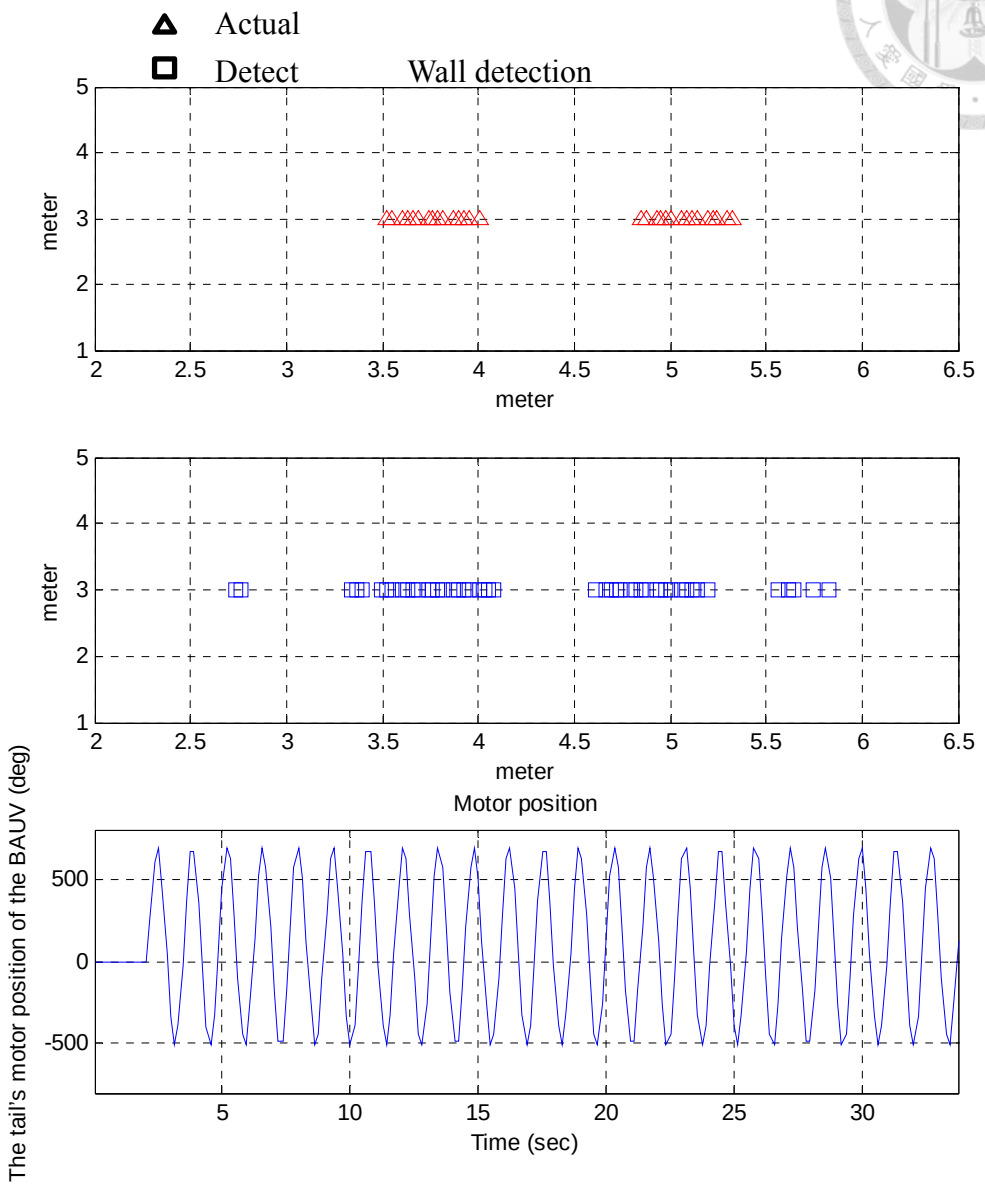

Fig. 4.28 The results of wall detection (case 1)

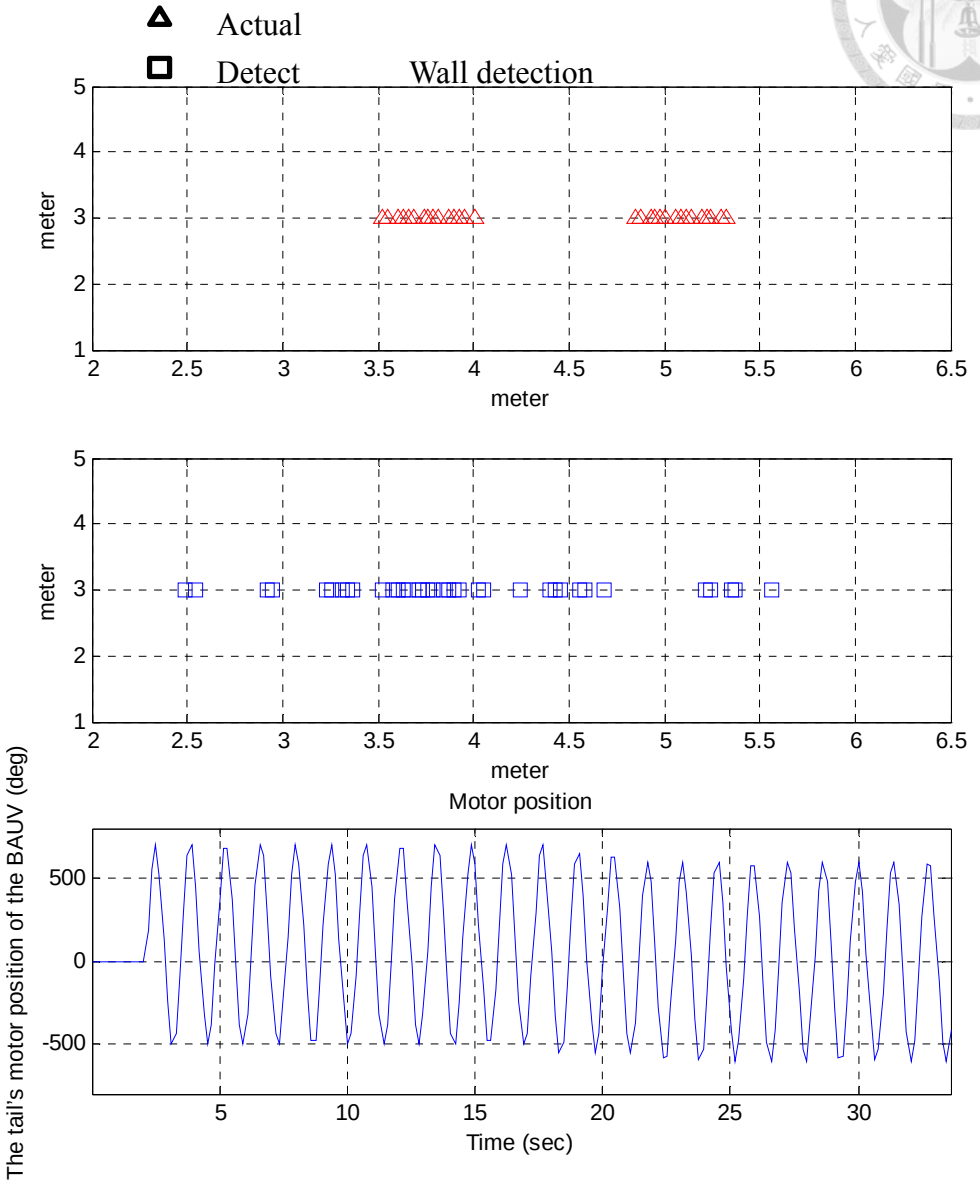

Fig. 4.29 The results of wall detection (case 2)

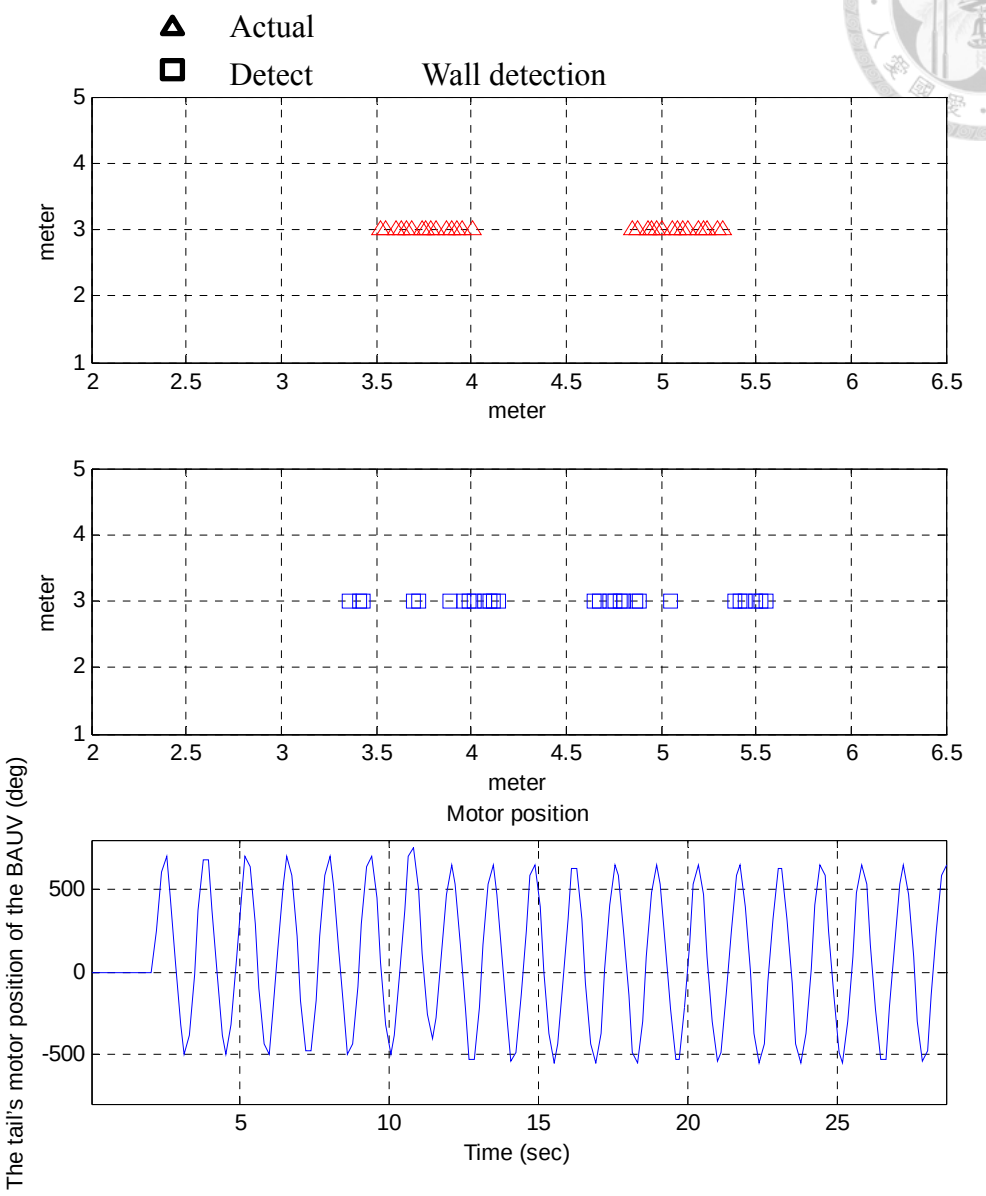

Fig. 4.30 The results of wall detection (case 3)

As Fig. 4.28 to Fig. 4.30 displayed, if we change the motor position of the tail fin in the experiment, it will affect the accuracy of our detection. For case1, the BAUV swam through the first wall and the second wall that the both distance are within detection range (the BAUV and the wall are apart about 20 ~ 50cm), so we has not changed the motor position of the tail fin, the result of wall detection showed that we can indeed sense the both wall.

For case 2 and case 3, we controlled the motor position of the tail fin to revise the distance from the robot and wall. The BAUV was pushed away the wall by the rebound force when it swam through the first wall in case 2, and we changed the motor position of the tail fin to make the robot swim close to the wall, the result of case 2 showed that it's not identify the second wall. The case 3 changed the motor position of the tail fin when it swam through the first wall, and the detection result is not good. The experiments proved that when the motor changes will affect our recognition rate.

The above experiments are based on the tail fin of the BAUV stable swimming forward, the results show the motor changes will affect our detection result. Thence, we try to add the measured pressure signals in training data when the BAUV changes the caudal fin, and we also make the motor position of the tail fin as a feature in training data. Fig. 4.31 to Fig. 4.33 show the improve results after adding new training data.

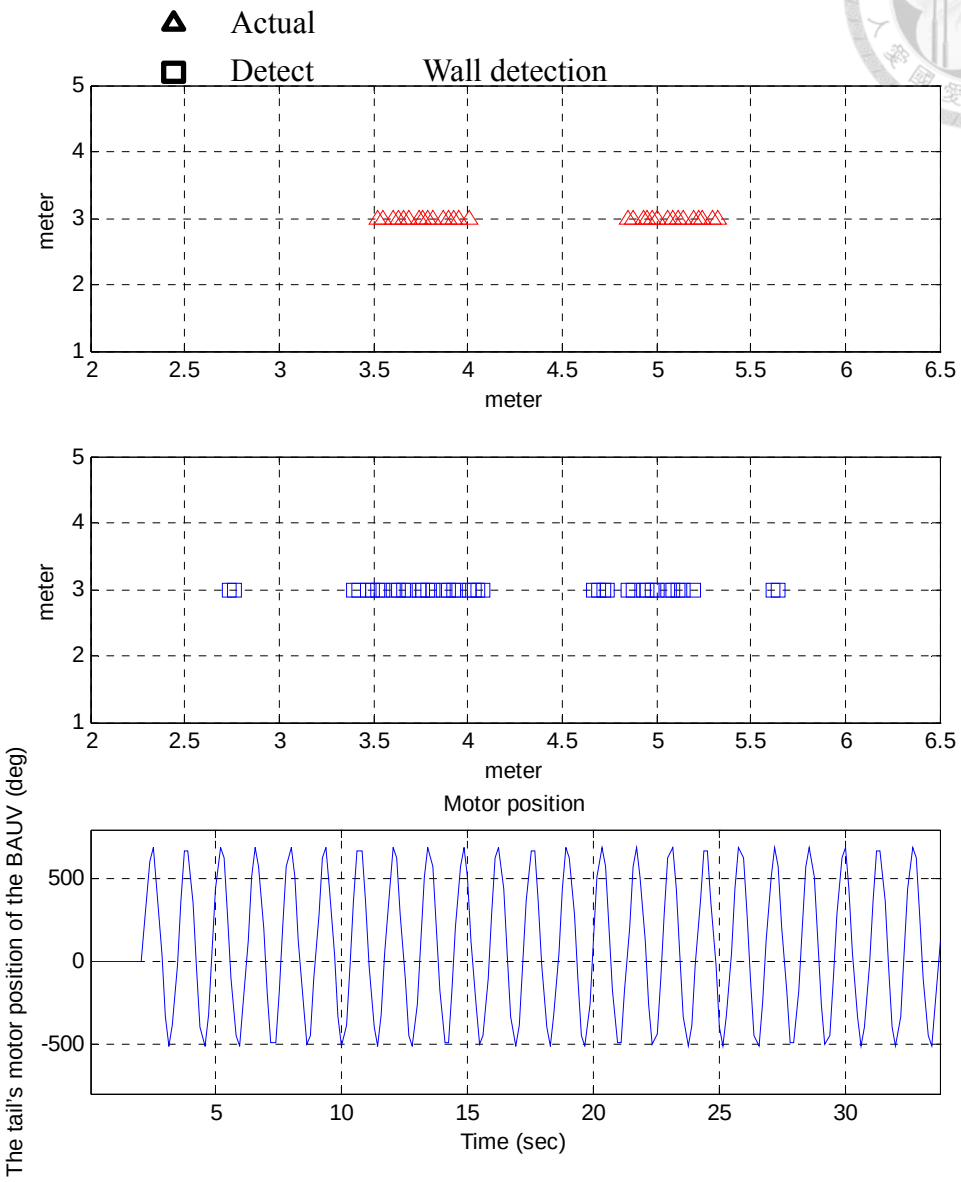

Fig. 4.31 The improved results of wall detection (case 1)

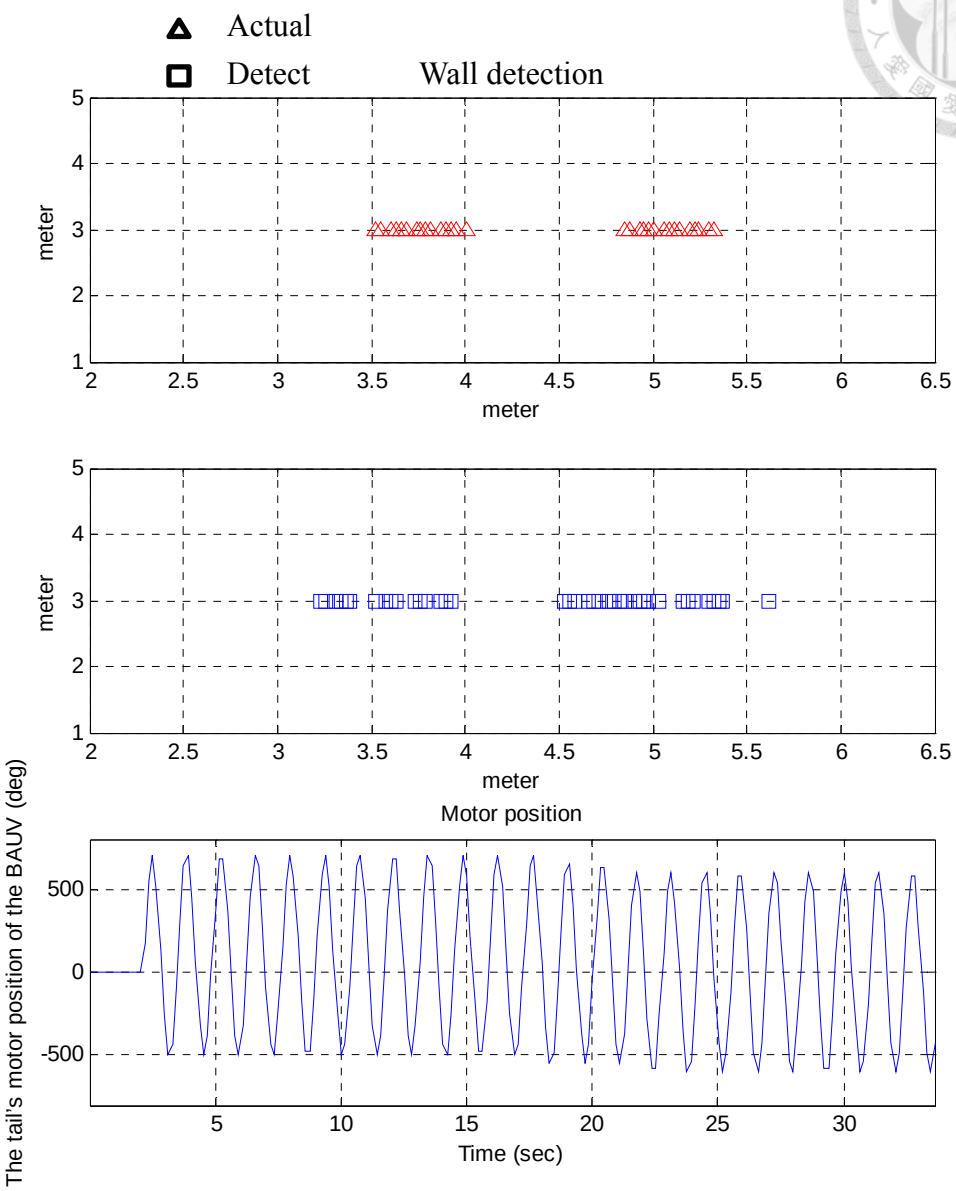

Fig. 4.32 The improved results of wall detection (case 2)

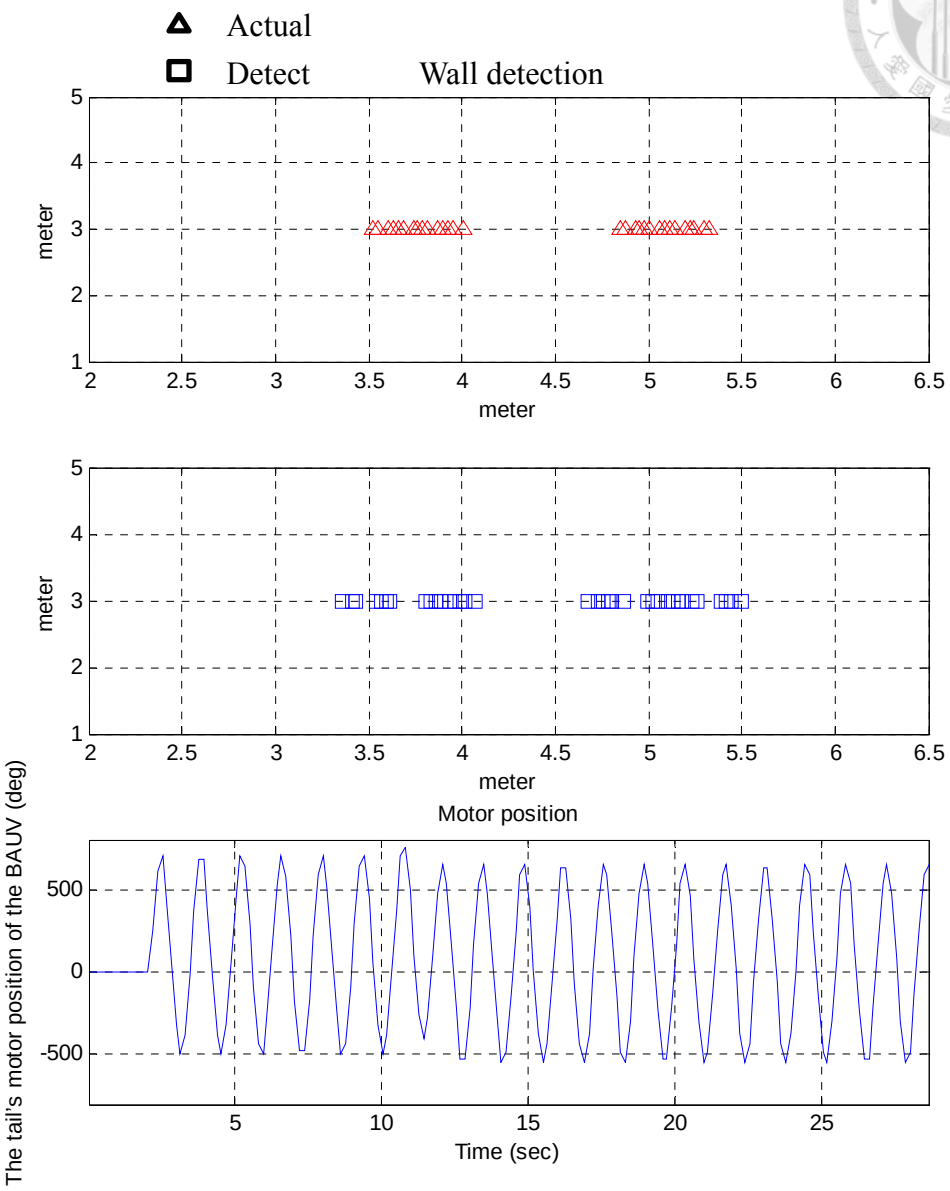

Fig. 4.33 The improved results of wall detection (case 3)

In Fig. 4.31 to Fig. 4.33, the results of wall detection have significant improvement, the dynamic pressure signal added to the training data when the BAUV changes the caudal fin and adds the motor position of the tail fin as a feature, the tail position effectively reduced the uncertainties in detecting the wall when the robot is turning.. Compare to the previous set of data which does not take account of the changes in the caudal fin, the detection rate that considers the tail fin motion is higher.

To verify the robustness of wall detection, we extend the experiment by adding one more task which is to turn and then move along a perpendicular solid wall. Total travel time of experiment is about 57 seconds. Fig. 4.34 shows the tail's motor position.

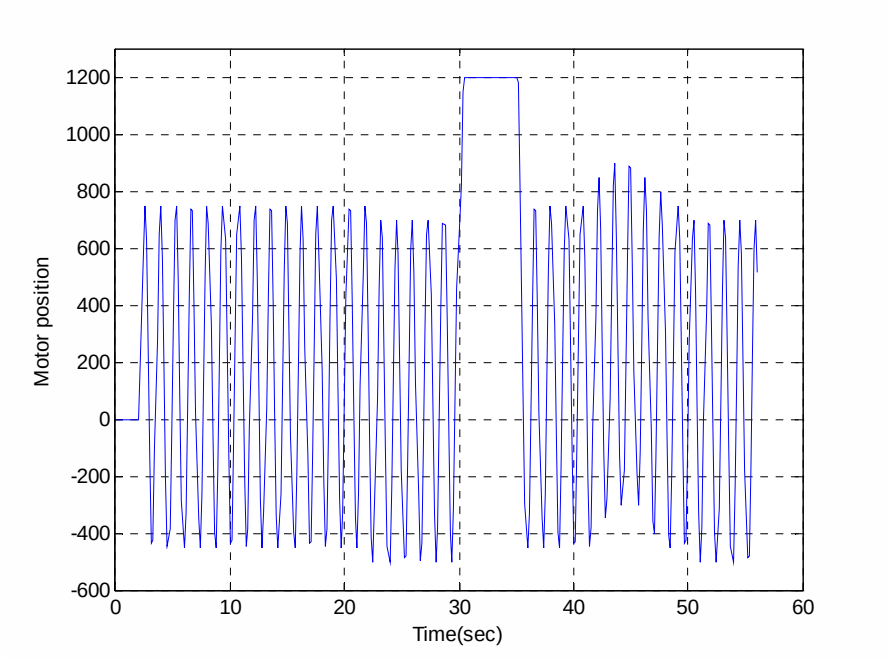

Fig. 4.34 Tail motor position

The selected features before the robot turning are shown in Figs. 4.35 to 4.37, the selected features after the robot turning are shown in Fig. 4.38 to Fig. 4.40. The BAUV passed through the first wall and the second wall at about 14 seconds and 20 seconds respectively.

In Figs. 4.35 to 4.37, we can find that data becomes increasing after 18 seconds, the reason is that the BAUV swam close the wooden wall. Furthermore, Figs. 38 to 40 display data when the BAUV was swimming along the concrete wall. They are relatively stable compared to the data along the wooden wall.

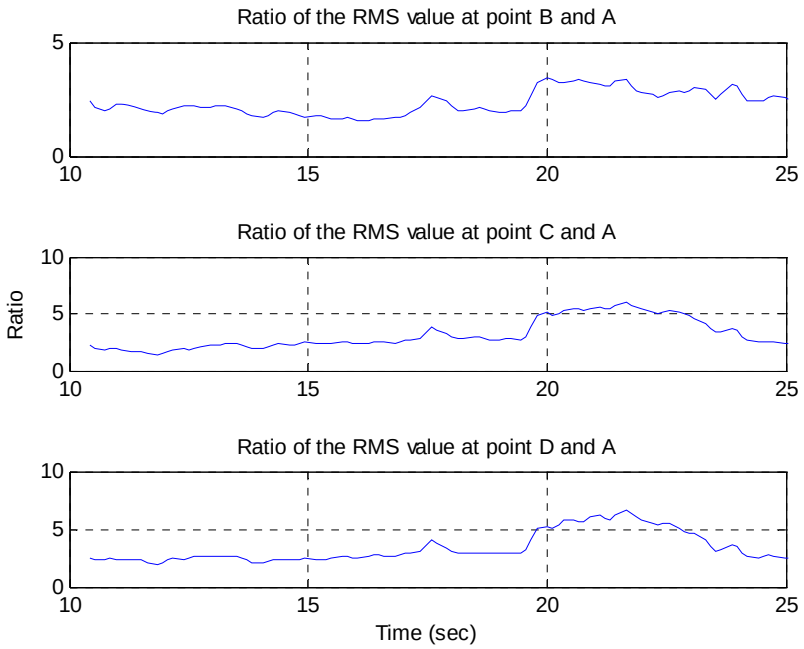

Fig. 4.35 Selected features of experimental results before the robot turning (3 features out of 10)

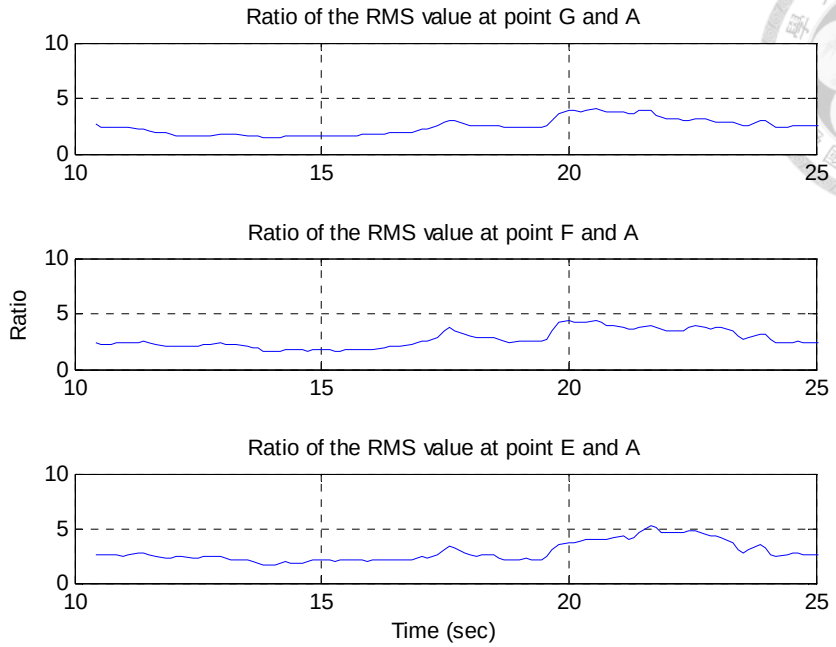

Fig. 4.36 Selected features of experimental results before the robot turning (another 3 features out of 10)

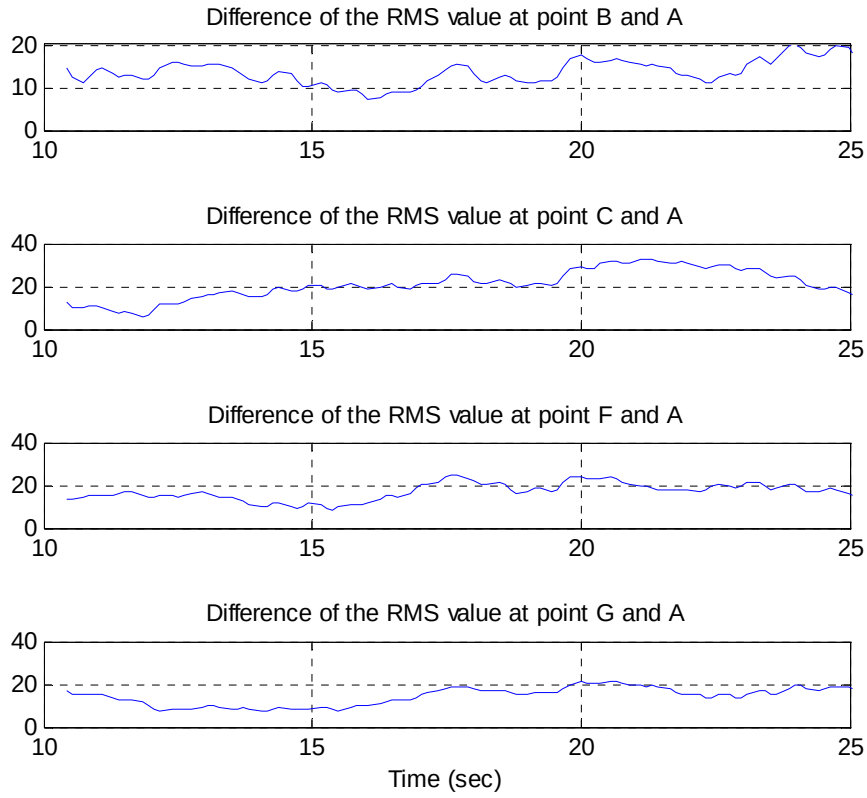

Fig. 4.37 Selected features of experimental results before the robot turning (4 features out of 10)

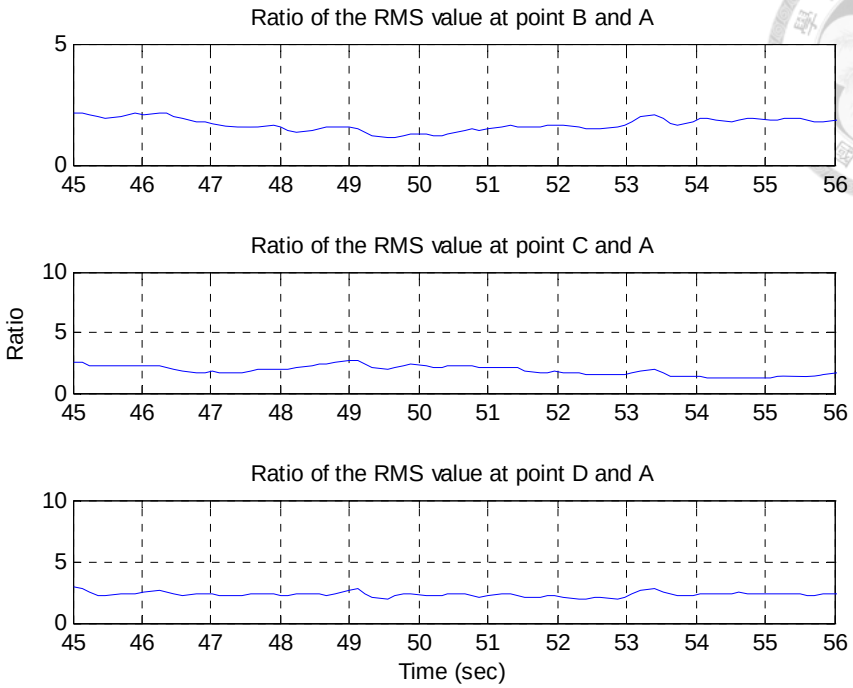

Fig. 4.38 Selected features of experimental results after the robot turning (3 features out of 10)

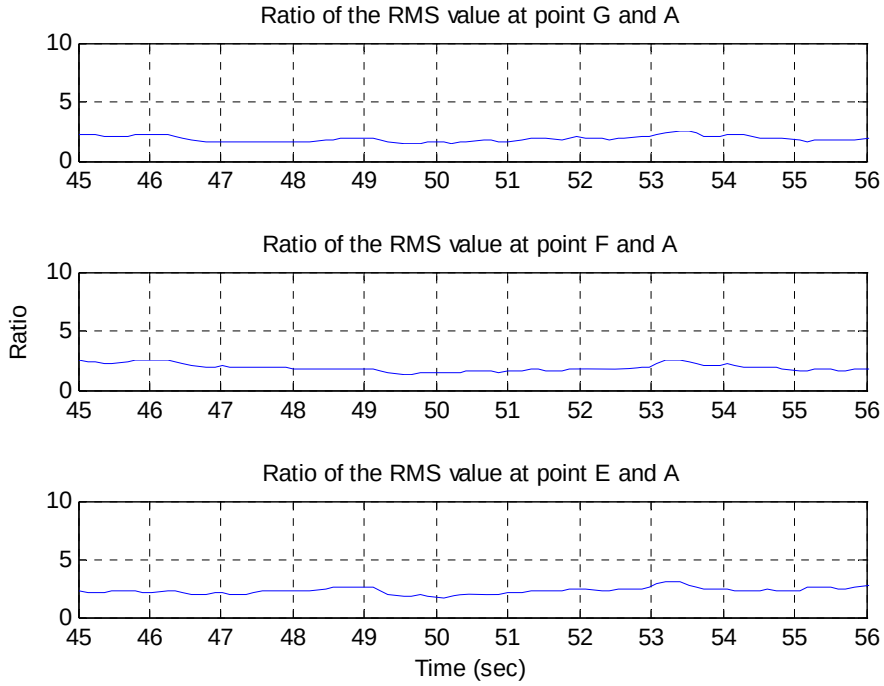

Fig. 4.39 Selected features of experimental results after the robot turning (another 3 features out of 10)

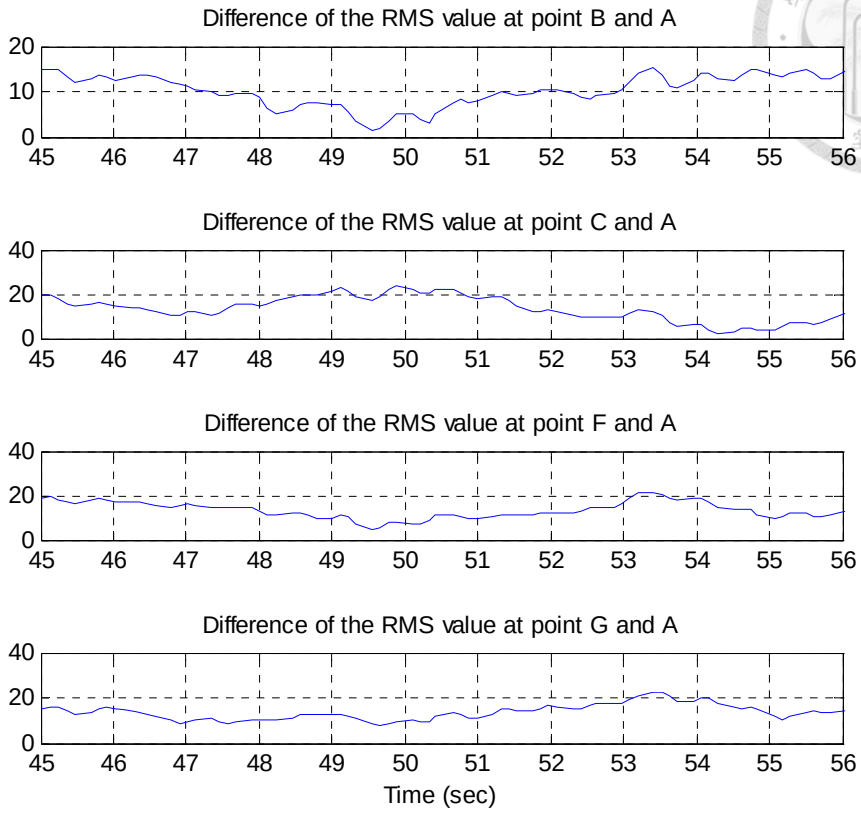

Fig. 4.40 Selected features of experimental results after the robot turning (4 features out of 10)

Fig. 4.41 illustrates the extended experiment results of wall detection. The total samples detected from the experiment are 226, and the samples have been classified into right group are 203, which means the detection rate is 89.8%, and therefore the BAUV can effectively perceive the appearance of walls. In the above experiment, the correct detection of the wooden walls was 138 samples out of 154, and the correct detection of the concrete wall was 65 samples out of 72. Note that, since the BAUV was not trained with the turning movement, the observation was halted during the cornering.

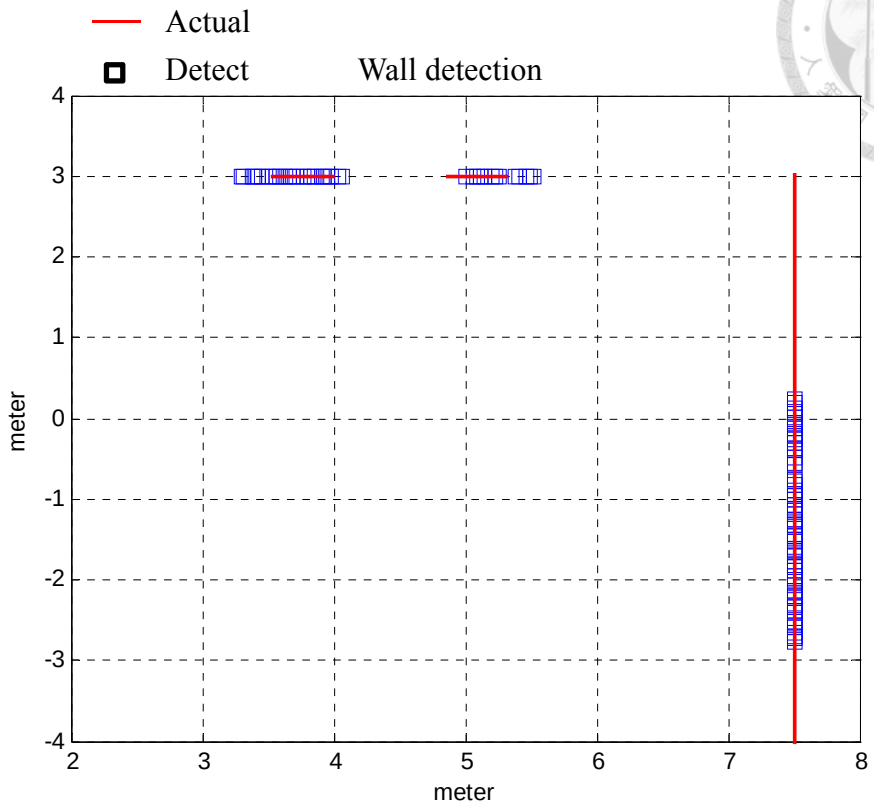

Fig. 4.41 The extended experiment results of wall detection

Chapter 5 Conclusions

This work implements a sensory system to mimic the sensory capabilities of the lateral line evolved in real fish. The dynamic pressure signals were measured by an array of pressure sensors embodied on a biomimetic vehicle. The measured pressure signal was processed to obtain the feature signals, and through the importance appraisals before feeding the feature vectors into a support vector machine classifier by the feature selection method. The pressure patterns were then learned to distinguish the patterns between the ones obtained in open space and in closer proximity to a solid wall. The results indicate that selected important feature vectors are useful to identify the wall presence by our pattern-recognition method. The correctness of the wall detection was further enhanced by including the tail's motor position changes as a feature. The tail position effectively reduced the uncertainties in detecting the wall when the robot is turning. Three sets of feature vectors are compared to find the difference of pressure statistics while the robot fish swimming along the wall and swimming in open water without a wall. Finally, 10 features selected by their importance were utilized, and the classification accuracy was 84%. The results indicate that the selected features are mostly related with the sensor on the forehead. It is found that the ratio and difference of the RMS values of each sensors on the lateral sides and on forehead sensor, the effect

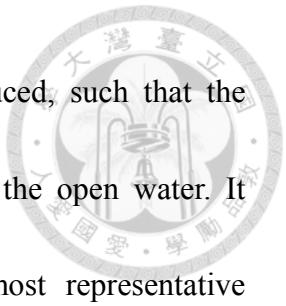

of water depth, the pitching of the vehicle body are greatly reduced, such that the classification can be accurately performed along the wall and in the open water. It proves that the feature selection method could pick out the most representative characteristics of the signals to distinguish the environmental situation. Furthermore, the correctness of the wall detection was enhanced to nearly 90% by including the tail's motor position changes as a feature. The tail position effectively reduces the uncertainties in detecting the wall when the robot is differentially adjusting its heading by the wall.

In future applications, dynamic pressure can be used as a new navigational information for an unmanned underwater vehicle in the proximity to environmental features. To recognize features' information, feature selection methods for various kinds of features, such as circular shaped, rectangular shaped, tubing objects etc., are to be developed and the important dimensions out of the extracted feature vectors for classification must be extensively studied.

REFERENCES

[1] C. B. B. Sheryl Coombs, "Information Processing by the Lateral Line System," in *Sensory Processing in Aquatic Environments*, S. P. Collin and N. J. Marshall, Eds., ed: Springer New York, 2003, pp. 122-138.

[2] D. Hoekstra and J. Janssen, "Non-visual feeding behavior of the mottled sculpin, Coitus bairdi, in Lake Michigan," *Environmental Biology of Fishes* vol. 12, pp. 111-117 1985.

[3] T. J. Pitcher, B. L. Partridge, and C. S. Wardle, "A Blind Fish Can School," *Science,* vol. 194, pp. 963-965, 1976.

[4] C. y. Campenhausen, I. Riess, and R. Weissert, "Detection of Stationary Objects by the Blind Cave Fish Anoptichthys jordani (Characidae)," *Journal of Comparative Physiology,* vol. 143, pp. 369-374, 1981.

[5] S. Coombs, "Smart Skins: Information Processing by Lateral Line Flow Sensors," *Autonomous Robots* vol. 11, pp. 255-261, 2001.

[6] V. I. Fernandez, A. Maertens, F. M. Yaul, J. Dahl, J. H. Lang, and M. S. Triantafyllou, "Lateral-Line-Inspired Sensor Arrays for Navigation and Object Identification," *Marine Technology Society Journal,* vol. 45, pp. 130-146, July/August 2011.

[7] Z. Fan, J. Chen, J. Zou, D. Bullen, C. Liu, and F. Delcomyn, "Design and fabrication of artificial lateral line flow sensors," *JOURNAL OF MICROMECHANICS AND MICROENGINEERING,* vol. 12, pp. 655-661, 2002.

[8] S. P. Windsor, S. E. Norris, S. M. Cameron, G. D. Mallinson, and J. C. Montgomery, "The flow fields involved in hydrodynamic imaging by blind Mexican cave fish (Astyanax fasciatus). Part I: open water and heading towards a wall," *The Journal of Experimental Biology,* pp. 3819-3831, August 2010.

[9] S. P. Windsor, S. E. Norris, S. M. Cameron, G. D. Mallinson, and J. C. Montgomery, "The flow fields involved in hydrodynamic imaging by blind Mexican cave fish (Astyanax fasciatus). Part II: gliding parallel to a wall," *The Journal of Experimental Biology,* pp. 3832-3842, August 2010.

[10] V. Vapnik, *Estimation of Dependences Based on Empirical Data*, 2006.

[11] C. J. C. Burges, "A Tutorial on Support Vector Machines for Pattern Recognition," *Data Mining and Knowledge Discovery,* vol. 2, pp. 121-167, 1998.

[12] C. Cortes and V. Vapnik, "Support-Vector Networks," *Machine Learning,* vol. 20, pp. 273-297, 1995.

[13] C. J. C. Burges and B. Scholkopf, "Improving the Accuracy and Speed of Support Vector Machines," *in Advances in Neural Information Processing System,* vol. 9, pp. 375-381, 1997.

[14] G. M. Fung, O. L. Mangasarian, and J. W. Shavlik, "Knowledge-Based Support VectorMachine Classifiersers," *in Advances in Neural Information Processing System,* 2002.

[15] T. Joachims, "Text Categorization with Support Vector Machines: Learning with Many Relevant Features," presented at the in Proceedings of ECML-98, 10th European Conference on Machine Learning (C. Nedellec and C. Rouveirol, eds.), (Chemnitz, DE), 1998.

[16] M.-J. Chung, "Classification of Epileptic EEG Signals by Using Support Vector Machine," 2009.

[17] C.-W. Hsu, C.-C. Chang, and C.-J. Lin, "A Practical Guide to Support Vector Classification," Department of Computer Science National Taiwan University, Taipei 106, Taiwan, 2010.

[18] S. S. Keerthi and C.-J. Lin, "Asymptotic behaviors of support vector machines with Gaussian kernel," *Neural computation*, vol. 15, pp. 1667-1689, 2003.

[19] H.-T. Lin and C.-J. Lin, "A study on sigmoid kernels for SVM and the training of non-PSD kernels by SMO-type methods," *submitted to Neural Computation*, pp. 1-32, 2003.

Appendix

Table 4 Commercial pressure sensors MS5803-01BA technical data

Sensor Performances				
Pressure	**Min**	**Typ**	**Max**	**Unit**
Range	10		1300	mbar
ADC		24		bit
Resolution		0.012		mbar
Accuracy 25℃, 750 to 1100 mbar	-1.5		+1.5	mbar
Response time		8.22		ms
Long term stability		-1		mbar/yr
Temperature	**Min**	**Typ**	**Max**	**Unit**
Range	-40		+85	℃
Resolution		<0.01		℃
Accuracy	-0.8		+0.8	℃